

**On the Regulation of Centriole Duplication in Human Cells:**

**Exploring the Interactions of Polo-Like Kinase 4 with the  
Centrosomal Proteins Cep192 and STIL**

**Inauguraldissertation**

zur Erlangung der Würde eines Doktors der Philosophie  
vorgelegt der  
Philosophisch-Naturwissenschaftlichen Fakultät  
der Universität Basel

von

**Anna-Maria Katarina Gabryjonczyk**  
aus Illnau-Effretikon ZH, Schweiz

Basel, 2015

Originaldokument gespeichert auf dem Dokumentenserver der Universität Basel

[edoc.unibas.ch](http://edoc.unibas.ch)

Genehmigt von der Philosophisch-Naturwissenschaftlichen Fakultät

auf Antrag von

Prof. Dr. Erich A. Nigg und Prof. Dr. Peter Scheiffele

Basel, den 23.06.2015

Dekan: Prof. Dr. Jörg Schibler

# TABLE OF CONTENTS

<b>1</b>	<b>SUMMARY</b> .....	<b>5</b>
<b>2</b>	<b>INTRODUCTION</b> .....	<b>6</b>
<b>2.1</b>	<b>Overview</b> .....	<b>6</b>
<b>2.2</b>	<b>Structure and function of the centrosome</b> .....	<b>7</b>
<b>2.3</b>	<b>The centrosome cycle</b> .....	<b>11</b>
<b>2.4</b>	<b>Control of centriole duplication in human cells</b> .....	<b>13</b>
2.4.1	“Cell cycle control” versus “copy number control” .....	13
2.4.2	Canonical versus <i>de novo</i> centriole formation .....	15
<b>2.5</b>	<b>Molecular mechanism of centriole biogenesis</b> .....	<b>16</b>
2.5.1	SAS-6 dictates the assembly of the cartwheel structure .....	18
2.5.2	STIL .....	20
2.5.3	Cep192 .....	21
2.5.4	Polo-like kinase 4 (PLK4).....	22
<b>3</b>	<b>AIM OF THIS PROJECT</b> .....	<b>26</b>
<b>4</b>	<b>RESULTS</b> .....	<b>27</b>
<b>4.1</b>	<b>Identification of PLK4-interacting proteins</b> .....	<b>27</b>
<b>4.2</b>	<b>On the PLK4/Cep192 interaction</b> .....	<b>30</b>
4.2.1	The Cep192 N-terminus (1-330) binds to the PB1-PB2 domain of PLK4 .....	30
4.2.2	Binding of Cep192 to PLK4 is direct.....	34
4.2.3	Cep192 is a substrate of PLK4.....	36
4.2.4	Cep152 and Cep192 display distinct centrosomal localizations .....	38
4.2.5	Cep192 and Cep152 cooperate in PLK4 recruitment and centriole duplication....	40
4.2.6	Excursion: Cep192 interacts with Aurora A and PLK1 .....	41
<b>4.3</b>	<b>On the PLK4/STIL interaction</b> .....	<b>43</b>
4.3.1	Interdependencies between PLK4, STIL, and SAS-6 centrosomal localizations ...	43
4.3.2	STIL and PLK4 interact functionally and physically.....	45
4.3.3	The STIL-CC motif is necessary and sufficient for PLK4 binding .....	48
4.3.4	The STIL-CC motif is essential for STIL self-association .....	50
4.3.5	The STIL-CC motif is essential for centriole duplication.....	52
4.3.6	The STIL-CC motif directly binds to PLK4-PB3 with nanomolar affinity .....	54
4.3.7	Does STIL-CC binding to PLK4-L1 depend on an intact DSG motif? .....	56
4.3.8	Analysis of the STIL-CC sequence properties.....	57

---

4.3.9	Mutational analysis of STIL-CC residues at positions b, c, and f.....	60
4.3.10	Structure-based analysis of the PLK4-PB3/STIL-CC complex.....	62
4.3.11	Structure-guided mutational analysis of the PLK4/STIL-CC interaction.....	64
4.3.12	Analysis of PLK4 self-interactions.....	67
<b>5</b>	<b>DISCUSSION.....</b>	<b>68</b>
5.1	PLK4 interacts with Cep192 and STIL.....	68
5.2	Exploring the PLK4/Cep192 interaction.....	69
5.3	Exploring the PLK4/STIL interaction.....	74
5.4	Speculative model for the initial steps of procentriole assembly.....	79
<b>6</b>	<b>MATERIALS AND METHODS.....</b>	<b>82</b>
6.1	Cell culture and transfections.....	82
6.2	Antibodies.....	82
6.3	Plasmids and cloning.....	83
6.4	Cell extracts, immunoprecipitations, and Western blotting.....	90
6.5	Recombinant protein purification and biochemical assays.....	90
6.6	Immunofluorescence microscopy.....	91
6.7	Miscellaneous.....	92
<b>7</b>	<b>ABBREVIATIONS.....</b>	<b>93</b>
<b>8</b>	<b>REFERENCES.....</b>	<b>95</b>
<b>9</b>	<b>PUBLICATIONS.....</b>	<b>111</b>
<b>10</b>	<b>ACKNOWLEDGEMENTS.....</b>	<b>112</b>

## 1 SUMMARY

Centrioles duplicate once in each cell cycle to give rise to two centrosomes that form the spindle poles during mitosis. Aberrant centriole duplication can result in the formation of supernumerary centrosomes, leading to incorrect spindle assembly and chromosome segregation errors, thereby possibly contributing to carcinogenesis (Ganem et al., 2009; Nigg, 2002; Zyss and Gergely, 2008). Thus, to ensure genome stability, centriole duplication has to be precisely regulated. Polo-like kinase 4 (PLK4) is a key regulator of centriole duplication (Bettencourt-Dias et al., 2005; Habedanck et al., 2005). PLK4 is characterized by an N-terminal Ser/Thr kinase domain and three C-terminal Polo-boxes (PB1-PB3) (Slevin et al., 2012). The PB1-PB2 domain is required for PLK4's centrosomal localization and binding to Cep152 (Cizmecioglu et al., 2010; Hatch et al., 2010; Slevin et al., 2012). In contrast to PB1-PB2, no binding partners have been described for PB3.

Here, we identify Cep192 and STIL as novel interaction partners of PLK4-PB1-PB2 and PLK4-PB3, respectively. In the first part of this study, we reveal that Cep192 directly binds PB1-PB2 via a short region within its N-terminus, which contains conserved patches of acidic residues. We show that also in the case of Cep152 a short N-terminal acidic region is critical for the binding to PB1-PB2. These acidic regions of Cep192 and Cep152 enable electrostatic interactions with positively charged residues of the PB1-PB2 domain in order to promote PLK4 centriolar recruitment (Sonnen et al., 2013). In the second part of this study, we identify STIL as the first known binding partner of PLK4-PB3. We show that the coiled-coil motif of STIL (STIL-CC) is necessary and sufficient for this interaction and thus important for centriole duplication. Based on a collaboration for crystallographic and NMR analyses, we furthermore demonstrate that PB3 adopts a canonical PB fold, and that the PLK4-PB3/STIL-CC binding mimics coiled-coil formation. Analysis of structure-guided STIL mutants suggests a dual binding mode of STIL-CC to PB3 and L1 of PLK4 (linker between the catalytic domain and the PB domains). Taken together, we propose a speculative model for the initial steps of procentriole assembly according to which PLK4 is recruited to centrioles by electrostatic interactions between PB1-PB2 and Cep192/Cep152, and thereafter is stabilized and activated via STIL-CC binding to PB3 and L1.

## 2 INTRODUCTION

### 2.1 Overview

The centrosome was first discovered and described in the late 19<sup>th</sup> century by Edouard van Beneden and Theodor Boveri (Boveri, 1887; Van Beneden, 1876). Although centrosomes are present in almost all eukaryotic cells, research on their structure and function has long been stagnant, mostly owing to technical limitations imposed by their small size and low copy number in cells. In the late 20<sup>th</sup> century, centrosome biology was rediscovered and since then has gained increasingly more attraction. To date, key functions of the centrosome have been unraveled, but the underlying molecular mechanisms are still incompletely understood. Recent proteomic analyses of the human centrosome have provided large-scale information on the composition of this tiny organelle, revealing hundreds of yet to be characterized centrosomal components (Andersen et al., 2003; Jakobsen et al., 2011). Thus, given its considerable complexity, the centrosome is expected to keep researchers busy for many years to come.

The centrosome plays principally two roles in cells: In proliferating cells, it serves as the main microtubule-organizing center (MTOC), and in quiescent or differentiated cells, it additionally provides the basal body for the formation of a cilium or flagellum. Furthermore, the centrosome has been proposed to serve as a hub for the integration of various signalling pathways, regulating for example cell cycle progression or the response to DNA damage (reviewed in Arquint et al., 2014; Doxsey et al., 2005). Importantly, deregulation of centrosome-related processes has been implicated in various human diseases, including cancer. Already Boveri proposed a direct link between cancer and centrosome abnormalities (Boveri, 1914). He postulated that centrosome aberrations might contribute to carcinogenesis through generating multipolar spindles, resulting in erroneous mitoses and hence aneuploidy. In fact, aneuploidy and numerical and/or structural centrosome abnormalities are characteristics of many aggressive human cancers (reviewed in Chan, 2011; Nigg, 2006; 2002; Zyss and Gergely, 2008). Yet, a direct genetic proof for a causal relationship between centrosome abnormalities and carcinogenesis is still lacking. By contrast, a direct genetic link

undoubtedly exists in the case of mutations in centrosomal genes that underlie various disorders such as ciliopathies, dwarfisms and microcephalies (Bettencourt-Dias et al., 2011; Nigg and Raff, 2009). Considering this variety of centrosome-related diseases, elucidation of the molecular mechanisms governing centrosomal functions will hopefully not only improve our conceptual knowledge of the centrosome but also contribute to the development of therapies that target centrosome-related disorders.

## **2.2 Structure and function of the centrosome**

Each centrosome comprises a pair of microtubule-based, cylindrical structures, the centrioles (a mother centriole and a daughter centriole), which are embedded in a protein matrix known as the pericentriolar material (PCM) (Figure 1a,b). The PCM contains a large number of high molecular-weight, coiled-coil proteins (Andersen et al., 2003), which are organized in a concentric fashion around the centriole pair (Fu and Glover, 2012; Lawo et al., 2012; Mennella et al., 2012; Sonnen et al., 2012). The centrioles and the PCM are closely linked, as removal of the centrioles results in dispersal of the PCM and, conversely, centriole biogenesis fails in the absence of PCM components (Bobinnec, 1998; Dammermann et al., 2004; Lončarek et al., 2008). In proliferating cells, centrioles are located next to the nucleus and duplicate once per cell cycle (Figure 1b), whereas in quiescent cells, centrioles can associate with the plasma membrane, where the older centriole forms a basal body to enable the formation of a cilium (Figure 1c). In human cells, the centriole barrel is about 450 nm in length, with inner and outer diameters of about 130 nm and 250 nm, respectively (reviewed in Gönczy, 2012). The barrel is composed of microtubule triplets that are arranged in a ninefold radial symmetry. The microtubule triplets consist of the A-, B-, and C-tubules, of which the A- and B-tubules span the entire length of a fully elongated centriole, whereas the C-tubule does not extend to the distal end of the centriole. Differences from this arrangement can be found for example in *Caenorhabditis elegans*, where centriole cylinders consist of nine microtubule singlets (Azimzadeh and Marshall, 2010; Delattre, 2004). In contrast to cytoplasmic microtubules, the centriolar microtubules are highly stable and, consequently, resistant to cold and detergent treatments. Their high stability is provided by posttranslational modifications (polyglutamylation and acetylation) of centriolar tubulin, which protects them from depolymerization (Bobinnec, 1998;

Piperno et al., 1987). The oldest, fully mature centriole of a mammalian cell is distinguished by the presence of distal and subdistal appendages (Graser et al., 2007a; Yoshio Nakagawa, 2001) (Figure 1a). These appendages are formed at the G2/M transition during centriole/centrosome maturation and, in quiescent cells, enable the centriole to dock to the plasma membrane in order to induce ciliogenesis (Tanos et al., 2013). Cilia and flagella are motile or immotile hair-like membrane protrusions, the functions of which range from cellular locomotion, movement of extracellular fluids to chemo- and mechanosensation (reviewed in Goetz and Anderson, 2010; Ishikawa and Marshall, 2011; Kim and Dynlacht, 2013). Interestingly, certain epithelial cells can form hundreds of centrioles near-simultaneously to provide the basal bodies for the formation of multi-ciliated surfaces (reviewed in Nigg and Raff, 2009) (Figure 1c).

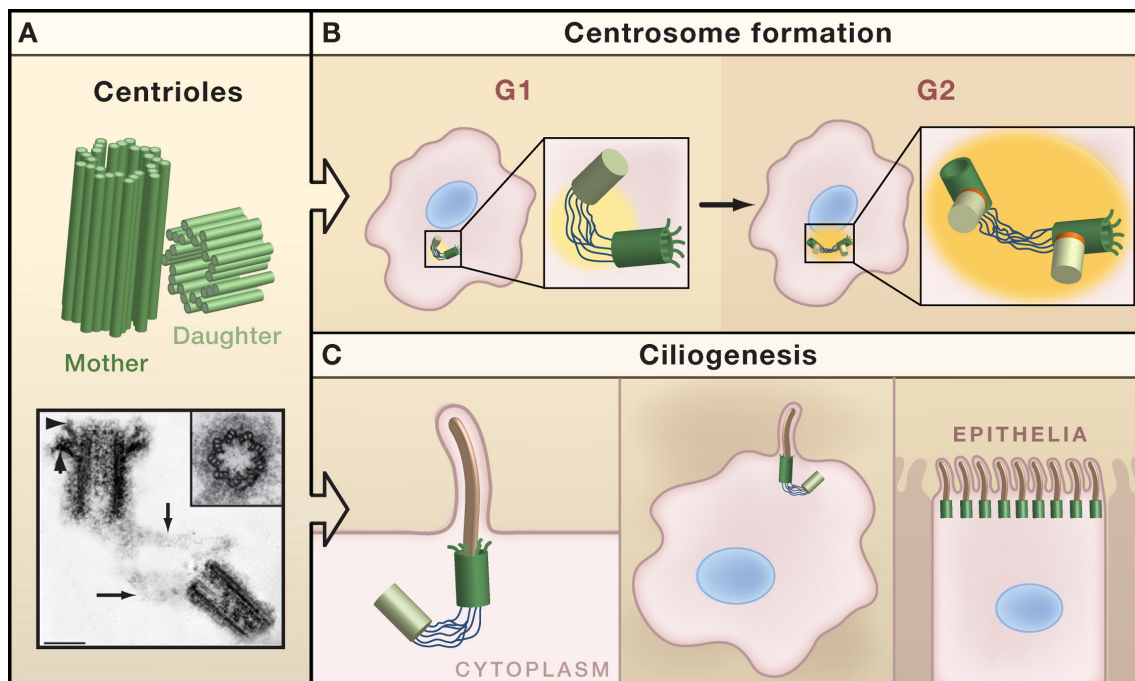


**Figure 1. Centrioles form cilia and centrosomes**

a) Schematic illustration of a centriole pair, consisting of a mother centriole and a daughter centriole (dark and light green, respectively). The EM image shows a centriole pair in G1. The older centriole is distinguished by distal and subdistal appendages (marked by arrowheads). The centrioles are linked by a flexible tether (arrows). Inset: cross-section of a centriole barrel. b) In proliferating cells, the centrioles duplicate in preparation for mitosis. In G1 phase, the single centriole pair organizes smaller amounts of PCM (light yellow) compared to the amount of PCM around duplicated centrioles in G2 (dark yellow). c) In quiescent cells, the older centriole docks to the plasma membrane, where it induces the formation of a cilium (brown). In some epithelial cells, hundreds of centrioles are formed at once to provide the basal bodies for the formation of multiciliated surfaces. (The EM image is courtesy of M. Bornens. Scale bar: 0.2  $\mu\text{m}$ ) (Adapted from Nigg and Raff, 2009)

The primary function of the centrosome in animal cells is to organize the microtubule network in time and space (reviewed in Lüders and Stearns, 2007). This MTOC activity is provided by the PCM-associated  $\gamma$ -tubulin ring complexes ( $\gamma$ -TuRCs), which nucleate and anchor microtubule minus-ends (Moritz et al., 1995). Based on the function as MTOC, the centrosome is involved in diverse microtubule-dependent cellular processes: During interphase, the centrosome contributes to cell shape, polarity, migration and intracellular transport. During mitosis, on the other hand, it plays a central role in mitotic spindle assembly (reviewed in Bettencourt-Dias and Glover, 2007; Bornens, 2012; Gadde and Heald, 2004). Mitotic spindle assembly starts during prophase, when the two centrosomes begin to move to the opposite sides of the cell (Figure 2). Once forming the poles of the mitotic spindle, the centrosomes are involved in the organization of kinetochore-, astral- and interpolar microtubules (reviewed in Meunier and Vernos, 2012). Kinetochore microtubules connect the chromosomes with the spindle poles in order to separate the sister chromatids during anaphase, while the astral microtubules emanate from the centrosomes and associate with the cell cortex to assist in spindle positioning (reviewed in Kotak and Gönczy, 2013). Spindle positioning will define the orientation of the cleavage furrow that forms during cytokinesis (Kaltschmidt et al., 2000). The interpolar microtubules are nucleated from the opposite poles and interact via their plus ends in the region of the spindle midzone, contributing to the orientation of the cleavage furrow (Cao and Wang, 1996). Due to these functions as spindle poles, centrosomes have been ascribed a pivotal role in asymmetric cell divisions, e.g. in the context of the developing brain (Wang et al., 2009; reviewed in Siller and Doe, 2009).

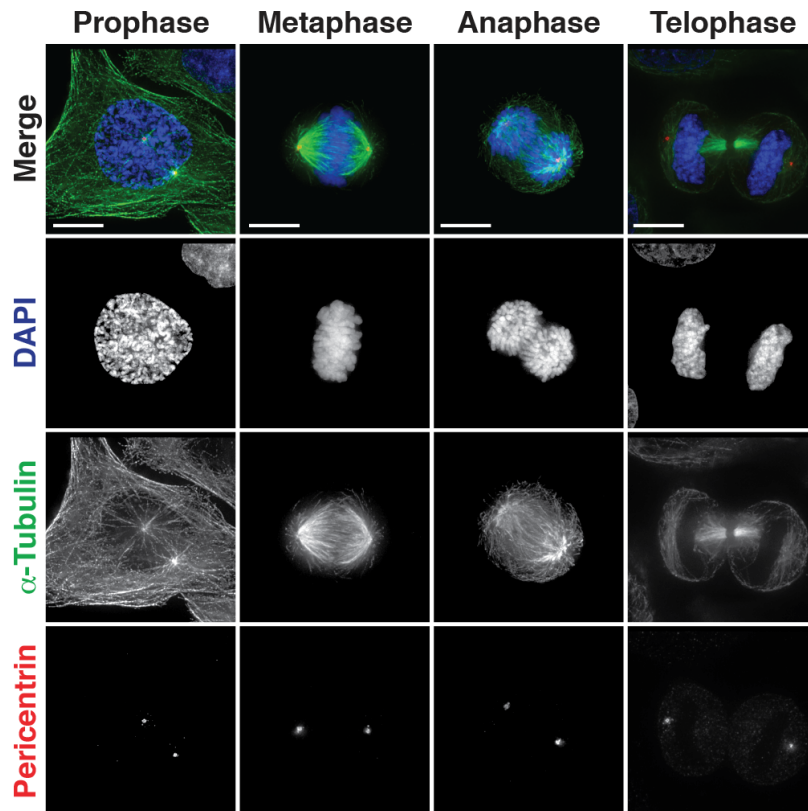


**Figure 2. Centrosomes form the poles of the spindle apparatus during mitosis**

Human HeLa cells were fixed and stained for the indicated proteins to visualize centrosomes during mitosis (from prophase until telophase). Anti-Pericentrin and anti- $\alpha$ -tubulin antibodies were used to mark the centrosomes (red) and microtubules (green), respectively. DNA was stained with the dye DAPI (blue). Scale bars: 10  $\mu$ m. (Images were acquired by 3D-SIM)

In contrast to most eukaryotic cells, where the centrosomes play a critical role in mitotic spindle assembly, some systems exist in which functional bipolar spindles are formed in the absence of centrosomes, e.g. in higher plants (Zhang and Dawe, 2011), female germ cells (Manandhar et al., 2005), and planarians (Azimzadeh et al., 2012). Furthermore, microtubules have been shown to organize acentrosomal spindles *in vitro* around artificial chromosomes in *Xenopus* cell extracts (Heald et al., 1996). Notably, acentrosomal spindles can also be formed in vertebrate somatic cells after removal of centrosomes by microsurgery or laser ablation (Hinchcliffe, 2001; Khodjakov and Rieder, 2001; Khodjakov et al., 2000). However, vertebrate somatic cells lacking centrosomes have been shown to exhibit a high rate of chromosomal instability and prolonged mitotic timing (Sir et al., 2013). In flies, centrosomes appear to be dispensable for most developmental aspects after the first embryonic cell divisions, as *Drosophila DSas-4* mutant embryos lacking centrioles after the first zygotic divisions

can develop into morphologically normal adult flies (Basto et al., 2006; Stevens et al., 2007). But similar to other organisms, flies rely on the presence of centrosomes for correct asymmetric cell divisions, e.g. during neurodevelopment (Basto et al., 2006; Yamashita and Fuller, 2008). The mechanisms underlying spindle formation in the absence of centrosomes include Ran-GTP-dependent, chromatin-directed microtubule assembly, and kinetochore-, CPC-, or Augmin-dependent pathways (reviewed in Duncan and Wakefield, 2011; Kalab and Heald, 2008; Meunier and Vernos, 2012; O'Connell and Khodjakov, 2007; Wadsworth and Khodjakov, 2004).

While in certain cases cells are able to form bipolar spindles despite a lack of centrosomes, the question arises as to whether the opposite situation, i.e., a surplus of centrosomes, interferes with bipolar spindle assembly. Interestingly, cancer cells have been found to divide in a bipolar fashion despite extra copies of centrosomes (reviewed in Acilan and Saunders, 2008; Godinho et al., 2009). The cellular mechanisms permitting these bipolar divisions include centrosome inactivation (Basto et al., 2008) and, predominantly, clustering of supernumerary centrosomes at both poles (Basto et al., 2008; Kwon et al., 2008; Quintyne, 2005; Saunders, 2005; Yang et al., 2008). However, albeit centrosome clustering can result in bipolar cell divisions, the presence of extra centrosomes appears to promote merotelic kinetochore-microtubule attachments (one kinetochore being attached to microtubules emanating from both spindle poles), leading to frequent chromosome missegregations (Ganem et al., 2009; Silkworth et al., 2009). Therefore, cells must nevertheless strictly control centrosome/centriole numbers throughout the entire cell cycle to ensure chromosome stability (see § 2.4).

### **2.3 The centrosome cycle**

In the course of cell cycle progression, centrosomes/centrioles undergo several processes: centriole duplication, centriole elongation, centriole and centrosome maturation, centrosome separation, and centriole disengagement (Elliott Robbins, 1968; Kuriyama and Boris, 1981; Nigg and Raff, 2009; Nigg and Stearns, 2011) (Figure 3). In G1 phase, a somatic cycling cell contains two centrioles. The cell keeps this centriole pair while traversing through G1 or when entering the quiescent state (G0), during which the older centriole forms a basal body to induce ciliogenesis. Once the cell re-

enters the cell cycle from G<sub>0</sub> phase, the cilium is resorbed and the centrioles start to duplicate at the G<sub>1</sub>/S phase transition. Centriole duplication gives rise to two daughter centrioles that are perpendicularly oriented and tightly connected to the proximal end of their respective mother centriole (engaged configuration). The daughter centrioles continue to elongate throughout S and G<sub>2</sub> phase (reviewed in Azimzadeh and Bornens, 2007) (Figure 3). At the G<sub>2</sub>/M transition, the centriole pairs accumulate more PCM during centrosome maturation. This step is governed by the mitotic protein kinases PLK1 (Lane and Nigg, 1996) and Aurora A (Berdnik and Knoblich, 2002), and leads to an overall increase in centrosome size and thus enhanced microtubule nucleation capacity (reviewed in Blagden and Glover, 2003). In parallel, the PLK1-Mst2-Nek2A kinase cascade triggers the removal of the linker proteins C-Nap1 and rootletin, which form the flexible tether between the centriole pairs during interphase (Bahe et al., 2005; Fry, 1998; Mardin et al., 2011; Mayor et al., 2000). Once the tether is removed, the kinesin-related motor Eg5 promotes separation of the two centrosomes, allowing mitotic spindle formation (reviewed in Mardin and Schiebel, 2012). At mitotic exit, mother and daughter centrioles lose their tight connection (engagement) upon centriole disengagement, an event that depends on the activities of the cysteine protease Separase and the kinase PLK1 (Tsou and Stearns, 2006a; 2006b; Tsou et al., 2009).

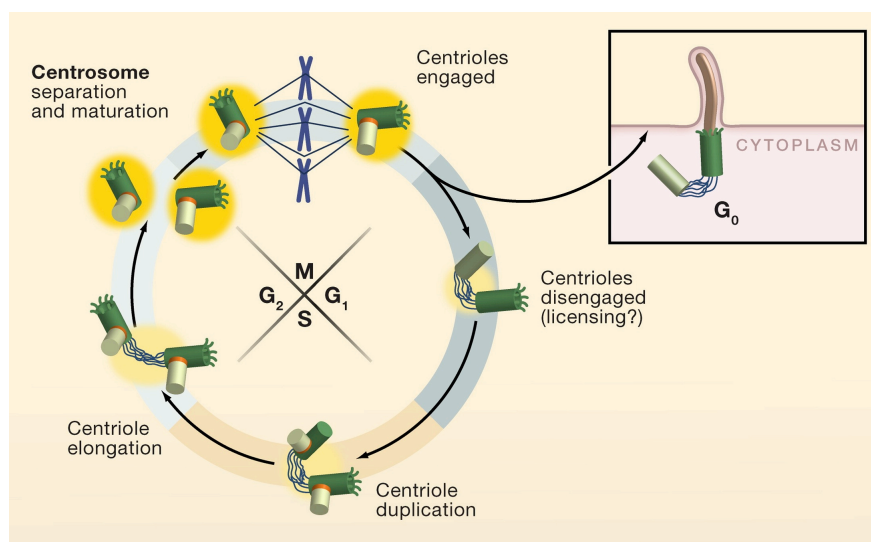


**Figure 3. Schematic illustration of the centrosome cycle**

At the end of mitosis, each daughter cell inherits two centrioles. Cells progress through G<sub>1</sub> phase or become quiescent (G<sub>0</sub>). During the quiescent state, certain cell types form a cilium. In proliferating cells, the centrioles start to duplicate upon entry into S phase. The newly forming daughter centrioles (light green) remain engaged (i.e., tightly connected) with their mother centrioles (dark green) and elongate until G<sub>2</sub>. In preparation for mitosis, the centrioles accumulate more PCM (yellow) and the two

centrosomes separate in order to form the poles of the mitotic spindle. During exit from mitosis, the centrioles disengage (i.e., they lose their tight connection), which prepares them for the next round of duplication. (Adapted from Nigg and Raff, 2009)

## **2.4 Control of centriole duplication in human cells**

### **2.4.1 “Cell cycle control” versus “copy number control”**

Centriole duplication must be tightly controlled in order to maintain constant centriole numbers throughout successive cell division cycles. Two conceptually distinct control mechanisms have been proposed: the “cell cycle control” and the “copy number control”. The “cell cycle control” ensures that centriole duplication occurs “once and only once” per cell cycle, while the “copy number control” warrants that “one and only one” daughter centriole is formed during each round of centriole biogenesis. Breaking either of the two control mechanisms can lead to aberrant centrosome numbers, a common feature of cancer cells (Nigg, 2006; 2007).

The “cell cycle control” ensures temporal coordination of centriole duplication with the cell cycle and prevents initiation of centriole re-duplication once centriole biogenesis has started. The onset of centriole duplication is synchronized with DNA replication as both processes rely on E2F and CDK2 activity and therefore start at the G1/S transition (Matsumoto et al., 1999; Meraldi et al., 1999). A block to centriole re-duplication during S and G2 phases was first demonstrated through cell fusion experiments. These experiments revealed that only disengaged unduplicated G1-centrioles, but not engaged duplicated G2-centrioles, are able to duplicate in an S phase cytoplasm (Wong and Stearns, 2003). Furthermore, experimental removal of an engaged daughter centriole by laser ablation allowed re-duplication of the corresponding mother centriole in the same S-phase (Lončarek et al., 2008). These findings indicate that the presence of an engaged procentriole during S and G2 phases imposes an intrinsic block to re-duplication. This block lasts until mitotic exit, when centriole disengagement licenses the centrioles for duplication in the next S-phase (reviewed in Nigg, 2007; Tsou and Stearns, 2006a). Such a licensing mechanism is highly reminiscent of the licensing known in the context of DNA replication. There, licensing is mediated by loading of the mini chromosome

maintenance (MCM) 2-7 helicases onto replication origins to build the pre-replicative complex (preRC) during late mitosis and G1 (Blow and Dutta, 2005). In contrast to DNA replication, the molecular mechanisms regulating licensing of centriole duplication are only beginning to be elucidated. So far, it has been shown that Separase and PLK1 are necessary for centriole disengagement and thus for licensing of centriole duplication (Tsou and Stearns, 2006b; Tsou et al., 2009). Recently, it has been suggested that the cohesin complex holds centrioles in the engaged configuration and that cleavage of the cohesin ring by Separase is required for centriole disengagement (in analogy to sister chromatid separation) (Schöckel et al., 2011). In addition, Kendrin (Pericentrin) has been identified as a crucial substrate for Separase in the licensing of centriole duplication (Matsuo et al., 2012), and, furthermore, the centrosome cohesion protein CDK5RAP2 (Cep215) has also been implicated in centriole engagement (Barrera et al., 2010; Graser et al., 2007b). As Separase and PLK1 are usually activated only in mitosis, these proteins provide a molecular cue for the synchronization of the centriole duplication cycle with the cell cycle. However, under certain circumstances the centrosome cycle and the nuclear cycle can become uncoupled and cells can undergo repeated rounds of centriole duplication during prolonged interphase, when Separase is inactive (e.g. during DNA damage checkpoint arrest) (Balczon et al., 1995; Dodson et al., 2004; Inanc et al., 2010; Kuriyama et al., 1986; Lončarek et al., 2010; Meraldi et al., 1999).

While the “cell cycle control” guarantees that a new round of centriole duplication can only be initiated after passage through mitosis, the “copy number control” ensures that only one daughter centriole is formed per pre-existing mother centriole. Polo-like kinase 4 (PLK4) has emerged as the key regulator exerting “copy number control”, because PLK4 protein levels directly correlate with procentriole numbers (Bettencourt-Dias et al., 2005; Habedanck et al., 2005). Loss of PLK4 blocks centriole duplication and leads to gradual reduction of centriole numbers throughout successive cell cycles. In contrast, excess PLK4 promotes the near-simultaneous formation of multiple daughter centrioles in a rosette-like arrangement around the mother centriole (Habedanck et al., 2005; Kleylein-Sohn et al., 2007). Likewise, overexpression of the centriole duplication factors STIL or SAS-6 triggers the formation of supernumerary procentrioles in a rosette-like configuration, while depletion of STIL or SAS-6 leads to

gradual loss of centrioles (Arquint et al., 2012; Strnad et al., 2007; Tang et al., 2011; Vulprecht et al., 2012). How PLK4 cooperates with STIL and SAS-6 to exert “copy number control” is still intensely investigated.

#### **2.4.2 Canonical versus *de novo* centriole formation**

Centrioles are usually formed via the canonical, semi-conservative manner, whereby the newly forming procentriole grows perpendicularly to its parental centriole and remains closely connected to it (i.e., engaged) until late mitosis. However, centrioles can also be formed *de novo* when no pre-existing centrioles are present. For example, in some epithelial cells, generation of hundreds of centrioles *de novo* precedes the formation of multiciliated surfaces. In this case, the centrioles grow around cytoplasmic protein assemblies, known as deuterosomes, and eventually form the basal bodies during ciliogenesis (Sorokin, 1968). This massive centriole amplification in multiciliated cells has been reported to rely on the deuterosomal proteins Deup1 and Ccdc78 (Klos Dehring et al., 2013; Zhao et al., 2013). Recently, deuterosomes have been shown to be formed at the proximal part of the younger centriole (at the same site where a procentriole is assembled), and shown to be released from there into the cytoplasm (Jord et al., 2014). Besides multiciliated cells, the mouse zygote provides another example for *de novo* centriole formation. In contrast to most mammalian zygotes, which contain sperm-derived centrioles, the first embryonic divisions in mouse zygotes occur in the absence of centrosomes, until the cells reach the blastomere stage. At this stage, centrioles are generated *de novo*, and from then on are propagated via the canonical pathway (Szollosi et al., 1972). Furthermore, in *Drosophila* and *Xenopus* oocytes, *de novo* centriole formation can be triggered by overexpression of PLK4 (Eckerdt et al., 2011; Peel et al., 2007; Rodrigues-Martins et al., 2007). *De novo* centriole formation has also been reported to occur in cycling somatic vertebrate cells after artificial removal of centrioles (Khodjakov et al., 2002; La Terra, 2005; Uetake et al., 2007). Removal of pre-existing centrioles in vertebrate cells is necessary as *de novo* formation is suppressed as long as one centriole is present (La Terra, 2005). Both modes of centriole formation, *de novo* and canonical, depend on a set of key centriole duplication proteins (see § 2.5) and thus represent variations of a similar mechanism (rather than two distinct pathways) (Jord et al., 2014; Peel et al., 2007).

## 2.5 Molecular mechanism of centriole biogenesis

Pioneering studies in *C. elegans* revealed a set of five core proteins required for centriole biogenesis: ZYG-1 (PLK4 in humans), SPD-2 (Cep192 in humans), SAS-6, SAS-5 (STIL in humans), and SAS-4 (CPAP in humans) (Dammermann et al., 2008; Delattre et al., 2004; Kemp et al., 2004; Kirkham et al., 2003; Leidel and Gönczy, 2003; 2005; Leidel et al., 2005; O'Connell et al., 2001; Pelletier et al., 2004). These proteins have been shown to act in a sequential order to promote procentriole assembly in *C. elegans* embryos (Delattre et al., 2006; Pelletier et al., 2006). First, shortly after fertilization of the oocyte, SPD-2 is recruited to the sperm-derived centriole. Next, SPD-2 triggers the recruitment of the kinase ZYG-1, which in turn recruits the SAS-5/SAS-6 complex. SAS-5 and SAS-6 promote the formation and elongation of the central tube (counterpart of the cartwheel structure, see § 2.5.1). In addition, SAS-5 and SAS-6 are required for centriolar recruitment of SAS-4. SAS-4 finally facilitates the deposition of centriolar microtubules onto the central tube, a process that also requires  $\gamma$ -tubulin (reviewed in Bettencourt-Dias and Glover, 2007) (Figure 4).

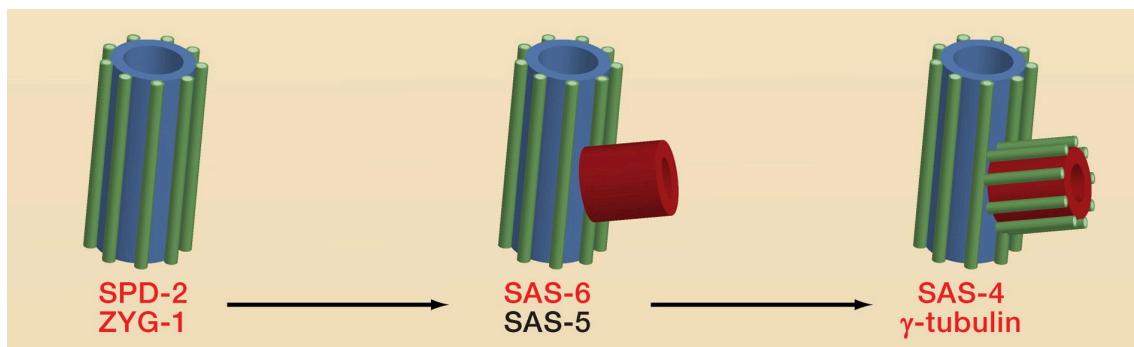


**Figure 4. Illustration of centriole duplication in *C. elegans***

SPD-2 recruits the protein kinase ZYG-1 to the mother centriole, which in turn recruits a complex of SAS-6 and SAS-5 that promotes the formation of a central tube (red) at the proximal end of the mother centriole. SAS-6 and SAS-5 recruit SAS-4, which facilitates the deposition of centriolar microtubules (green) onto the central tube;  $\gamma$ -tubulin is also required at this stage. (Adapted from Nigg and Raff, 2009)

In human cells, procentriole assembly follows a very similar pathway as in *C. elegans*. Upon discovery of PLK4 as a master regulator of centriole duplication (Bettencourt-Dias et al., 2005; Habedanck et al., 2005), key steps of the human centriole assembly pathway have been uncovered (Kleylein-Sohn et al., 2007). Similar to the *C. elegans*

counterpart ZYG-1, human PLK4 acts upstream in the pathway and promotes sequential recruitment of further components to the procentriole assembly site. After SAS-6 recruitment, CPAP (*C. elegans* SAS-4) and Cep135 localize to the procentriole, followed by the recruitment of  $\gamma$ -tubulin, which most likely is responsible for the nucleation of centriolar microtubules. Elongation of nascent centrioles is thought to occur via insertion of tubulin subunits underneath a “cap” formed by CP110, which marks the distal tips of both mother and daughter centrioles. Interestingly, CP110 and CPAP antagonize each other in centriole length control, as overexpression of CPAP gives rise to extra long centrioles and simultaneous overexpression of CP110 blocks this effect, and, accordingly, depletion of CP110 phenocopies CPAP overexpression (Kohlmaier et al., 2009; Schmidt et al., 2009; Tang et al., 2009).

As outlined above, the recruitment of ZYG-1 to centrioles in *C. elegans* depends on the protein SPD-2 (Delattre et al., 2006; Pelletier et al., 2006). At the beginning of this study it was unknown how human PLK4 is recruited to centrioles and whether Cep192, the human counterpart of *C. elegans* SPD-2 (Pelletier et al., 2004), plays a role in this process. In *Drosophila*, the corresponding protein D-SPD-2 plays no apparent role in PLK4 recruitment (Dix and Raff, 2007; Giansanti et al., 2008). Instead, PLK4 recruitment in flies depends on Asterless (Dzhindzhev et al., 2010), which has been reported to be the ortholog of the vertebrate protein Cep152 (Blachon et al., 2008). Similar to Asterless, human Cep152 is important for centriole duplication and directly binds the PB1-PB2 domain of PLK4 via its N-terminal region (residues 1-217) (for PLK4 domain organization see § 2.5.4) (Cizmecioglu et al., 2010; Dzhindzhev et al., 2010; Hatch et al., 2010). However, it had remained unclear to what extent human Cep152 might contribute to PLK4 recruitment. On the one hand, it was reported that depletion of Cep152 had no effect on PLK4 centriolar recruitment (Cizmecioglu et al., 2010; Dzhindzhev et al., 2010; Hatch et al., 2010), on the other hand, one study showed that Cep152 is necessary for centrosomal localization of newly synthesized PLK4 (Cizmecioglu et al., 2010). During the course of this study, human Cep152 was found to cooperate with Cep192 in PLK4 recruitment (Kim et al., 2013; Sonnen et al., 2013), clarifying the earlier, controversial reports on the roles of Cep152 and Cep192 in centriole duplication (Cizmecioglu et al., 2010; Gomez-Ferreria et al., 2007; Hatch et al., 2010; Zhu et al., 2008).

### 2.5.1 SAS-6 dictates the assembly of the cartwheel structure

The early phase of procentriole formation involves the formation of the cartwheel structure (which corresponds to the central tube found in *C. elegans*) (reviewed in Hirono, 2014). The cartwheel serves as a scaffold for the assembly of the centriolar microtubules and thus is crucial for conveying the characteristic ninefold radial symmetry to the centriole (Hirono, 2014; Winey and O'Toole, 2014). The overall architecture of the cartwheel has been best studied by electron microscopy in unicellular organisms, such as *Chlamydomonas reinhardtii* (Figure 5a,b). The cartwheel consists of nine spokes that emanate from a central hub and are connected to the sets of triplet microtubules (A-C) via pinhead structures. In human cells, the cartwheel is located at the proximal end of daughter centrioles (Figure 5c,d) and is thought to be assembled and disassembled in every cell cycle (reviewed in Gönczy, 2012). Recent cryo-electron tomography analysis of the *Trichonympha* centriole proximal region has provided a remarkable 3D map of the detailed cartwheel organization (Guichard et al., 2013) (Figure 5e).

On the molecular level, the ninefold symmetry of the cartwheel is imparted by the key centriole duplication factor SAS-6 (Nakazawa et al., 2007), which has been shown to self-assemble *in vitro* into structures that closely resemble the central part of the cartwheel (Guichard et al., 2013; Kitagawa et al., 2011; van Breugel et al., 2011; 2014). Interestingly, *C. elegans* SAS-6 has been shown to self-assemble into a distinct, spiral arrangement, possibly explaining the presence of a central tube instead of a cartwheel in this species (Hilbert et al., 2013). The organization of human SAS-6 molecules into cartwheel-like structures has recently been proposed to be templated by the proximal lumen of mother centrioles (Fong et al., 2014).

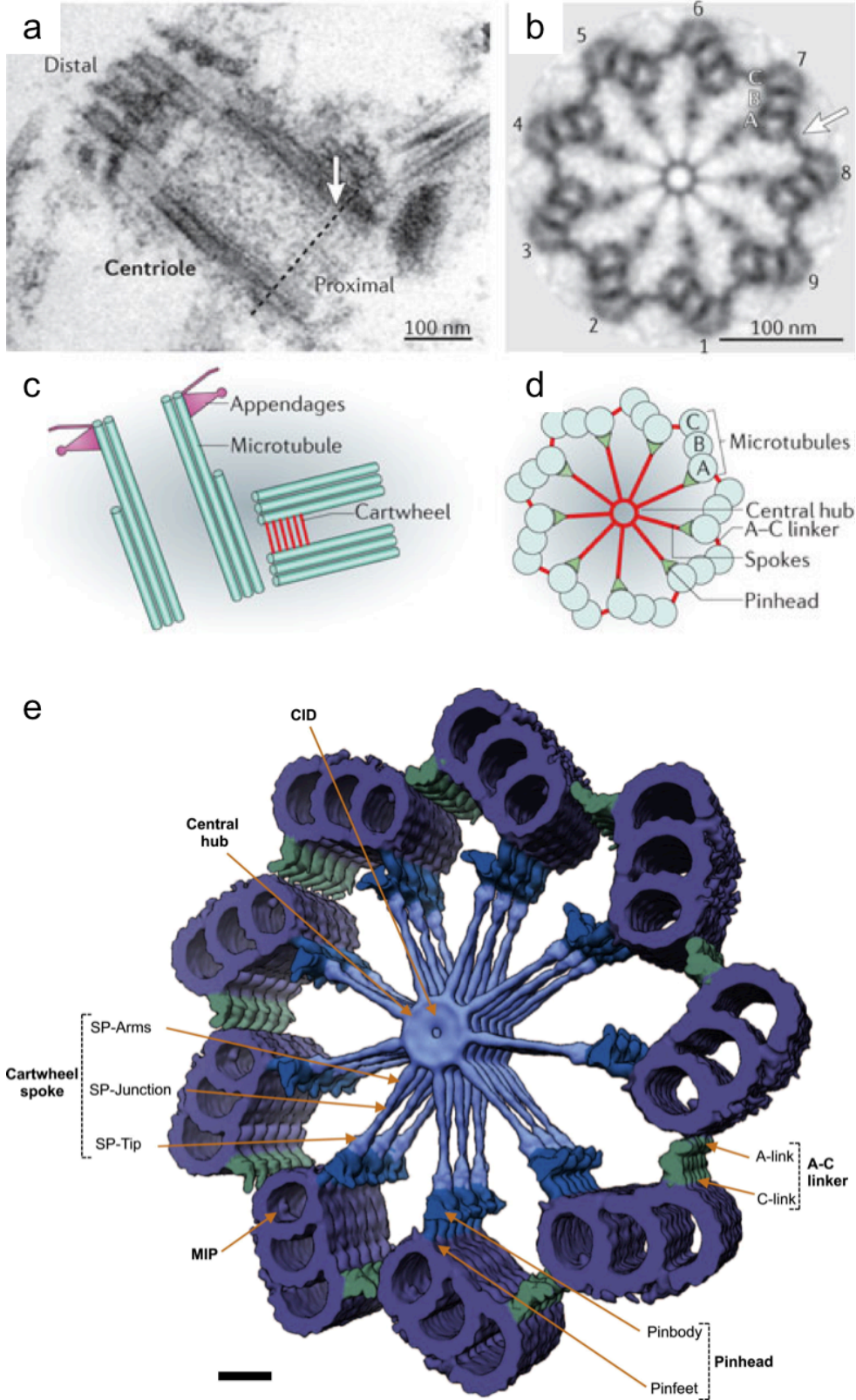


**Figure 5. Cartwheel architecture**

a-b) Electron microscopy images of resin-embedded samples of *Chlamydomonas reinhardtii*. a) Side view of a centriole, with the cartwheel (arrow) at its proximal end. b) Cross-section of the proximal part of a centriole, displaying the characteristic ninefold symmetry of the cartwheel structure. c) Schematic illustration of a mother and daughter centriole pair in a human cell. The cartwheel is located at the

proximal end of the daughter centriole (which bears no appendages). d) Illustration of the cartwheel structure. The cartwheel consists of nine spokes that emanate from a central hub and are connected to the microtubule triplets (A-C) via pinhead structures. The A and C microtubules are connected via the A-C linkers. e) Cryo-electron tomography 3D map illustrating the cartwheel structure of a *Trichonympha* centriole. Scale bar: 20 nm. a-d) Adapted from Gönczy, 2012 (images in a and b are courtesy of P. Guichard). e) Adapted from Guichard et al., 2013.

## 2.5.2 STIL

The human *STIL* gene (or *SIL*; *SCL/TAL1* interrupting locus) was first described in the context of a chromosomal rearrangement that causes T-cell acute lymphoblastic leukemia (Aplan et al., 1991; 1990), and later shown to be pivotal for vertebrate embryonic development (Izraeli et al., 1999; Pfaff et al., 2007). Recently, *STIL* has emerged as the proposed human counterpart of *C. elegans* SAS-5, which in *Drosophila*, on the other hand, is referred to as Ana2 (Arquint et al., 2012; Stevens et al., 2010a; Tang et al., 2011). Like *PLK4* and *SAS-6*, *STIL* is a key centriole duplication factor involved in the “copy number control” (see § 2.4.1), as overexpression of *STIL* leads to the formation of extra copies of centrioles, whereas depletion of *STIL* blocks centriole assembly, resulting in a progressive loss of centrioles (Arquint et al., 2012; Tang et al., 2011; Vulprecht et al., 2012). *STIL* displays a strikingly similar localization pattern compared to *SAS-6*, raising the intriguing possibility that *STIL* might cooperate with *SAS-6* in cartwheel assembly. Both *STIL* and *SAS-6* are recruited to the centrosome at the onset of procentriole assembly and colocalize at the cartwheel region of daughter centrioles. The centriolar levels of both proteins increase towards mitosis, until both *STIL* and *SAS-6* are lost from centrioles during mitotic progression (Arquint and Nigg, 2014; Arquint et al., 2012; Strnad et al., 2007; Tang et al., 2011). Interestingly, in *Drosophila*, Ana2 forms a complex with *SAS-6*, and ectopic expression of both proteins leads to the formation of cartwheel-like tubules (Stevens et al., 2010a; 2010b). In *C. elegans*, SAS-5 and *SAS-6* also form a complex and, furthermore, strictly depend on each other for their centrosomal localization (Leidel et al., 2005). In human cells, *STIL* and *SAS-6* have been shown to largely depend on each other for efficient and robust centriolar association; however, at the beginning of this study, no direct interaction between these two proteins had been demonstrated (Arquint et al., 2012; Tang et al., 2011; Vulprecht et al., 2012). Also, a possible interaction between *STIL* and *PLK4* had not been reported.

STIL is roughly three times larger than *C. elegans* SAS-5 or *Drosophila* Ana2, and sequence similarity is restricted to two short motifs: the coiled-coil motif (STIL-CC), encompassing residues 720-751, and the STIL/Ana2 (STAN) motif, spanning residues 1061-1147 (Stevens et al., 2010a) (Figure 6). The STAN motif had previously been shown to be important for centriole duplication (Vulprecht et al., 2012). However, the function of the STIL-CC motif was unknown at the beginning of this study.

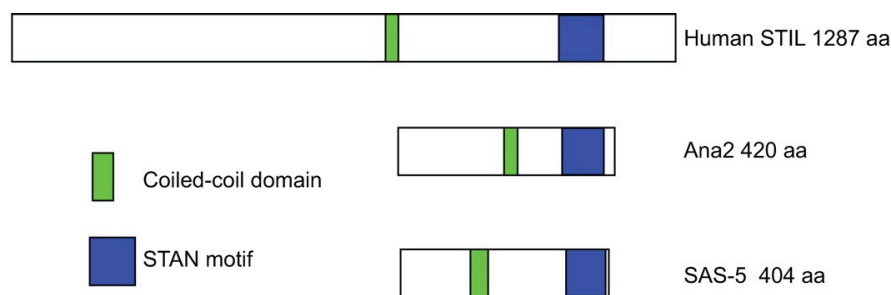


**Figure 6. Schematic representation of human STIL in comparison with *Drosophila* Ana2 and *C. elegans* SAS-5**

The three amino acid sequences share a short coiled-coil domain (green) and the STIL/Ana2 (STAN) motif (blue). In human STIL, the coiled-coil domain (STIL-CC) spans residues 720-751, and the STAN motif covers amino acids 1061-1147. (Adapted from Stevens et al., 2010a)

### 2.5.3 Cep192

Human Cep192 has been reported to be the homolog of *C. elegans* SPD-2 (Pelletier et al., 2004). Initially, *C. elegans* SPD-2 was identified in a genetic screen for conditional cell division mutants and reported to be involved in mitotic spindle assembly (O'Connell et al., 1998). Further analysis revealed that SPD-2 is a coiled-coil protein that is associated with centrioles during interphase and spreads into the PCM during mitosis, mirroring its dual role in procentriole formation and PCM recruitment (Kemp et al., 2004; Pelletier et al., 2004). In the centriole duplication pathway, SPD-2 acts most upstream, as it is responsible for the centriolar recruitment of the kinase ZYG-1 (Delattre et al., 2006; Pelletier et al., 2006). Similar to *C. elegans* SPD-2, Cep192 localizes to centrosomes throughout the entire cell cycle. At the G2/M transition, Cep192 accumulates in a PLK1-dependent manner to promote centrosome maturation

(Haren et al., 2009; Santamaria et al., 2010). Herein, it recruits the PCM components Nedd1/GCP-WD and  $\gamma$ -tubulin, and facilitates Aurora A centrosomal localization and activation; consequently, depletion of Cep192 impairs mitotic spindle formation (Gomez-Ferreria et al., 2007; Joukov et al., 2010; Zhu et al., 2008). In contrast to the established functions in centrosome maturation and spindle assembly, contradicting data have been reported on Cep192's role in centriole duplication: While Zhu and colleagues (2008) have claimed that Cep192 is required for centriole duplication, Gomez-Ferreira and co-workers (2007) have reported that Cep192 is dispensable for this process. A role for Cep192 in PLK4 recruitment (in analogy to *C. elegans* SPD-2) had not been explored at the beginning of this study. In *Drosophila*, the corresponding protein D-SPD-2 plays no apparent role in PLK4 recruitment or centriole duplication; there, D-SPD-2 primarily functions in PCM recruitment (Dix and Raff, 2007; Giansanti et al., 2008).

#### **2.5.4 Polo-like kinase 4 (PLK4)**

PLK4 belongs to the PLK family, which in vertebrates comprises the four members PLK1-4. PLK family members regulate key cell cycle events, such as mitotic entry, the metaphase-to-anaphase transition, mitotic exit, cytokinesis, the DNA damage response, and, in the case of PLK4, centriole duplication (reviewed in Archambault and Glover, 2009; Barr et al., 2004; Zitouni et al., 2014). All members are characterized by an N-terminal Ser/Thr-kinase domain and a C-terminal region comprising two or three Polo-box (PB) folds (reviewed in Archambault and Glover, 2009; Lowery et al., 2005). Among the PLK members, PLK1 is the best characterized: In its C-terminal region it contains two PBs, PB1 and PB2, which form an intramolecular heterodimer that is referred to as the Polo-box domain (PBD). The PBD controls substrate recognition and subcellular localization through binding to target proteins, generally in a phosphorylation-dependent manner (Cheng et al., 2003; Elia et al., 2003a; 2003b). Specifically, the PBD usually interacts with target proteins via a consensus motif after its phosphorylation ("priming") on the Ser/Thr sites (Ser-[pSer/pThr]-[Pro/X]) (Elia et al., 2003a). As an exception to this binding mode, *Drosophila* Map205 has been found to interact with the PBD in a distinct, phosphorylation-independent manner (Archambault et al., 2008).

PLK4 is distinguished from the other PLK family members by the presence of three, rather than two, PBs within its C-terminal part (PB1-PB3). The central conserved region lying upstream of the third PB had initially been referred to as the “cryptic polo box” (CPB) (Swallow et al., 2005), until structural analysis based on *Drosophila* PLK4 unveiled the presence of two tandem polo boxes, PB1 and PB2 (Slevin et al., 2012). Both PB1 and PB2 exhibit a canonical PB architecture, which consists of a six-stranded antiparallel  $\beta$ -sheet and a C-terminal  $\alpha$ -helix that runs diagonally to the  $\beta$ -strands, similar to the arrangement of the PB folds in PLK1 (Cheng et al., 2003; Elia et al., 2003b; Slevin et al., 2012) (Figure 7). In contrast to the PBD of PLK1, however, the PB1-PB2 domain of PLK4 binds its target proteins in a phosphorylation-independent manner and forms an intermolecular homodimer (Slevin et al., 2012). Importantly, PB1-PB2 homodimerization leads to PLK4 autophosphorylation in *trans*, resulting in phosphorylation of the DSG motif, hence causing capture by the E3 ubiquitin ligase SCF- $\beta$ TrCP and consequent proteasomal degradation (Cunha-Ferreira et al., 2013; 2009; Guderian et al., 2010; Holland et al., 2010a; 2010b; Klebba et al., 2013; Rogers et al., 2009). In addition to mediating PLK4 dimerization, the PB1-PB2 domain is crucial for the centrosomal localization of PLK4 and allows binding to centrosomal protein(s), such as Cep152/Asterless (Cizmecioglu et al., 2010; Dzhinzhev et al., 2010; Habedanck et al., 2005; Hatch et al., 2010; Slevin et al., 2012).

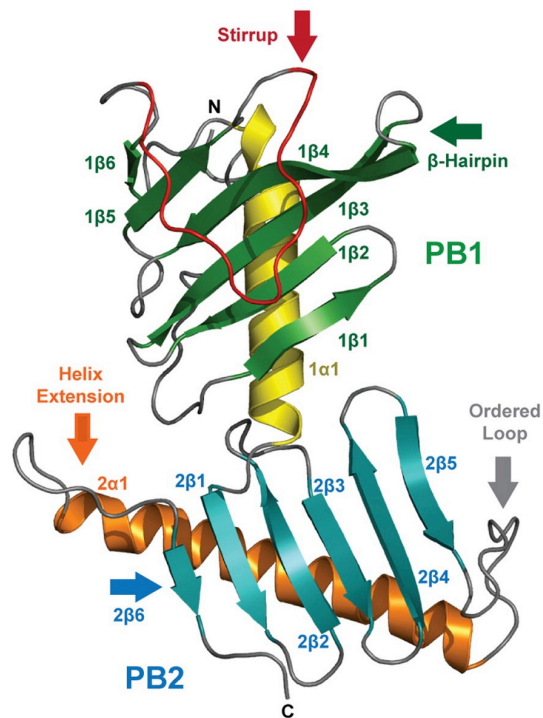


**Figure 7. Structure of the PB1-PB2 protomer of *Drosophila* PLK4**

Structure of the *Drosophila* PLK4 PB1-PB2 domain (one protomer of the PB1-PB2 homodimer is shown). Both PB1 and PB2 adopt a canonical PB fold, which is characterized by an N-terminal, six-stranded antiparallel  $\beta$ -sheet ( $\beta$ 1– $\beta$ 6) and a C-terminal  $\alpha$ -helix. (PB1:  $\beta$ -strands are shown in green,  $\alpha$ -helix is depicted in yellow; PB2:  $\beta$ -strands are shown in blue,  $\alpha$ -helix is represented in orange.) (Adapted from Slevin et al., 2012)

In contrast to PB1 and PB2 of PLK4, no interaction partner has been described for PB3. Furthermore, PB3 displays rather weak centrosome targeting activity (Leung et al., 2002; Slevin et al., 2012), and a construct of human PLK4 lacking PB3 (residues 1-888) has been shown to maintain the ability to drive centriole amplification upon overexpression in cells, suggesting that PB3 might be dispensable for PLK4 functionality (however, the endogenous pool of PLK4 might have provided functionality in those experiments) (Habadanck et al., 2005). Notably, crystal-structure analysis of murine PB3 has revealed an intermolecular, domain-swapped homodimer, in which four  $\beta$ -strands ( $\beta$ 6,  $\beta$ 1,  $\beta$ 2, and  $\beta$ 3) from one monomer form a continuous antiparallel  $\beta$ -sheet with two  $\beta$ -strands ( $\beta$ 4 and  $\beta$ 5) from the other monomer (Leung et al., 2002) (Figure 8).

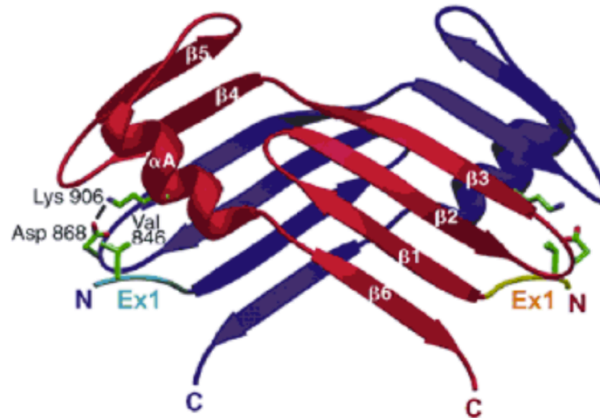


**Figure 8. Structure of homodimeric murine PB3**

Structure of a murine PB3 homodimer. Note the domain-swapped conformation, in which the  $\beta$ -strands  $\beta_6$ ,  $\beta_1$ ,  $\beta_2$ , and  $\beta_3$  from one monomer form a continuous antiparallel  $\beta$ -sheet with the strands  $\beta_4$  and  $\beta_5$  from the other monomer. (Adapted from Leung et al., 2002)

Human PLK4 contains 970 amino acid residues (Figure 9). The residues 1-265 encode the catalytic domain, which is followed by the linker region L1 that extends up to residue 586, where the PB1-encoding sequence starts. PB2 is closely connected to PB1, whereas PB3 is separated from PB2 via the linker L2 (residues 814-887). The DSG motif, which mediates the interaction with the E3 ubiquitin ligase SCF- $\beta$ TrCP, is located just downstream of the kinase domain (residues 284-289).

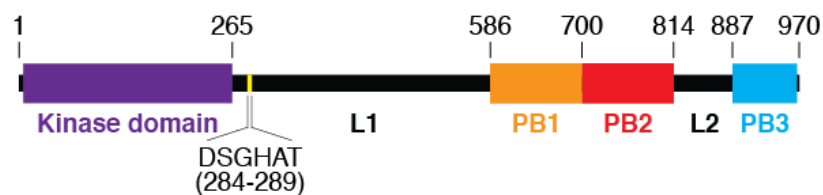


**Figure 9. Scheme of PLK4 domain organization**

PLK4 comprises an N-terminal Ser/Thr-kinase domain (amino acids 1-265) and three C-terminal Polo-boxes (PB1-PB3, spanning amino acids 586-970). The DSG motif (residues 284-289) is located within the linker L1 region, just downstream of the kinase domain. PB3 is separated from PB2 via the linker L2. Scheme is drawn to scale. (Amino acid numbering based on Slevin et al., 2012)

### 3 AIM OF THIS PROJECT

PLK4, the key regulator of centriole duplication, comprises an N-terminal Ser/Thr kinase domain and three C-terminal PBs, PB1-PB3. The PB1-PB2 domain has been shown to bind to Cep152 (Cizmecioglu et al., 2010; Dzhindzhev et al., 2010; Hatch et al., 2010), and, recently, the detailed PB1-PB2 architecture has been unveiled via crystallography (Slevin et al., 2012). A crystal structure has also been presented for PB3 (Leung et al., 2002). However, it has remained unclear whether the reported domain-swapped dimer of murine PB3 represents the conformation adopted in *in vivo* interactions as, so far, no binding partners of PB3 have been described. Here, we set out to identify novel binding partners of PLK4 PB1-PB3. In the first part of this study we characterize the PB1-PB2 binding partner Cep192, and in the second part we explore the interaction between PB3 and STIL. Based on a collaboration for crystallography and NMR analysis, we examine the novel PB3 binding mode in detail and compare the conformation of human PB3 with the previously reported structure of the murine counterpart (Leung et al., 2002).

## 4 RESULTS

### 4.1 Identification of PLK4-interacting proteins

To investigate PLK4 function, we generated a set of U2OS Flp-In T-REx cell lines for the inducible expression of full-length PLK4 or fragments encompassing either the N-terminal catalytic domain and the linker region L1 (residues 1-570) or C-terminal pieces comprising PB1-PB3 (570-970), PB1-PB2 (570-820) or L2-PB3 (814-970) (Figure 10). All constructs were N-terminally fused to an S-peptide-EGFP tag to enable analysis of the subcellular localization by fluorescence microscopy (via EGFP detection) in parallel to affinity purification experiments coupled to mass spectrometry (via S-peptide pulldowns). To test the subcellular localization of the PLK4 constructs, we induced transgene expression for 24 hours and scored colocalization with the centrosome as strong, weak, or not detectable (Figure 10). The two C-terminal fragments encompassing PB1-PB3 (570-970) and PB1-PB2 (570-820) displayed robust centrosome localization, similar to full-length PLK4. However, PB3 alone (814-970, including L2) showed rather weak centrosomal localization, and the N-terminal PLK4 fragment (1-570) was completely absent from centrosomes (Figure 10). These observations indicate that the PB1-PB2 domain of PLK4 is crucial for PLK4 centrosomal targeting, confirming previous data (Habedanck et al., 2005; Leung et al., 2002; Slevin et al., 2012).

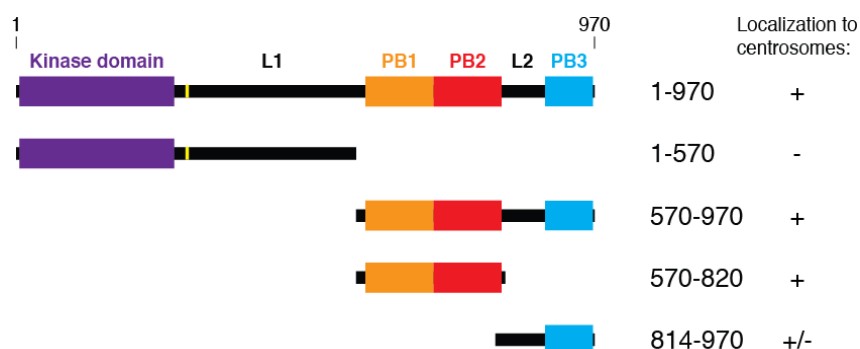


**Figure 10. Illustration of PLK4 constructs used to generate U2OS Flp-In T-REx cell lines**

The schemes illustrate the constructs of full-length PLK4 or fragments containing either the N-terminal kinase domain and linker L1 (residues 1-570) or C-terminal parts comprising PB1-PB3 (570-970), PB1-PB2 (570-820) or L2-PB3 (814-970) (all N-terminally fused to an S-peptide-EGFP tag). The efficiency of centrosomal localization (as determined via EGFP fluorescence microscopy) is indicated on the right (+, strong; +/-, weak; -, not detectable).

Although the C-terminus of PLK4 had clearly emerged to be crucial for PLK4 localization to centrosomes (Habedanck et al., 2005; Slevin et al., 2012) (Figure 10), the identity of the corresponding centrosomal docking proteins had remained elusive. To identify centrosomal binding partners of the PLK4 C-terminus, we performed an affinity purification experiment coupled to mass spectrometry. We induced expression of the C-terminal PLK4 fragment comprising PB1-PB3 (residues 570-970) in the corresponding transgenic U2OS cell line. After transgene expression for 24 hours, we subjected the cell extracts to S-peptide pulldowns and analyzed the co-purifying proteins via mass spectrometry. As control cell lines we used the parental U2OS cell line and the cell line expressing the N-terminal half of PLK4 (residues 1-570). Using this approach, we identified a set of centrosomal proteins that were brought down specifically with PLK4 PB1-PB3. Among these proteins were Cep152 and Cep192 (sixteen and four identified peptides, respectively), the key centriole duplication factor STIL (one peptide identified) (Arquint et al., 2012), the Nuclear distribution protein nudE homolog 1 (NDE1) (6 peptides), Cep63 (4 peptides), and Aurora kinase A (2 peptides) (Table 1).

**Table 1.** List of proteins that co-purified with the C-terminal PLK4 fragment encompassing PB1-PB3 (residues 570-970), which was isolated via an S-peptide pulldown from a U2OS Flp-In T-REx cell line. The long and short names of the proteins are indicated as well as the numbers of peptides that were identified via mass spectrometry.

Protein Full Name	Short Name	# of Peptides
Centrosomal protein of 152 kDa	CEP152	16
Nuclear distribution protein nudE homolog 1	NDE1	6
Centrosomal protein of 192 kDa	CEP192	4
Centrosomal protein of 63 kDa	CEP63	4
Aurora kinase A	AURKA	2
SCL-interrupting locus protein	STIL	1

Of these six proteins that co-purified with the C-terminal PLK4 fragment, Cep152 was already known to bind to PLK4's PB1-PB2 domain and to be essential for centriole duplication (Cizmecioglu et al., 2010; Dzhindzhev et al., 2010; Hatch et al., 2010). Furthermore, at the beginning of this study, Cep63 had been shown to form a complex

with Cep152 (Sir et al., 2011) and thus was detected here in the pulldown probably due to its interaction with Cep152. Likewise, Aurora A possibly co-purified in an indirect manner through interacting with Cep192 (Joukov et al., 2010). In the case of NDE1, no interaction with PLK4 had previously been described. Because NDE1 is a centrosomal protein and mutations in NDE1 have been associated with microcephaly (Alkuraya et al., 2011; Bakircioglu et al., 2011; Feng and Walsh, 2004), it will be interesting to see if future experiments will unveil a direct physical and/or functional interaction between NDE1 and PLK4. In the present study, we chose to focus on the interactions of PLK4 with Cep192 and STIL (§ 4.2-4.3).

## 4.2 On the PLK4/Cep192 interaction

### 4.2.1 The Cep192 N-terminus (1-330) binds to the PB1-PB2 domain of PLK4

Earlier studies on human Cep192 had generally focused on the short isoform (Gomez-Ferreria et al., 2007; 2012). However, data from our laboratory revealed that the predominantly expressed isoform of Cep192 (predicted molecular weight of 279 kDa) harbors an N-terminal extension that is essential for mediating the interaction with PLK4 (amino acids 1–519) (Sonnen et al., 2013). To characterize the PLK4/Cep192 interaction in more detail, we performed co-immunoprecipitation experiments to determine the minimal protein regions that are required for the binding. In order to map the region in PLK4, we expressed GFP-tagged PLK4 full-length or truncated versions together with FLAG-tagged N-terminal Cep192 (residues 1-330) in HEK293T cells and subjected the cell extracts to GFP-immunoprecipitations (Figure 11a,b). We found that the PLK4 PB1-PB2 domain (residues 570-820) is required for the interaction, whereas the individual PB1 or PB2 domains (residues 570-708 and 677-820, respectively) are not sufficient. The third Polo-box PB3, including L2 (construct spanning residues 814-970), and the N-terminus of PLK4 (residues 1-570) did not bring down Cep192 (1-330). Similar results were obtained in another co-immunoprecipitation experiment using beads coated with anti-FLAG antibodies to pull down Cep192 (1-330) and Cep152 (1-220) fragments, which had been co-expressed with the different GFP-tagged PLK4 constructs (Figure 11a,c). Detection via immunoblotting clearly revealed that PLK4 PB1-PB2 co-purified with N-terminal Cep192 (1-330) as well as with the previously known binding partner Cep152 (1-220) (Cizmecioglu et al., 2010; Dzhindzhev et al., 2010; Hatch et al., 2010).

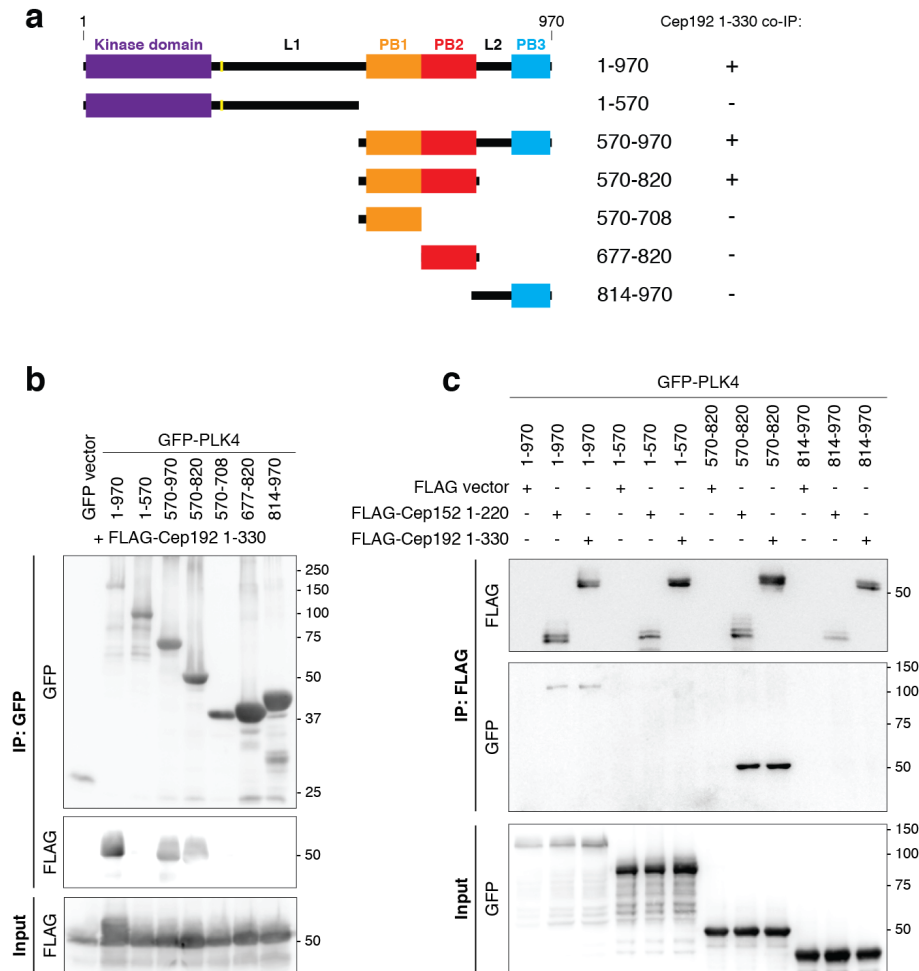


**Figure 11. The Cep192 N-terminus (residues 1-330) binds to the PB1-PB2 domain of PLK4**

a) Schemes of PLK4 constructs used for the co-immunoprecipitations to map the Cep192-binding domain of PLK4. On the right, the ability of the constructs to interact with Cep192 (1-330) is indicated (+, interaction detected; -, no interaction detected). b-c) HEK293T cells were co-transfected with the indicated plasmids and cell extracts were subjected to anti-GFP (b) or anti-FLAG (c) co-immunoprecipitations followed by immunoblotting with the indicated antibodies.

To precisely determine the PLK4-binding region within the N-terminal part of Cep192 (residues 1-330), we next co-transfected HEK293T cells with plasmids coding for Myc-PLK4 and GFP-tagged pieces of the N-terminal Cep192 fragment. Upon cell lysis, we subjected the cell extracts to an anti-GFP co-immunoprecipitation experiment and analyzed the results via Western blotting using GFP- and Myc antibodies. We found that the N-terminal Cep192 region spanning amino acids 190-240 is necessary and sufficient for the binding to PLK4 (Figure 12a). In the case of Cep152, a similar anti-GFP co-immunoprecipitation experiment followed by Western blot analysis revealed that the N-terminal Cep152 fragment containing residues 1-46 is necessary and

sufficient for the interaction with PLK4 (Figure 12b). Interestingly, these minimal PLK4-binding regions of both Cep192 and Cep152 (residues 190–240 and 1–46, respectively) comprise conserved stretches of negatively charged amino acids (Figure 12c), suggesting that binding to PLK4 is mediated through electrostatic interactions between these negatively charged residues and positively charged residues on the PB1-PB2 domain (Slevin et al., 2012).

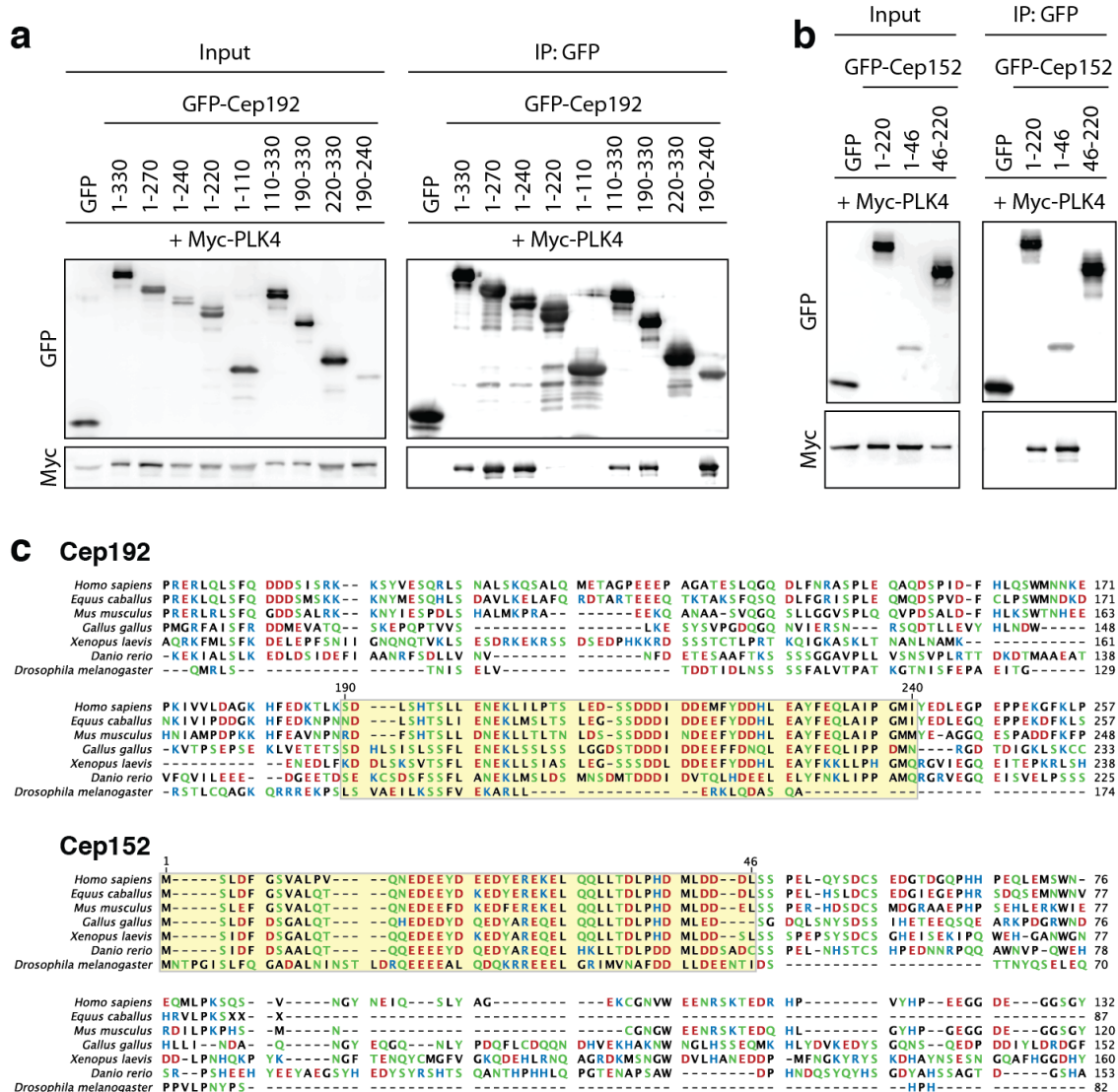


**Figure 12. The PLK4-binding regions within Cep192 1-330 and Cep152 1-220 contain conserved stretches of acidic residues**

a-b) Myc-PLK4 was co-expressed with GFP-tagged pieces of Cep192 (a) or Cep152 (b) in HEK293T cells. Cell extracts were subjected to anti-GFP immunoprecipitations and Western blot analysis with the indicated antibodies. Cep192 residues 190-240 (a) and Cep152 residues 1-46 (b) are necessary and sufficient for PLK4 binding. c) Alignments of the PLK4-interacting regions within Cep192 and Cep152 proteins from different species. Yellow shadings highlight the minimal PLK4-binding regions as determined in this study for the human proteins (residues 190-240 and 1-46 within Cep192 and Cep152, respectively). Amino acid residues are color-coded (red, acidic; blue, basic; green, polar; black, non-polar).

We next tested whether overexpression of the minimal PLK4-binding fragments of Cep192 and Cep152 affects the centrosomal localization of endogenous PLK4. To this end, GFP-tagged versions of the corresponding protein fragments were overexpressed for 24 hours in U2OS cells, and the cells were fixed and stained with antibodies against PLK4 and  $\gamma$ -tubulin for analysis via immunofluorescence microscopy. We found that the Cep192 and Cep152 fragments did not localize to centrosomes, but, instead of that, caused loss of PLK4 from the centrosomes (Figure 13), corroborating the conclusion that the fragments encompassing residues 190-240 and 1-46 of Cep192 and Cep152, respectively, are necessary and sufficient for the interaction with PLK4.

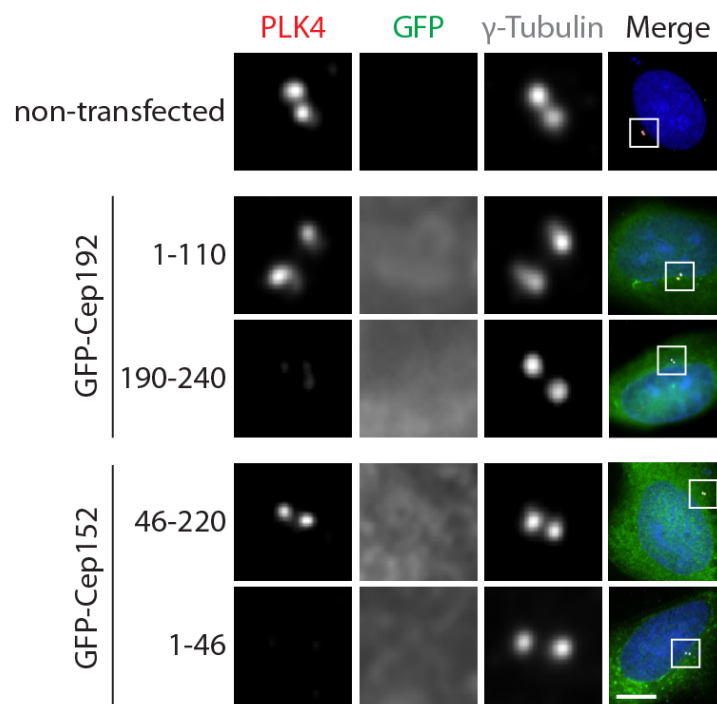


**Figure 13. PLK4 is lost from centrosomes in cells expressing GFP-tagged Cep192 190-240 or Cep152 1-46**

U2OS cells were transfected with the indicated plasmids for 24 hours. Cells were fixed and stained with antibodies against PLK4 and  $\gamma$ -tubulin; DNA was stained with DAPI. Scale bar: 5  $\mu$ m

To verify the importance of Cep192's N-terminal acidic residues for PLK4 binding, we generated two mutant Cep192 constructs, in both of which three sequential acidic amino acids were substituted with alanine residues. The mutant Cep192-M1 contained the residue substitutions D218A, D219A, and E220A, whereas Cep192-M2 comprised the amino acid replacements D214A, D215A, D216A. GFP-tagged versions of these two Cep192 mutants were co-expressed with Myc-PLK4 in HEK293T cells and the cell

extracts were used for anti-GFP co-immunoprecipitations that were analyzed via immunoblotting. Both Cep192-M1 and Cep192-M2 displayed slightly reduced PLK4 binding compared to Cep192-WT (Figure 14), indicating that the selected acidic residues indeed contribute to PLK4 binding. However, the non-mutated acidic residues appeared to maintain the PLK4 binding capacity to a substantial degree. More stringent washing of the immunocomplexes and/or insertion of additional mutations would probably result in a more pronounced reduction of the interaction.

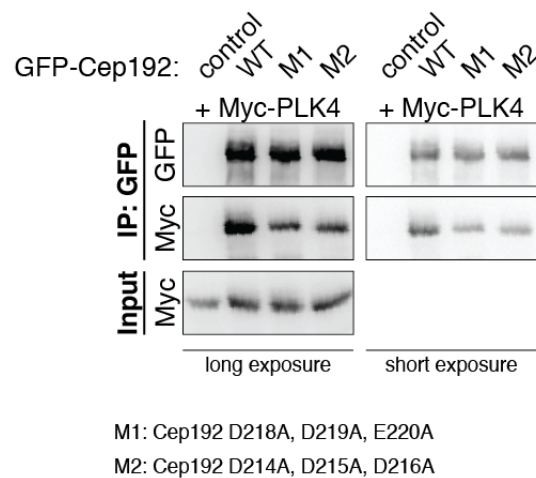


**Figure 14. Two Cep192 mutants (M1 and M2) display slightly reduced PLK4 binding**

Two Cep192 mutants were generated by replacing three acidic residues within the PLK4-interacting region with alanine residues; Cep192-M1 (D218A, D219A, E220A), Cep192-M2 (D214A, D215A, D216A). HEK293T cells were transfected with the indicated control- and Cep192-plasmids and cell extracts were subjected to GFP-co-immunoprecipitations. The immunoprecipitates were analyzed by immunoblotting with the indicated antibodies.

#### 4.2.2 Binding of Cep192 to PLK4 is direct

In the case of Cep152, a direct interaction with the PB1-PB2 domain of PLK4 had previously been demonstrated (Cizmecioglu et al., 2010; Dzhindzhev et al., 2010; Hatch et al., 2010). We thus asked whether Cep192 might also directly bind to PB1-PB2. To address this question, we carried out *in vitro* binding assays with bacterially expressed GST-Cep192 (residues 1-330). In the first binding experiment, we incubated this recombinant Cep192 fragment with *in vitro*-translated Myc-PLK4 and analyzed the precipitates via Western blotting using anti-GST and anti-Myc antibodies (Figure 15a). Myc-PLK4 specifically brought down the Cep192 fragment, indicating that the two

proteins interact in a direct manner. For the second binding experiment, Myc-PLK4-WT and Myc-PLK4-KD (kinase-dead PLK4) were overexpressed in HEK293T cells and isolated via anti-Myc immunoprecipitation. The beads were washed and incubated with GST-tagged Cep192 (1-330), and bound proteins were analyzed by immunoblotting (Figure 15b). We found that the Cep192 fragment was present in the immunoprecipitates of both PLK4-WT and -KD, revealing a direct interaction and showing that Cep192 has similar binding affinity to catalytically active and inactive PLK4. Thus, PLK4 kinase activity is not necessary for the Cep192 interaction. Finally, we performed a GST-pulldown assay with bacterially expressed NusA-His-tagged Cep192 (residues 1-330). As a control we used a shorter piece of Cep192, encompassing residues 1-110, which is not able to interact with PLK4 (Figure 12a). We mixed these Cep192 fragments with GST-tagged PLK4 PB1-PB2 (570-820) or GST alone (as control). The Cep192 fragment (1-330) consistently bound to PLK4 PB1-PB2, whereas the control fragment (1-110) did not, confirming that the interaction between Cep192 and PLK4 is direct (Figure 15c).

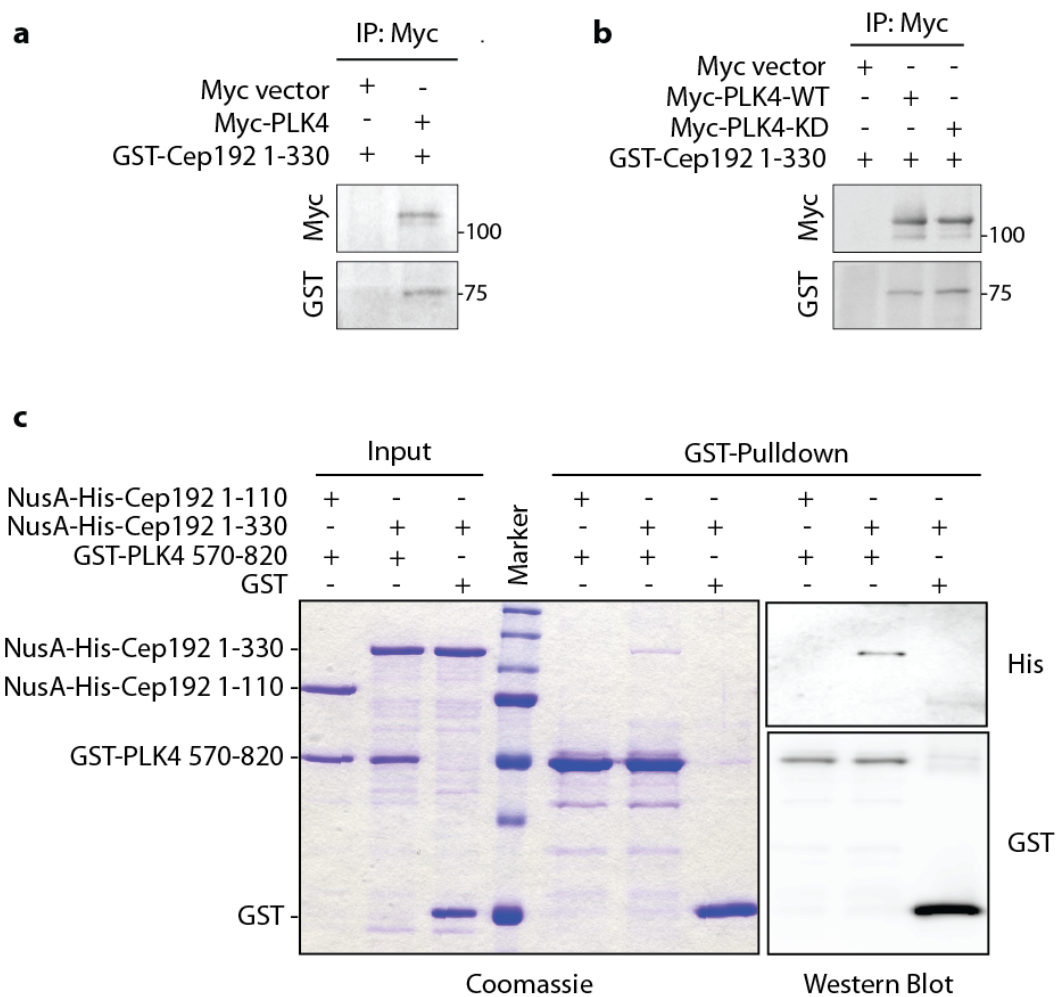


**Figure 15. Binding of Cep192 to PLK4 is direct**

a) *In vitro* binding assay with bacterially expressed GST-Cep192 (1-330) and Myc-PLK4, which was generated by coupled *in vitro* transcription-translation and isolated via anti-Myc immunoprecipitation. Proteins were analyzed by Western blotting with the indicated antibodies. b) HEK293T cells were transfected with control-, Myc-PLK4-WT and Myc-PLK4-KD (kinase dead) constructs for 48 hours. Proteins were isolated by anti-Myc immunoprecipitations and the beads were washed, resuspended, and incubated with equal amounts of bacterially expressed GST-Cep192 (1-330). After washing, the precipitates were analyzed by immunoblotting with the indicated antibodies. c) GST pulldown assay with the indicated constructs, which were purified from *E. coli*. Samples were subjected to SDS-PAGE followed by Coomassie Blue staining or immunoblotting with the indicated antibodies.

### 4.2.3 Cep192 is a substrate of PLK4

Because PLK4 directly binds to Cep192, we next asked whether Cep192 is a phosphorylation target of PLK4. To test this possibility, we performed an *in vitro* kinase assay with recombinant, bacterially expressed GST-PLK4 and FLAG-tagged Cep192 (1-330) that was overexpressed in HEK293T cells and then isolated using FLAG-

antibody coated beads. We incubated the beads with GST-PLK4 in the presence of  $\gamma$ -[ $^{32}$ P]-ATP. Detection by autoradiography and Western blotting revealed that the Cep192 fragment was indeed phosphorylated by PLK4 (Figure 16a). In another *in vitro* kinase experiment, we incubated GST-PLK4 with bacterially expressed GST-Cep192 (1-330). Again, we found that the Cep192 fragment was readily phosphorylated by PLK4, whereas GST alone was not (Figure 16b). Thus, Cep192 can be added to the growing list of PLK4 substrates, which so far contains Cep152, the F-box protein FBXW5, CPAP, and the  $\gamma$ -TuRC protein GCP6 (Bahtz et al., 2012; Chang et al., 2010; Hatch et al., 2010; Puklowski et al., 2011).

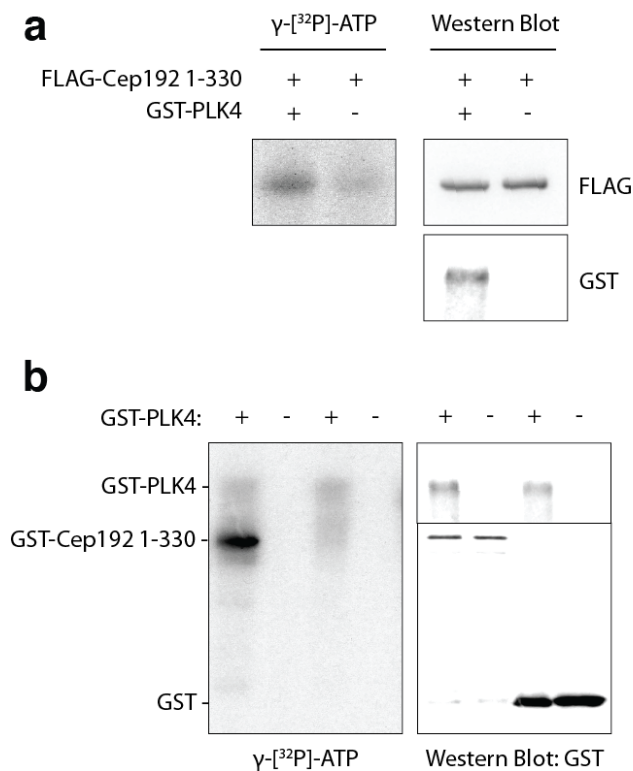


**Figure 16. Cep192 1-330 is phosphorylated by PLK4 *in vitro***

*In vitro* kinase assays with bacterially expressed GST-PLK4. a) FLAG-Cep192 1-330 was expressed in HEK293T cells and immunoprecipitated using FLAG-antibody coupled beads. The beads were incubated with  $\gamma$ -[ $^{32}$ P]-ATP in the presence or absence of GST-PLK4 for 30 min at 30 °C. Samples were analyzed by autoradiography and Western blotting with the indicated antibodies. b) Same as in (a) except that bacterially expressed GST-Cep192 1-330 was used as substrate. GST was analyzed for control. The PLK4 autoradiography signal appeared as a diffuse band, presumably because bacterial expression of full-length PLK4 was inefficient, yielding a substantial amount of background protein (probably PLK4 degradation products).

#### 4.2.4 Cep152 and Cep192 display distinct centrosomal localizations

As shown above, both Cep152 and Cep192 share the ability to directly bind to the PB1-PB2 domain of PLK4 (§ 4.2.1-4.2.2) (Cizmecioglu et al., 2010; Dzhindzhev et al., 2010; Hatch et al., 2010). However, it had been unclear at the beginning of this study to what extent the two proteins might share similar centrosomal functions. As a first approach to analyze the centrosomal functions of Cep152 and Cep192, we compared the precise centriolar localization patterns of the two proteins via 3D-structured illumination microscopy (3D-SIM). For analysis of the localization in interphase cells, we stained U2OS cells for Cep152, Cep192, and either CP110, a marker for the distal ends of centrioles, or glutamylated tubulin (GT335), which marks the centriolar walls (Figure 17a,b). In interphase cells, anti-Cep192 antibodies consistently labeled both mother and daughter centrioles along their entire walls, reflecting the staining pattern of glutamylated tubulin (GT335). In contrast, antibodies against Cep152 stained only the proximal halves of mother centrioles, in line with previous data (Cizmecioglu et al., 2010; Lukinavičius et al., 2013; Sir et al., 2011). For analysis of the localization patterns in mitotic cells, we used anti-Cep152 and anti-Cep192 antibodies in conjunction with antibodies against the PCM marker  $\gamma$ -tubulin (Figure 17c). Both Cep192 and Cep152 localized to the centrosomes/spindle poles during mitosis. However, whereas Cep192 was distributed throughout the PCM, Cep152 remained restricted to the proximal halves of mother centrioles. The expansion of Cep192 into the PCM in mitotic cells reflects the role of Cep192 in centrosome maturation and spindle assembly (Gomez-Ferreria et al., 2007; Joukov et al., 2010; Zhu et al., 2008). Taken together, Cep192 shows a wider distribution at centrioles than Cep152 in interphase cells, and the difference in the distribution is even more pronounced when Cep192 spreads throughout the PCM in mitotic cells.

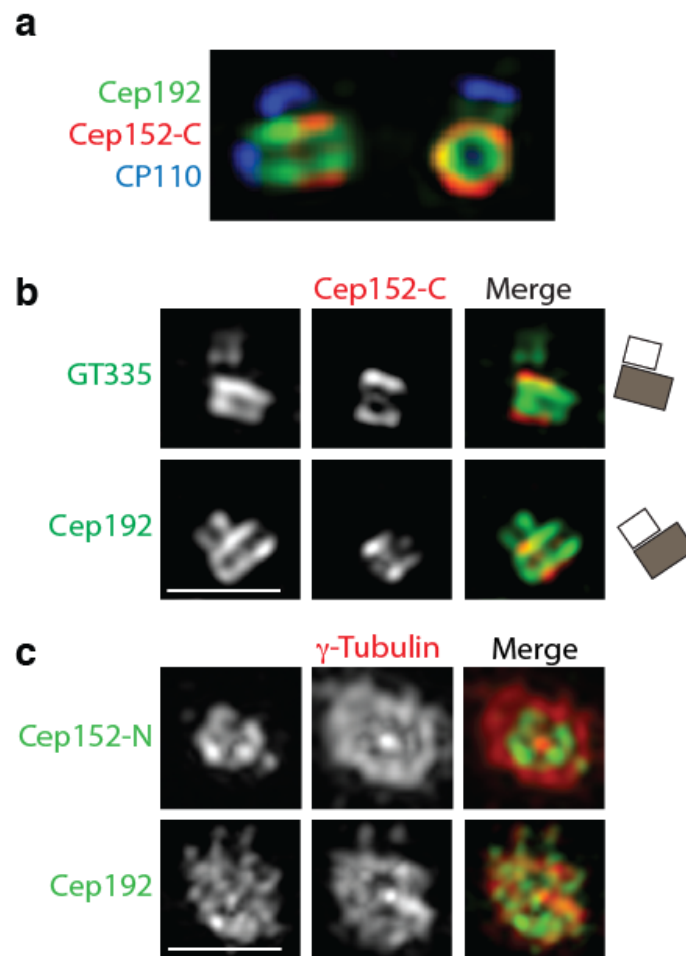


**Figure 17. Cep152 and Cep192 display distinct cell cycle-specific centrosome localizations**  
 U2OS cells were fixed and stained for 3D-structured illumination microscopy (3D-SIM) with the indicated antibodies. Interphase (a-b) and mitotic cells (c) were analyzed (they were distinguished by the distance between the centriole pairs). In b), the centriole orientation is illustrated schematically (on the right). Cep152-C and -N indicate antibodies targeting C- and N-terminal epitopes of Cep152, respectively. Scale bars: 1  $\mu$ m

#### 4.2.5 Cep192 and Cep152 cooperate in PLK4 recruitment and centriole duplication

The Cep192 counterpart SPD-2 in *C. elegans* (Pelletier et al., 2004) had emerged as a key centrosomal recruitment factor for ZYG-1 (Delattre et al., 2006; Pelletier et al., 2006), and an analogous role for PLK4 recruitment in *Drosophila* had been assigned to Asterless, the counterpart of human Cep152 (Blachon et al., 2008). Thus, RNAi depletion experiments were carried out to test a possible role for Cep192 and/or Cep152 in the centrosomal recruitment of human PLK4 (Sonnen et al., 2013). RNAi-mediated

depletion of Cep152 from U2OS cells did not impair PLK4 targeting to centrioles. Instead, PLK4 levels were found to be slightly enhanced in these cells, in agreement with previous reports (Cizmecioglu et al., 2010; Dzhindzhev et al., 2010; Hatch et al., 2010) (Figure 18a,b). By contrast, depletion of Cep192 resulted in significantly reduced centrosomal PLK4 levels, and simultaneous depletion of both Cep152 and Cep192 completely interfered with PLK4's centrosomal localization (Figure 18a,b), indicating that the two proteins cooperate to promote centriolar recruitment of PLK4. The effects upon depletion of Cep192 and Cep152 were not caused by a reduction of overall PLK4 levels, as verified by Western blot analysis (Sonnen et al., 2013). Furthermore, depletion of Pericentrin (analyzed for control) had no significant impact on the centrosomal localization of PLK4 (Figure 18a,b) (Sonnen et al., 2013).

Having found that Cep192 and Cep152 cooperate in PLK4 recruitment, the role of these two proteins in centriole duplication was assessed (Sonnen et al., 2013). To do so, the proteins were depleted from U2OS cells, either individually or simultaneously, and the centriole numbers were determined by quantifying the CP110-positive dots in the cells (Figure 18c,d). Co-depletion of both proteins led to a strong reduction of centriole duplication, as about 60 % of the corresponding cells exhibited less than two centrioles (Sonnen et al., 2013). In contrast, only about 35 % of cells contained less than two centrioles after single-depletions of either Cep192 or Cep152. Notably, the effect of simultaneous depletion of both Cep192 and Cep152 was comparable to that observed upon depletion of the duplication factor SAS-6 (which yields 70 % of cells with less than two centrioles) (Figure 18c,d). Taken together, Cep192 and Cep152 cooperate in centriole duplication, presumably through their joint function in the centrosomal recruitment of PLK4 (Sonnen et al., 2013).

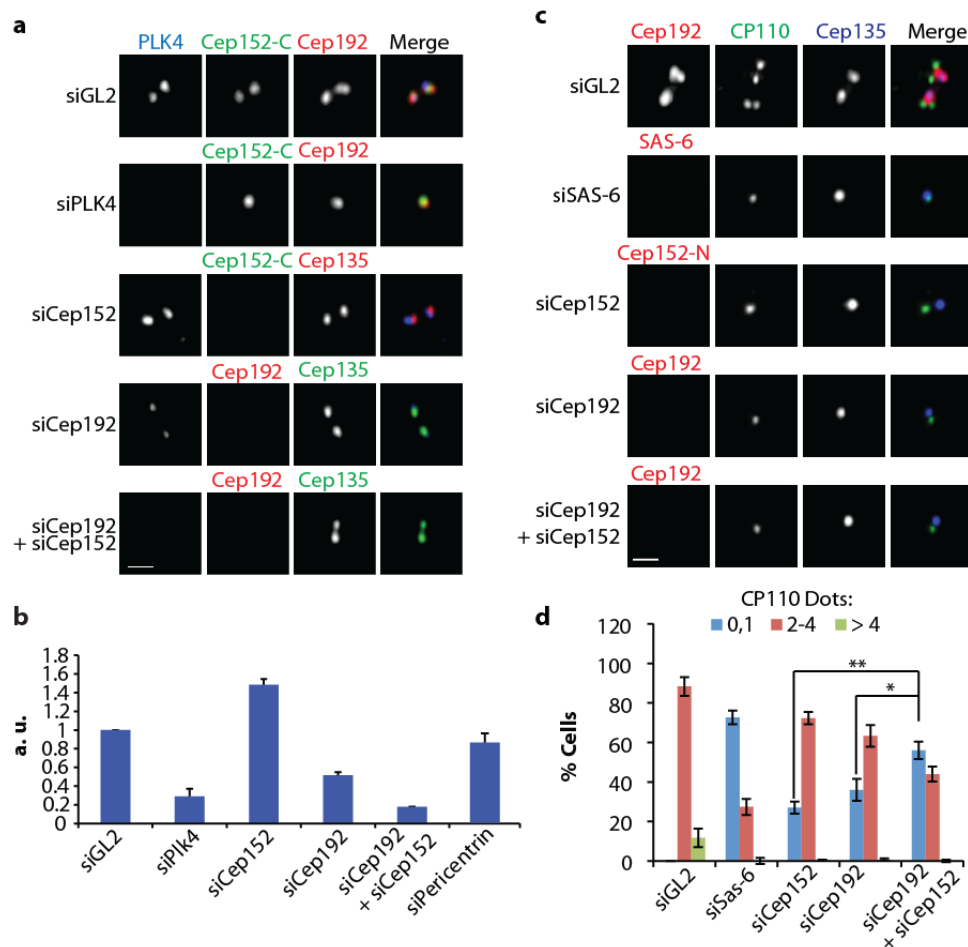


**Figure 18. Cep192 and Cep152 cooperate in PLK4 recruitment and centriole duplication**

a) U2OS cells were transfected with the indicated siRNA oligonucleotides for 72 hours. The cells were fixed and stained with the indicated antibodies. PLK4 levels at centrosomes were analyzed. b) Quantification of centrosomal PLK4 levels in cells treated as described in a) (three independent experiments, 10-15 cells each; error bars denote SEM). c) U2OS cells were transfected with the indicated siRNA oligonucleotides for 72 hours. After fixation, the cells were stained with the indicated antibodies to determine centriole numbers via immunofluorescence microscopy. d) Quantification of centriole numbers in cells treated as described in c) (three independent experiments, 100 cells each; error bars denote SEM); \* $P < 0.05$ , \*\* $P < 0.01$ . Cep152-C and -N indicate antibodies targeting C- and N-terminal epitopes of Cep152, respectively. Scale bars: 1  $\mu\text{m}$ . These experiments were performed by K. Sonnen (figures are courtesy of K. Sonnen). (Adapted from Sonnen et al., 2013)

#### 4.2.6 Excursion: Cep192 interacts with Aurora A and PLK1

Cep192 has been ascribed a pivotal role in centrosome maturation and mitotic spindle assembly (Gomez-Ferreria et al., 2007; Zhu et al., 2008), and in this context has been shown to bind and to activate the kinase Aurora A (Joukov et al., 2010). The centrosomal accumulation of Cep192 at the G2/M transition is thought to depend on PLK1 activity, as inhibition of PLK1 severely interferes with Cep192 recruitment

(Haren et al., 2009; Santamaria et al., 2010). Here, we wished to verify the interaction between Cep192 and Aurora A and, in parallel, to test if the N-terminal fragment of Cep192, which is responsible for PLK4 binding, can also bind PLK1. First, we transfected HEK293T cells with plasmids encoding Myc-Aurora A and FLAG-Cep192 and subjected the cell extracts to anti-FLAG co-immunoprecipitations. Western blot analysis revealed that Aurora A was present in the precipitate of Cep192, confirming the previously reported interaction (Figure 19a) (Joukov et al., 2010). Next, we carried out an anti-Myc co-immunoprecipitation experiment with overexpressed Myc-PLK1 and GFP-tagged N-terminal Cep192 (residues 1-330). We found that the N-terminus of Cep192 was efficiently brought down by Myc-PLK1 (Figure 19b). Notably, the upshift of the Cep192 1-330 band upon SDS-PAGE indicated that Cep192 is phosphorylated by PLK1 (Figure 19b), as has been suggested previously (Santamaria et al., 2010). Recently, the Cep192/PLK1 interaction has been analyzed in great detail, and it has been shown that Cep192-dependent activation of both Aurora A and PLK1 is crucial for centrosome maturation and mitotic spindle assembly (Joukov et al., 2014). Thus, Cep192 serves as a multifunctional scaffold that regulates various centrosomal processes at different stages of the cell cycle.

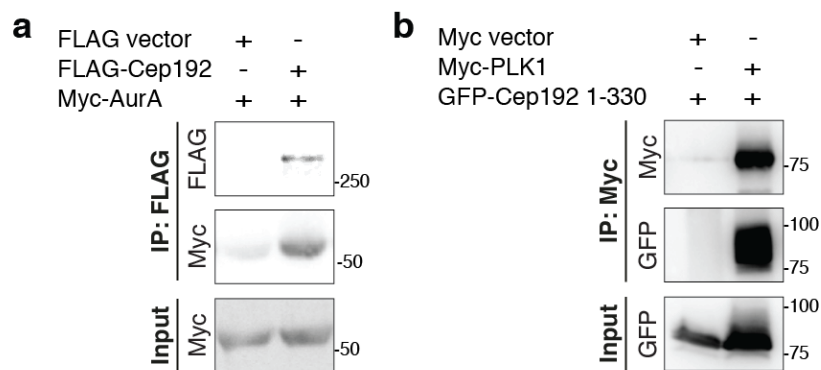


**Figure 19. Cep192 interacts with Aurora A and PLK1**

a-b) HEK293T cells were transfected with the indicated plasmids. Cell extracts were subjected to co-immunoprecipitation experiments using beads coated with anti-FLAG (a) or anti-Myc antibodies (b). The immunoprecipitates were analyzed by Western blotting with the indicated antibodies.

### 4.3 On the PLK4/STIL interaction

#### 4.3.1 Interdependencies between PLK4, STIL, and SAS-6 centrosomal localizations

STIL is a key centriole duplication factor in human cells, as depletion of STIL results in a failure of centriole duplication, whereas STIL overexpression gives rise to extra copies of centrioles that are arranged in a rosette-like pattern around the mother centriole (Arquint et al., 2012; Tang et al., 2011; Vulprecht et al., 2012). These depletion and overexpression phenotypes are similar to those observed in the case of PLK4 and SAS-6 (Habedanck et al., 2005; Leidel et al., 2005; Strnad et al., 2007). At the beginning of this study, however, no interaction between STIL and PLK4 had been reported. Since we had found STIL co-purifying with PLK4 PB1-PB3 in the S-peptide pulldown (Table 1), we set out to explore the anticipated physical and functional interaction in more detail. First, we conducted 3D-SIM imaging in U2OS cells to precisely determine the localizations of STIL and PLK4. We found that the two proteins largely colocalize at the proximal end of daughter centrioles (Figure 20), at the site where the cartwheel component SAS-6 is located, indicating that STIL and PLK4 might cooperate with SAS-6 in cartwheel formation (Arquint et al., 2012; Sonnen et al., 2012; Strnad et al., 2007; Tang et al., 2011).

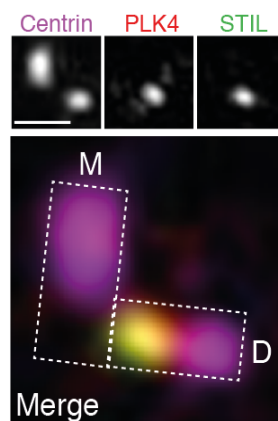


**Figure 20. PLK4 and STIL colocalize at the proximal end of daughter centrioles**

U2OS cells were fixed and stained with the indicated antibodies for 3D-SIM imaging. A representative 3D-SIM image is shown, demonstrating the colocalization of PLK4 and STIL at the daughter centriole. Top panel: Centrin (purple), PLK4 (red), STIL (green). Scale bar: 0.5  $\mu\text{m}$ . Bottom panel: Magnified view of the centrioles (overlay image). The rectangles illustrate the orientation of the mother (M) and daughter (D) centrioles.

Because of the colocalization of STIL, PLK4 and SAS-6, we next examined whether these three proteins depend on each other for their centriolar association. First, we tested whether the centrosomal localization of STIL and SAS-6 depends on the presence of PLK4. To this end, we transfected U2OS cells with siRNA oligonucleotides targeting PLK4. To this end, we transfected U2OS cells with siRNA oligonucleotides targeting PLK4 for 72 hours and, after fixation, stained the cells with antibodies against STIL and SAS-6. In addition, we used antibodies against CP110 to label individual centrioles, and anti- $\gamma$ -tubulin or anti-Cep135 antibodies to mark the centrosomes. We conducted immunofluorescence microscopy analysis to assess the centrosomal signal intensities of STIL and SAS-6 in prophase cells that harbored one to two centrioles (indicative of successful PLK4 depletion) (Figure 21). The centrosomal association of both STIL and SAS-6 was severely impaired in the absence of PLK4. Thus, PLK4 is required for SAS-6 and STIL centriolar recruitment and/or maintenance, confirming earlier reports (Strnad et al., 2007; Tang et al., 2011).

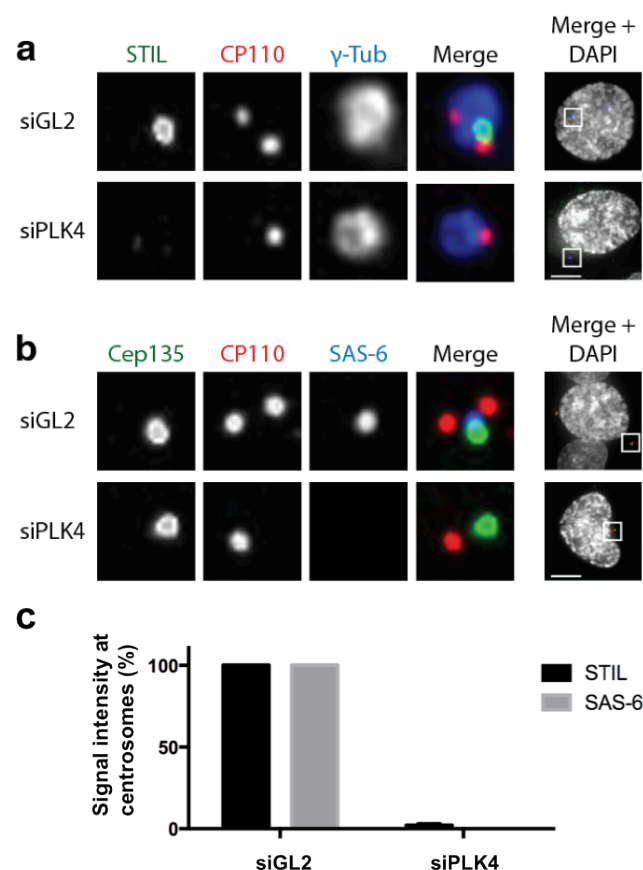


**Figure 21. The centrosomal localization of STIL and SAS-6 depends on PLK4**  
a-b) U2OS cells were transfected with control (siGL2) or PLK4 (siPLK4) siRNA oligonucleotides (for 72 hours) and stained with the indicated antibodies, DNA was stained with DAPI. The centriolar

association of STIL (a) and SAS-6 (b) was analyzed in prophase cells harboring 1-2 centrioles (indicative of successful PLK4 depletion). Scale bar: 5  $\mu$ m. c) Quantification of STIL and SAS-6 signal intensities at centrosomes in cells treated as described in a) and b) (three independent experiments, 10 cells each).

### 4.3.2 STIL and PLK4 interact functionally and physically

Having observed that PLK4 is required for STIL association with centrosomes (Figure 21a,c), we next tested whether, conversely, STIL is required for the centrosomal localization of PLK4. We transfected U2OS cells with control or three different STIL siRNA oligonucleotides for 72 hours and stained the cells using antibodies against STIL, PLK4, and CP110. Immunofluorescence microscopy analysis revealed that the centrosomal signal intensity of endogenous PLK4 was not reduced in the absence of STIL; in contrast, we found that PLK4 association with centrosomes was remarkably enhanced in STIL-depleted cells, and that PLK4 displayed a ring- rather than a dot-like pattern (Figure 22a,b). Immunoblotting showed that PLK4 protein levels were generally elevated in cells depleted of STIL (Arquint et al., 2015). The STIL depletion phenotype is similar to that observed after depletion of the F-box protein  $\beta$ TrCP (Figure 22a,b). Depletion of  $\beta$ TrCP results in elevated PLK4 levels due to abrogated proteasomal degradation of PLK4 (Guderian et al., 2010; Holland et al., 2010b). We suggest that, accordingly, depletion of STIL causes accumulation of PLK4 due to impaired PLK4 degradation in the absence of STIL (discussed in § 5.3-5.4).

Given the above observations pointing at a functional relationship between STIL and PLK4, we next investigated a possible physical interaction between these two proteins. For this purpose, HEK293T cells were transfected with plasmids encoding FLAG-tagged STIL and Myc-PLK4-WT or Myc-PLK4-ND (a non-degradable mutant of PLK4 (S285A, T289A), which is known to be stabilized in cells (Guderian et al., 2010)). After cell lysis, anti-Myc co-immunoprecipitations were performed and analyzed via immunoblotting with anti-Myc and anti-STIL antibodies. STIL was present in the precipitates of both PLK4-WT and PLK4-ND, indicating that STIL interacts with both versions of PLK4 (Arquint et al., 2015) (Figure 22c). In the precipitate of PLK4-ND more STIL protein was present than in the case of PLK4-WT, most likely due to the increased intracellular abundance of PLK4-ND compared to PLK4-WT. We therefore

used PLK4-ND (instead of WT) in the following co-immunoprecipitation experiments. Co-expression of PLK4-ND with STIL furthermore revealed that STIL is a substrate of PLK4 *in vivo*, as judged by the upshift of the STIL band on Western blot (Figure 22c). Thus, taken together, STIL and PLK4 interact functionally and physically.

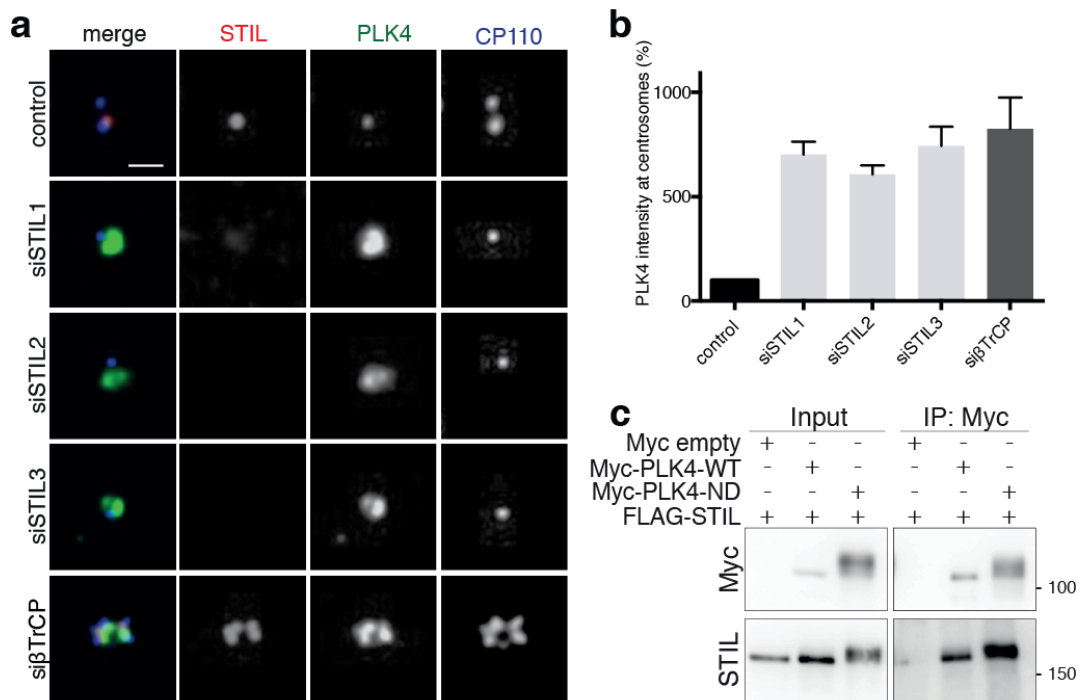


**Figure 22. STIL and PLK4 interact functionally and physically**

a) PLK4 levels are elevated in STIL-depleted cells. U2OS cells were transfected with the indicated siRNA oligonucleotides targeting STIL (siSTIL1-3) or  $\beta$ TrCP (si $\beta$ TrCP, analyzed for control). After 72 hours, cells were fixed and stained with the indicated antibodies for immunofluorescence microscopy. Representative images are shown. Scale bar: 1  $\mu$ m. b) Quantification of centrosomal PLK4 levels in cells treated as described in a) (three independent experiments, 15 cells each, error bars denote SEM) c) PLK4 binds and phosphorylates STIL. HEK293T cells were transfected to co-express FLAG-STIL with Myc-PLK4-WT or Myc-PLK4-ND (non-degradable mutant of PLK4 (S285A, T289A)). Cell extracts were subjected to anti-Myc co-immunoprecipitations and Western blot analysis. PLK4-ND is stabilized in cells (Guderian et al., 2010) and thus facilitates visualization of STIL binding. The upshift of the STIL band upon co-expression with PLK4-ND indicates that STIL is phosphorylated by PLK4. This figure is courtesy of C. Arquint. (Adapted from Arquint et al., 2015)

Having observed that STIL is phosphorylated by PLK4 (Figure 22c and Arquint et al., 2015), we next addressed the question of whether PLK4's catalytic activity is required for STIL binding. To this end, HEK293T cells were co-transfected with FLAG-STIL and Myc-PLK4-ND or Myc-PLK4-KD (kinase-dead PLK4), and the cell extracts were subjected to anti-Myc co-immunoprecipitations and subsequent Western blot analysis (Figure 23). PLK4-ND efficiently brought down STIL, as expected. In addition, we

could detect STIL in the precipitate of PLK4-KD, indicating that PLK4's catalytic activity is not required for STIL binding. (Whether the apparent increased levels of STIL in the presence of PLK4-ND (Figure 23, lane 2 of the input blot) reflect PLK4-ND-dependent stabilization, cannot be judged based on this single experiment. To address this issue, further experimentation would be required.)

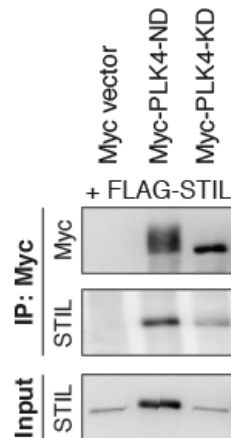


**Figure 23. PLK4 catalytic activity is not required for STIL binding**

HEK293T cells were transfected with the indicated plasmids and incubated for 36 hours. Cell extracts were subjected to anti-Myc co-immunoprecipitations and immunocomplexes were analyzed by Western blotting with the indicated antibodies. The upshift of the PLK4-ND band indicates PLK4 autophosphorylation. The upshift of the STIL band caused by PLK4-mediated phosphorylation (as shown in Figure 22c) is not visible here (presumably because of higher-percentage gels used for SDS-PAGE).

STIL and SAS-6 have been shown to mutually depend on each other for efficient and robust centriole association (Arquint et al., 2012; Tang et al., 2011; Vulprecht et al., 2012), mirroring earlier analogous observations in *C. elegans* (Leidel et al., 2005). In *C. elegans*, the STIL counterpart SAS-5 has furthermore been shown to form a stable complex with SAS-6 (Leidel et al., 2005), and likewise, *Drosophila* Ana2 has been reported to physically interact with DSAS-6 (Stevens et al., 2010a). However, in the case of human STIL and SAS-6, previous co-immunoprecipitation experiments had failed to demonstrate a direct, stable interaction between the two proteins (Arquint et al., 2012; Tang et al., 2011; Vulprecht et al., 2012). We hypothesized that in human cells PLK4 might be required to facilitate stable STIL/SAS-6 complex formation, possibly through phosphorylation of STIL. To test this possibility, we co-transfected HEK293T cells with plasmids encoding Myc-PLK4-ND, FLAG-STIL and Myc-SAS-6 and subjected the overexpressed proteins to a co-immunoprecipitation experiment, using

FLAG-STIL as bait. Strikingly, in this experimental constellation, not only PLK4 but also SAS-6 was brought down by STIL (Figure 24). This result is in agreement with parallel studies that concur to demonstrate a functional interplay between PLK4, STIL, and SAS-6 in procentriole assembly. Specifically, these studies have shown that PLK4-dependent phosphorylation on residues within the STAN motif of STIL is required for STIL/SAS-6 complex formation and SAS-6 recruitment (Dzhinzhev et al., 2014; Ohta et al., 2014; Kratz et al., 2015).

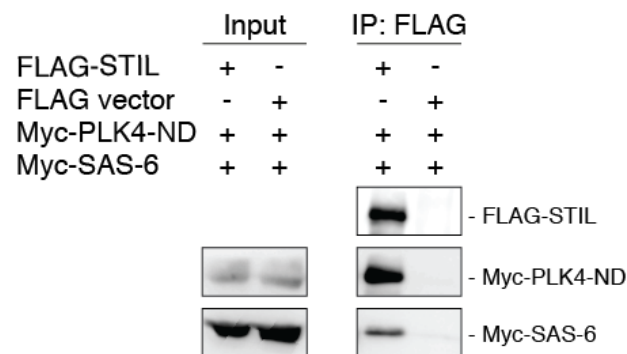


**Figure 24. PLK4 facilitates the interaction between STIL and SAS-6**

HEK293T cells were transfected with the indicated plasmids. Cell extracts were used for anti-FLAG co-immunoprecipitations, followed by Western blot analysis with anti-FLAG and anti-Myc antibodies.

### 4.3.3 The STIL-CC motif is necessary and sufficient for PLK4 binding

To further characterize the interaction between STIL and PLK4, we set out to map the region of STIL that is required for the binding to PLK4. For this purpose, we generated various fragments of STIL (Figure 25a). We then co-expressed Myc-tagged PLK4-ND with FLAG-tagged STIL fragments that covered either the N-terminal part of STIL (N-ter., residues 1-440), the middle domain (MD, residues 441-880) or the C-terminal part (C-ter., residues 881-1287), and subjected the overexpressed proteins to anti-Myc co-immunoprecipitations and Western blot analysis. We found that neither the N- nor the C-terminal part of STIL was able to efficiently interact with PLK4, in contrast to the middle domain of STIL, which displayed strong PLK4 binding (Figure 25a,b). Correspondingly, two STIL fragments lacking the N- or C-terminus but containing an

intact middle region (STIL- $\Delta$ N, residues 441-1287; STIL- $\Delta$ C, residues 1-880), were readily brought down by Myc-PLK4-ND (Figure 25a,b). To test whether the predicted coiled-coil motif within the middle region of STIL (STIL-CC, residues 720-751) (Stevens et al., 2010a) is required for PLK4 binding, we further truncated the middle domain of STIL and examined the ability of these truncated fragments to interact with Myc-PLK4-ND. Western blot analysis revealed that binding to PLK4 was not impaired as long as the STIL-CC motif was intact (Figure 25a,c). However, shortening or deleting the STIL-CC motif strongly interfered with PLK4 binding, indicating that the PLK4/STIL interaction critically depends on the STIL-CC motif.

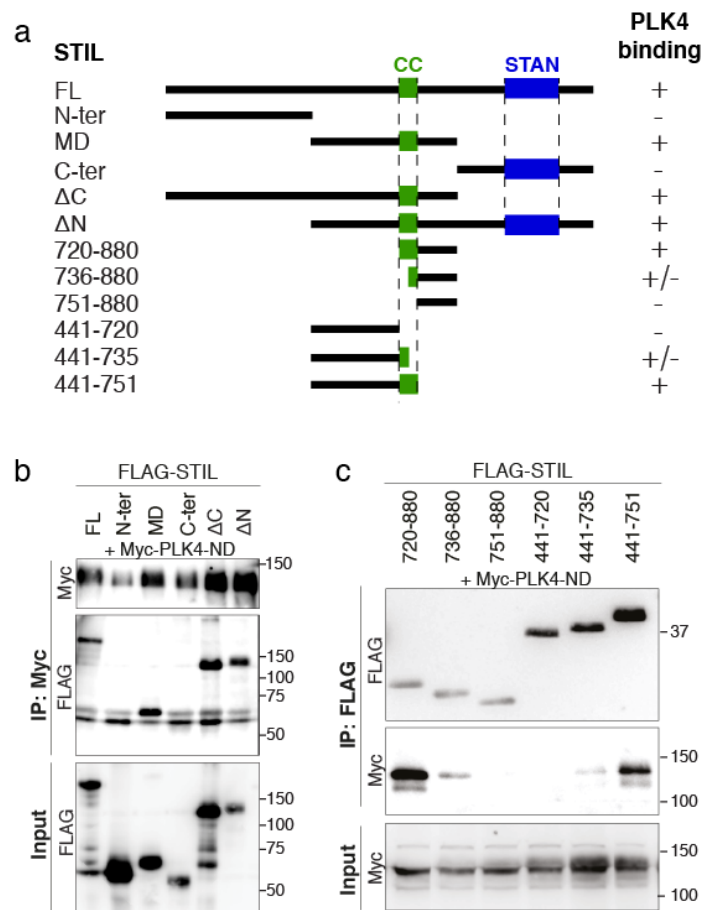


**Figure 25. Mapping of the PLK4-binding region in STIL**

a) Schematic representation of the STIL constructs that were used in the co-immunoprecipitation experiments shown in b) and c). On the right, the relative strengths of the interactions are indicated (+, strong; +/-, weak; -, not detected). b-c) HEK293T cells were transfected for 36 hours with the indicated plasmids encoding STIL fragments and Myc-PLK4-ND. Cell lysates were subjected to co-immunoprecipitations with anti-Myc or anti-FLAG antibodies. Western blot analysis was performed with the indicated antibodies. Panel b is courtesy of C. Arquint. (Adapted from Arquint et al., 2015)

To test if the STIL-CC motif is sufficient to mediate binding to PLK4, we co-expressed Myc-PLK4-ND and GFP-STIL-CC and performed an anti-GFP co-immunoprecipitation experiment. GFP-STIL-CC efficiently brought down Myc-PLK4-ND, indicating that the short STIL-CC segment is indeed sufficient for PLK4 binding (Figure 26a,b). Furthermore, a mutant of STIL lacking the CC motif (STIL- $\Delta$ CC) was not able to bind PLK4, while deletion of another conserved region in STIL, the STAN domain (STIL- $\Delta$ STAN), did not affect PLK4 binding (Figure 26a,c). Thus, the CC motif is both necessary and sufficient for STIL binding to PLK4.

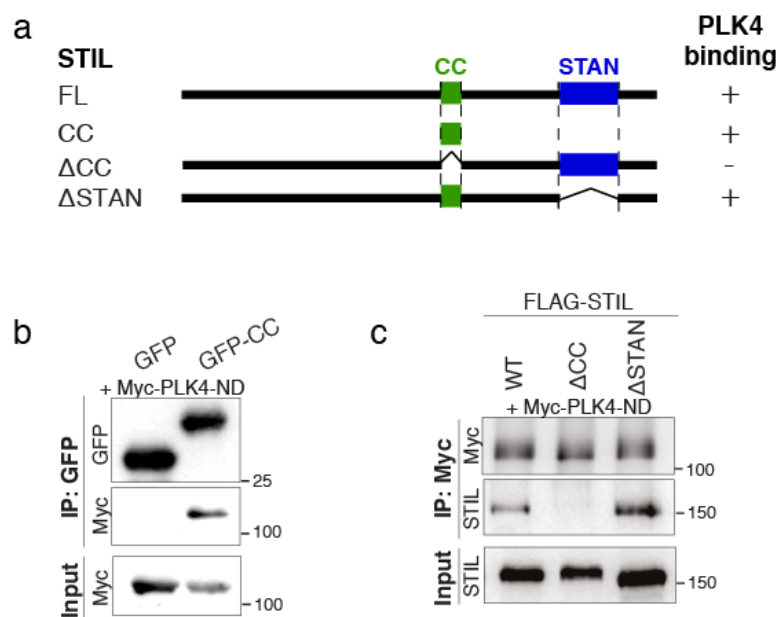


**Figure 26. The STIL-CC motif is necessary and sufficient for PLK4 binding**

a) Schematic representation of the STIL constructs that were used in the co-immunoprecipitation experiments shown in b) and c). On the right, the relative strengths of the analyzed interactions are indicated (+, strong; -, not detected). b-c) HEK293T cells were transfected for 36 hours with the indicated plasmids. Cell lysates were used for co-immunoprecipitation experiments with beads coated with anti-GFP or anti-Myc antibodies. Western blot analysis was performed with the indicated antibodies. (Adapted from Arquint et al., 2015)

#### 4.3.4 The STIL-CC motif is essential for STIL self-association

In an earlier study STIL had been shown to self-associate (Tang et al., 2011). Therefore, we tested which region of STIL is involved in this process. We transfected HEK293T cells with the above-mentioned plasmids encoding full-length or truncated versions of

STIL and subjected the cell lysates to a co-immunoprecipitation experiment followed by Western blot analysis (Figure 27a,b). We did not observe an interaction between full-length STIL and the N- or C-terminal fragments of STIL (N-ter., residues 1-440; C-ter., residues 881-1287), but we discovered that the middle region of STIL (MD, residues 441-880) displayed strong binding to the full-length STIL protein. The two STIL fragments lacking the N- or C-terminus of STIL but comprising an intact middle region (STIL- $\Delta$ N, residues 441-1287; STIL- $\Delta$ C, residues 1-880) also efficiently brought down full-length STIL. Thus, the middle region of STIL is both necessary and sufficient for the self-interaction. This finding led us to predict that the STIL-CC motif within the middle region of STIL might be essential for the self-interaction. Our prediction was indeed met as FLAG-tagged STIL-MD readily brought down GFP-STIL-CC in an anti-FLAG co-immunoprecipitation experiment (Figure 27a,c). Moreover, deletion of the CC motif severely impaired the self-association of STIL, while removal of the STAN domain had no impact (Figure 27a,d). Thus, the STIL-CC motif is not only pivotal for the interaction with PLK4 but is also important for STIL self-association.

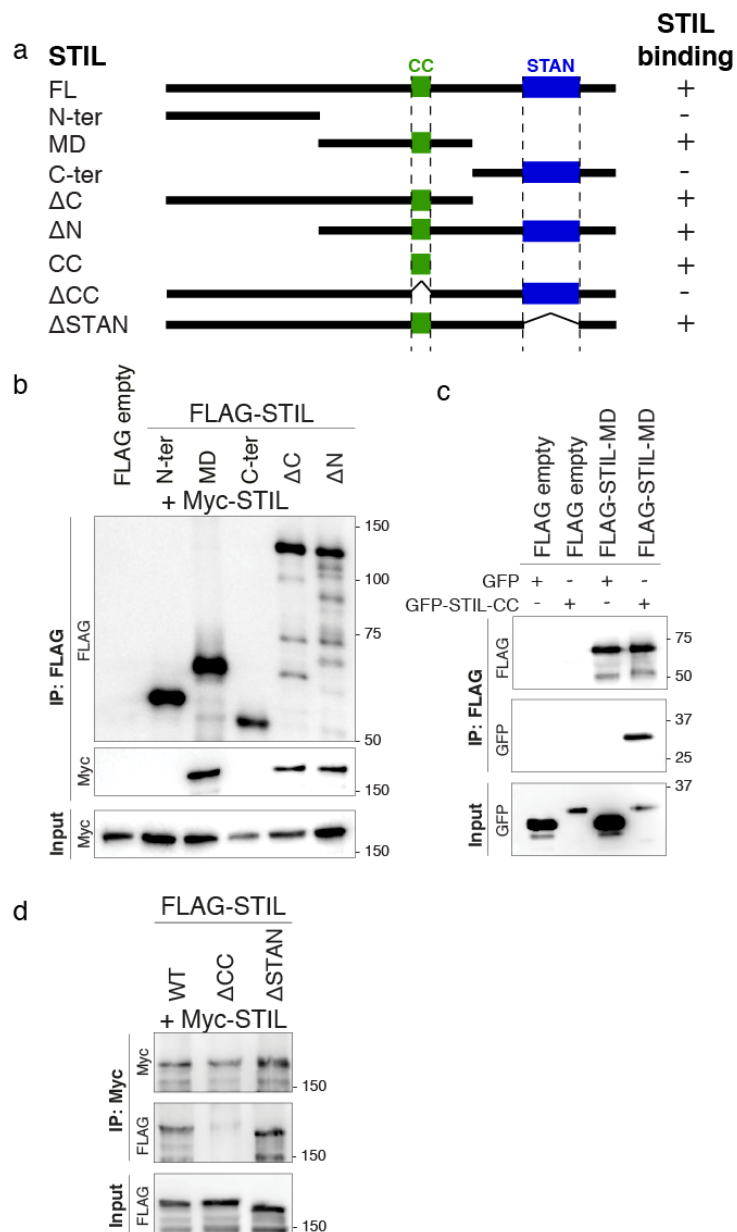


**Figure 27. The STIL-CC motif is essential for STIL self-association**

a) Schematic representation of the STIL constructs used for the co-immunoprecipitation experiments shown in b), c), and d). On the right, the relative strengths of the interactions are indicated (+, strong; -, not detected). b-d) Western blot analyses of co-immunoprecipitation experiments. HEK293T cells were transfected with the indicated plasmids. After co-expression of the STIL constructs for 24-36 hours, cells were lysed and co-immunoprecipitations were performed with beads coupled to anti-FLAG or anti-Myc antibodies. (Adapted from Arquint et al., 2015)

#### 4.3.5 The STIL-CC motif is essential for centriole duplication

The above results showed that the CC motif of STIL is crucial for PLK4 binding and STIL self-association. We next examined the importance of the CC motif for STIL functionality in centriole biogenesis. For this purpose, EGFP-tagged STIL-WT, STIL- $\Delta$ CC and STIL- $\Delta$ STAN (for control) were transiently overexpressed in U2OS cells and the levels of centriole amplification (i.e., centriole overduplication) were assessed via immunofluorescence microscopy (numbers of cells with more than four centrioles were determined) (Figure 28a,b). In the case of STIL-WT, we observed centriole amplification in 45 % of transfected cells (20 % of cells displayed a rosette-like centriole arrangement, resulting from the near-simultaneous formation of multiple procentrioles around one mother centriole (Arquint et al., 2012)). In contrast to STIL-WT, overexpression of STIL- $\Delta$ CC did not cause significant centriole amplification. In the case of STIL- $\Delta$ CC, the percentage of cells with more than four centrioles was comparable to that observed in the control condition (EGFP overexpression). Likewise, the STIL- $\Delta$ STAN mutant was not able to significantly drive centriole amplification, as expected due to the previously reported requirement for the STAN domain in centriole duplication (Vulprecht et al., 2012) (Figure 28a,b). Importantly, deletion of the STAN domain only slightly interfered with the localization of STIL to centrioles, whereas deletion of the STIL-CC motif drastically reduced centriolar association of STIL (Figure 28a,c). These results, together with the finding that depletion of PLK4 causes loss of STIL from centrioles (Figure 21a,c), suggest that the PLK4/STIL-CC interaction is required for STIL localization to the site of procentriole assembly.

Next, we addressed the question of how STIL overexpression affects PLK4 centriolar association. We monitored the localization of endogenous PLK4 after transient overexpression of EGFP-tagged STIL-WT, STIL- $\Delta$ CC, or STIL- $\Delta$ STAN in U2OS cells. Overexpression of STIL- $\Delta$ CC did not affect centriolar localization of PLK4 (Figure 28e,g). In contrast, upon overexpression of STIL-WT, endogenous PLK4 accumulated in a ring-like arrangement around the proximal ends of mother centrioles, from which the daughter centrioles grew near-simultaneously, suggesting that STIL stabilizes PLK4 at centrioles (Figure 28d,g). Strikingly, overexpression of

STIL- $\Delta$ STAN resulted in a similar ring-like PLK4 distribution around mother centrioles even though this mutant is not able to promote centriole formation (Figure 28f,g). We conclude that STIL can stabilize PLK4 at centrioles independently of promoting centriole formation.

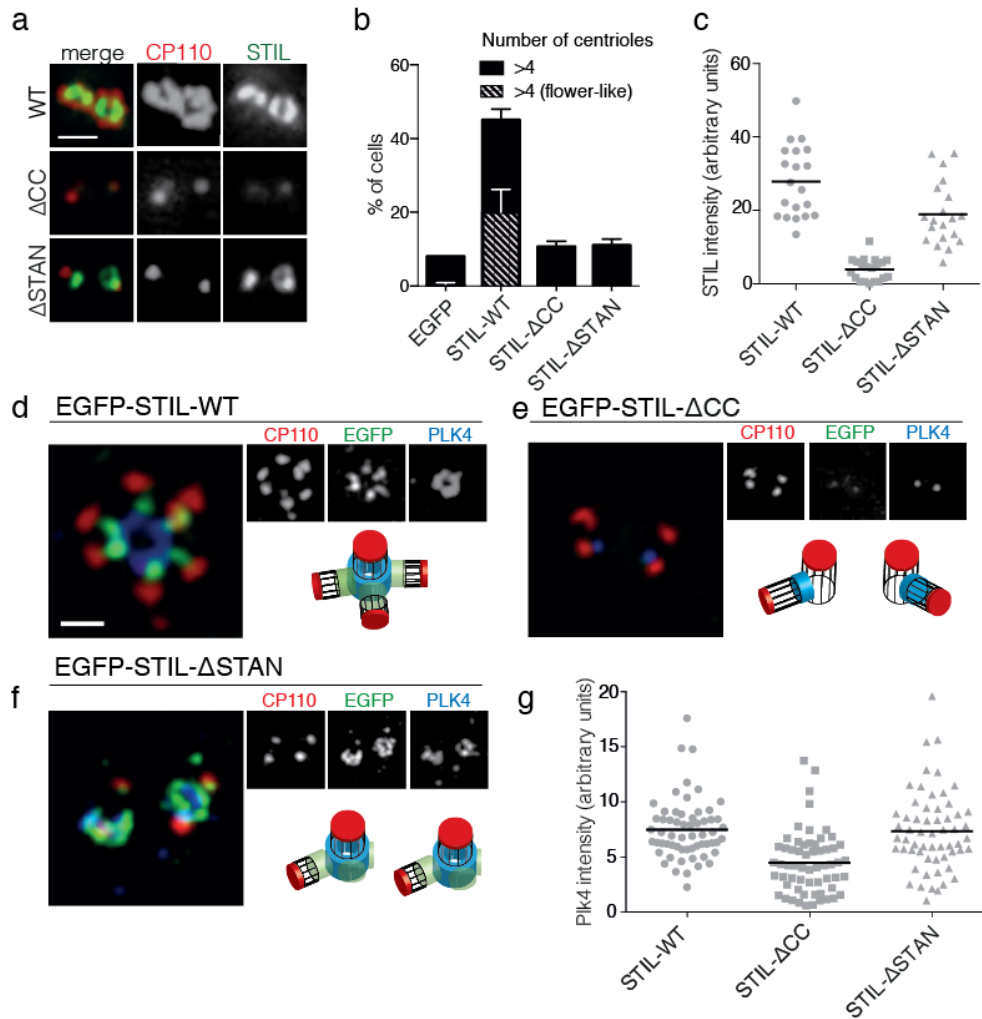


**Figure 28. The STIL-CC motif is essential for centriole duplication**

a) U2OS cells were transfected with plasmids encoding EGFP-tagged STIL-WT, STIL- $\Delta$ ACC or STIL- $\Delta$ STAN for 48 hours. Cells were fixed and stained with the indicated antibodies. Centriole amplification was analyzed by immunofluorescence microscopy. Scale bar: 1  $\mu$ m. b) Quantification of centriole numbers in U2OS cells after overexpression of the indicated STIL plasmids (three experiments, a total of 300 cells was analyzed for each condition). Error bars denote SD. c) Scatter plot to illustrate STIL signal intensities at centrosomes, after overexpression of STIL-WT, STIL- $\Delta$ ACC or STIL- $\Delta$ STAN (20 centrosomes were analyzed for each condition). d-f) 3D-SIM images of U2OS cells that were transfected with EGFP-tagged STIL-WT, STIL- $\Delta$ ACC and STIL- $\Delta$ STAN and stained with the indicated antibodies. Scale bar: 1  $\mu$ m. g) Scatter plot to illustrate PLK4 signal intensities at centrosomes, after overexpression of STIL-WT, - $\Delta$ ACC or - $\Delta$ STAN (60 centrosomes were analyzed for each condition). This figure is courtesy of C. Arquint. (Reproduced from Arquint et al., 2015)

#### 4.3.6 The STIL-CC motif directly binds to PLK4-PB3 with nanomolar affinity

To map the STIL-binding region(s) of PLK4, we performed co-immunoprecipitation experiments using a set of PLK4 fragments that contained either the N-terminal PLK4 part (residues 1-570), comprising the catalytic domain (1-271) and the linker region L1 (265-570), or the C-terminal part, including the Polo-boxes (PB1-PB3, residues 570-970; PB1-PB2, residues 570-820; L2-PB3, residues 814-970; PB3, residues 880-970) (Figure 29a). We first co-expressed GFP-tagged versions of these PLK4 fragments with FLAG-tagged full-length STIL in HEK293T cells and subjected the cell extracts to an anti-GFP co-immunoprecipitation experiment. Western blot analysis revealed that the N-terminal PLK4 fragment (residues 1-570) and the C-terminal fragments containing PB3 were sufficient to mediate the interaction with full-length STIL (Figure 29b). Next, we transfected HEK293T cells with FLAG-tagged versions of the PLK4 fragments and GFP-STIL-CC and subjected the overexpressed proteins to an anti-FLAG co-immunoprecipitation experiment. We found that STIL-CC was sufficient for the interactions with the PLK4 N-terminal fragment (residues 1-570) and the C-terminal fragments comprising PB3 (PB1-PB3, residues 570-970, and PB3, residues 880-970) (Figure 29c). Further narrowing down the STIL-binding region within the N-terminal part of PLK4 revealed that the linker L1 (residues 265-570) was involved in the interaction, whereas the catalytic domain itself (residues 1-271) was not (Figure 29d).

To determine the binding affinity of the PLK4-PB3/STIL-CC interaction, isothermal titration calorimetry was performed by collaborators from the Maier laboratory (Figure 29e). For this analysis, a synthetic STIL-CC peptide was titrated into a solution of recombinant, bacterially purified PLK4-PB3 (residues 884-970). The integrated raw data were fitted by a one-site binding model, indicating a direct binding between STIL-CC and PB3 with equimolar stoichiometry and a dissociation constant  $K_d$  of  $280 \pm 60$  nM (Figure 29e).



#### 4.3.7 Does STIL-CC binding to PLK4-L1 depend on an intact DSG motif?

The DSG-motif of PLK4 (DSGHAT, residues 284-289) lies just downstream of the kinase domain within the linker L1 region, which we have identified as a second binding region for STIL-CC (Figure 29d). We thus asked whether STIL-CC binding to L1 might require the presence of the intact DSG motif. Such a requirement would raise the interesting prospect that STIL-CC might interfere with PLK4 degradation by competing with  $\beta$ TrCP for binding to the DSG motif (Guderian et al., 2010).

To test if STIL-CC binding to L1 depends on the intact DSG motif, we introduced the previously mentioned double-alanine mutation S285A/T289A (referred to as DSG<sup>AA</sup>) (Guderian et al., 2010) into the PLK4 fragment spanning residues 1-570. We overexpressed FLAG-tagged WT and mutant PLK4 1-570 in combination with GFP-STIL-CC in HEK293T cells and used the cell extracts for an anti-FLAG co-immunoprecipitation experiment that we analyzed via Western blotting (Figure 30). The mutant PLK4 1-570 (DSG<sup>AA</sup>) was able to efficiently bring down STIL-CC, similar to the WT counterpart, suggesting that STIL-CC binding to PLK4-L1 does not depend on an intact DSG motif. However, albeit we did not detect a requirement for the DSG motif in STIL-CC binding, STIL could nonetheless prevent  $\beta$ TrCP binding to PLK4, e.g. through steric hindrance. Additional experiments are required to examine this possibility.

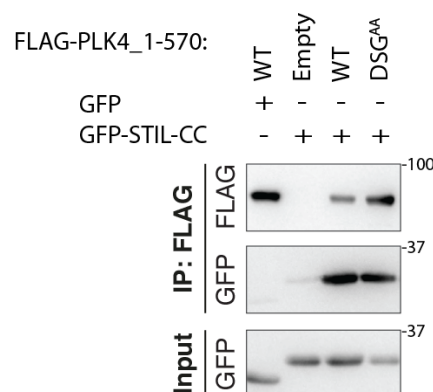


**Figure 30. STIL-CC binding to PLK4-L1 does not require an intact DSG motif**

HEK293T cells were transfected with the indicated FLAG-tagged constructs of PLK4 1-570 WT or mutant (DSG<sup>AA</sup>, S285A/T289A) for 36 hours. Cell extracts were subjected to anti-FLAG co-immunoprecipitations followed by Western blot analysis with the indicated antibodies.

#### 4.3.8 Analysis of the STIL-CC sequence properties

Having discovered that the STIL-CC motif is crucial for the function of STIL in centriole duplication – due to its roles in PLK4 binding, STIL self-association, and STIL centriolar recruitment (§ 4.3.3-4.3.6) – we next analyzed the sequence properties of this motif in more detail. First, we used the COILS program to determine the coiled-coil probability of the STIL-CC sequence. This computer program compares a protein sequence to a database of known two-stranded parallel coiled-coils and calculates the probability of the sequence to adopt a coiled-coil conformation (Lupas et al., 1991). According to this computational prediction, the coiled-coil probability for the STIL-CC motif is very high (Figure 31a). Next, we analyzed the STIL-CC motif via multiple sequence alignment using the software ClustalW. Comparison of the STIL-CC region from different species revealed high sequence similarity and showed that the STIL-CC sequence conforms to the general sequence properties of left-handed coiled-coils (which is the most commonly observed type of coiled coils) (Mason and Arndt, 2004) (Figure 31b). Specifically, the STIL-CC sequence can be divided into five heptad repeats (labeled H1-H5) (Figure 31b), i.e., patterns of hydrophilic and hydrophobic residues that are periodically repeated every seven residues. The seven residues within each heptad repeat are denoted a, b, c, d, e, f, and g on one helix, and a', b', c', d', e', f', and g' on the other (Figure 31c). The residues at the positions a and d are predominantly nonpolar (e.g. leucine, valine, or isoleucine) and form the hydrophobic interface between the two helices, thereby contributing to the stabilization of helix dimerization. On the other hand, the residues at positions e and g, as well as b, c, and f, are solvent-exposed and hence predominantly polar (Mason and Arndt, 2004) (Figure 31c).

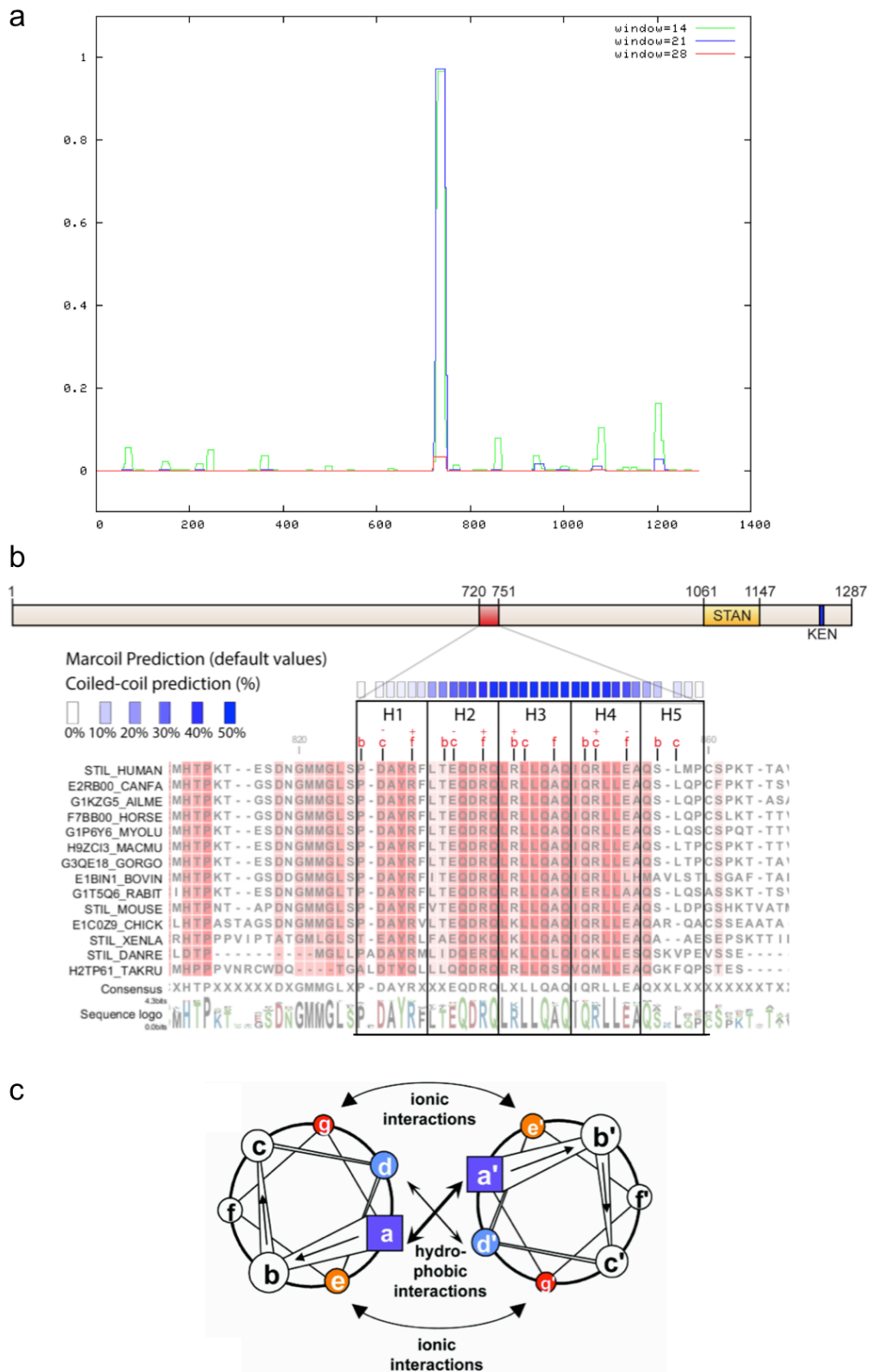


**Figure 31. Analysis of the STIL-CC sequence (residues 720-751)**

a) Computational prediction of the coiled-coil segment in the central region of STIL. The amino acid sequence of human STIL (1-1287) was analyzed using the COILS program (Lupas et al., 1991). b) Top: Schematic representation of the human STIL protein. The CC motif (residues 720-751) is depicted in red (STAN domain, yellow; KEN box, blue). Bottom: Alignment of STIL-CC motif sequences from different

species (ClustalW) to illustrate sequence similarity as well as the coiled-coil features of the STIL-CC motif (residues 720-751 of human STIL). The sequence is divided into five heptad repeats H1-H5, the residues of which are designated a-g (only the b, c, and f residues are marked on top in red). The CC probability (according to MARCOIL prediction) is depicted in blue on top of the alignment. c) Schematic representation of a parallel dimeric coiled-coil (adapted from Mason and Arndt, 2004). The residues are designated a-g in the left helix and a'-g' in the right helix. The hydrophobic core (a/a' and d/d') and the hydrophilic interactions are shown.

#### 4.3.9 Mutational analysis of STIL-CC residues at positions b, c, and f

Given the well-defined amino acid arrangement of coiled-coil sequences (Mason and Arndt, 2004) (Figure 31b,c), we next aimed at comparing the contribution of selected residues within STIL-CC to PLK4-PB3 binding versus STIL self-association. For this purpose, we used site-directed mutagenesis to generate five STIL-CC mutants in which we introduced alanine residues at the positions b, c and f within a heptad repeat (mutants CC\_H1 to CC\_H5) (Table 2): CC\_H1 (P720A, D721A, R724A), CC\_H2 (T727A, E728A, R731A), CC\_H3 (R734A, L735A), CC\_H4 (Q741A, R742A, E745A), CC\_H5 (S748A, L749A). We anticipated that these mutations of the b, c, and f residues would specifically interfere with PB3 binding and would not affect the self-association of STIL, as the latter is expected to be mediated via the predominantly hydrophobic residues at positions a and d (Figure 31c).

**Table 2. STIL-CC b/c/f mutants generated via site-directed mutagenesis**

Overview of the STIL-CC mutants harboring alanine substitutions at positions b, c and f in the respective heptad repeats. On the left, the numbers of the amino acids (AA) spanning STIL-CC (720-751) as well as the positions (a-g) in the heptad repeats (H1-H5) are indicated. The STIL-CC variants are termed CC\_WT (wild-type), CC\_H1 (P720A, D721A, R724A), CC\_H2 (T727A, E728A, R731A), CC\_H3 (R734A, L735A), CC\_H4 (Q741A, R742A, E745A), CC\_H5 (S748A, L749A).

AA		CC_WT	CC_H1	CC_H2	CC_H3	CC_H4	CC_H5
720	b	P	A	P	P	P	P
721	c	D	A	D	D	D	D
722	d	A	A	A	A	A	A
723	e	Y	Y	Y	Y	Y	Y
724	f	R	A	R	R	R	R
725	g	F	F	F	F	F	F
726	a	L	L	L	L	L	L
727	b	T	T	A	T	T	T
728	c	E	E	A	E	E	E
729	d	Q	Q	Q	Q	Q	Q

730	e	<b>D</b>	D	D	D	D	D
731	f	<b>R</b>	R	<b>A</b>	R	R	R
732	g	<b>Q</b>	Q	Q	Q	Q	Q
733	a	<b>L</b>	L	L	L	L	L
734	b	<b>R</b>	R	R	<b>A</b>	R	R
735	c	<b>L</b>	L	L	<b>A</b>	L	L
736	d	<b>L</b>	L	L	L	L	L
737	e	<b>Q</b>	Q	Q	Q	Q	Q
738	f	<b>A</b>	A	A	<b>A</b>	A	A
739	g	<b>Q</b>	Q	Q	Q	Q	Q
740	a	<b>I</b>	I	I	I	I	I
741	b	<b>Q</b>	Q	Q	Q	<b>A</b>	Q
742	c	<b>R</b>	R	R	R	<b>A</b>	R
743	d	<b>L</b>	L	L	L	L	L
744	e	<b>L</b>	L	L	L	L	L
745	f	<b>E</b>	E	E	E	<b>A</b>	E
746	g	<b>A</b>	A	A	A	A	A
747	a	<b>Q</b>	Q	Q	Q	Q	Q
748	b	<b>S</b>	S	S	S	S	<b>A</b>
749	c	<b>L</b>	L	L	L	L	<b>A</b>
750	d	<b>M</b>	M	M	M	M	M
751	e	<b>P</b>	P	P	P	P	P

To analyze the impact of the alanine mutations on STIL-CC self-association, we co-transfected HEK293T cells with plasmids encoding FLAG-EGFP- and HA-S-EGFP-tagged versions of WT and mutant STIL-CC. The cell extracts were used for anti-HA co-immunoprecipitations that were analyzed via immunoblotting, revealing that the STIL-CC mutants did not show significantly altered self-interaction (Figure 32a). To examine the ability of the STIL-CC mutants to bind PB3, the mutants were co-expressed with HA-S-EGFP-PB3, and the cell extracts were processed for anti-HA co-immunoprecipitations followed by Western blot analysis. Unexpectedly, we detected no reduction in PB3 binding (Figure 32b). Thus, the alanine substitutions at positions b, c and f within the heptad repeats do neither disturb STIL self-interaction nor PB3 binding.

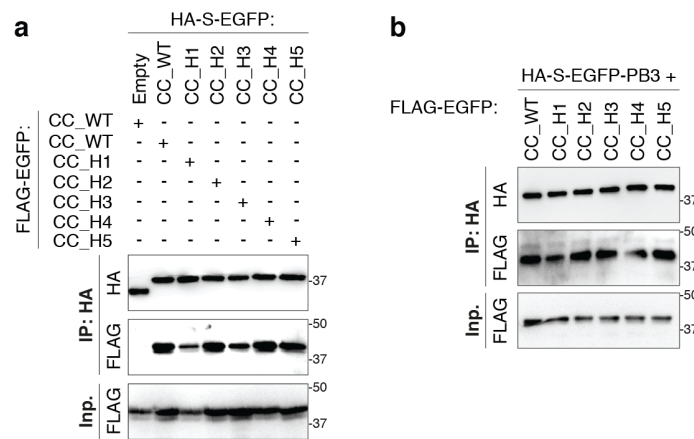


**Figure 32. Analysis of STIL-CC b/c/f mutants (CC\_H1 to CC\_H5)**

HEK293T cells were transfected with the indicated STIL-CC variants: CC\_WT (wild-type), CC\_H1 (P720A, D721A, R724A), CC\_H2 (T727A, E728A, R731A), CC\_H3 (R734A, L735A), CC\_H4 (Q741A, R742A, E745A), CC\_H5 (S748A, L749A). Cells were lysed and the cell lysates were subjected to anti-HA co-immunoprecipitations followed by Western blot analysis. a) Analysis of STIL-CC self-interaction. b) STIL-CC mutants were co-expressed with HA-S-EGFP-PB3 in order to analyze binding to PLK4-PB3.

#### 4.3.10 Structure-based analysis of the PLK4-PB3/STIL-CC complex

To characterize the PLK4-PB3/STIL-CC interaction on a structural basis, we started a collaboration with the Maier and Hiller laboratories at the Biozentrum. The structure of PLK4-PB3 (residues 884-970) was determined via solution NMR spectroscopy (Figure 33a). For this PB3 construct, no crystals diffracting to high resolution were found. But for the PLK4-PB3/STIL-CC complex, crystals diffracting to 2.6 Å resolution were obtained, and the structure was successfully solved (Figure 33b). The solution NMR structure of PB3 and the crystal structure of the PLK4-PB3/STIL-CC complex exhibit an overall PB3 configuration that comprises a six-stranded antiparallel  $\beta$ -sheet ( $\beta$ 1– $\beta$ 6) and a C-terminal  $\alpha$ -helix ( $\alpha$ 1), resembling the canonical fold of related PBs (Cheng et al., 2003; Elia et al., 2003b) (Figure 33c). STIL-CC interacts along its entire helix with PLK4-PB3 via a hydrophobic interface that is formed by both the  $\beta$ -sheet and the  $\alpha$ 1 helix of PB3. The key interacting residues on PB3 are V907, L917, V919, I926 and Y928 (on the  $\beta$ -sheet), and I948, L952, L955 and L959 (on the  $\alpha$ 1 helix). In addition, the residue L944 on the linker leading into the  $\alpha$ 1 helix is also involved (Figure 33d). On STIL-CC, the key interacting residues are leucine and isoleucine residues, such as L733, L736, I740, L743, L744. Additionally, backbone-backbone hydrogen bonds are formed between PB3<sub>G922</sub>-STIL<sub>Q739</sub> and PB3<sub>K943</sub>-STIL<sub>M750</sub>

(Figure 33d). Overall, the interaction between the STIL-CC and PB3 helices resembles a leucine zipper interaction.

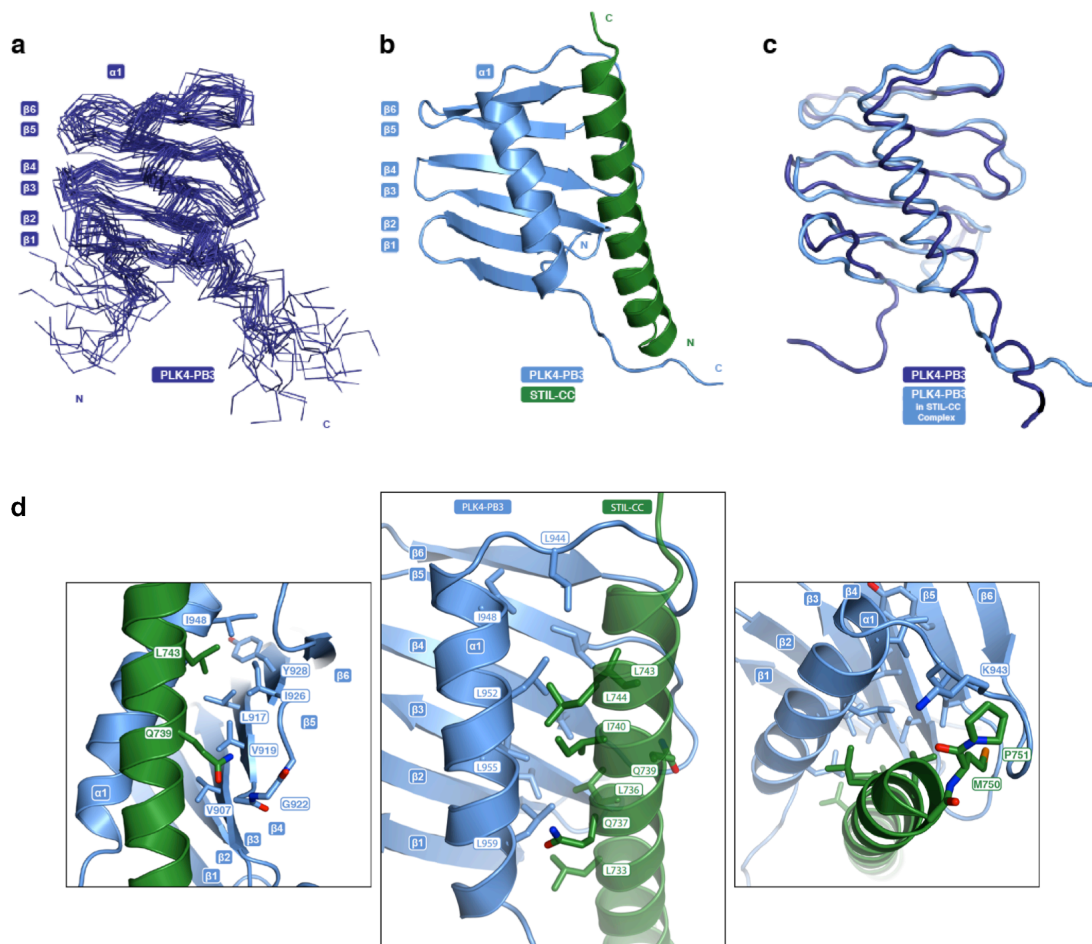


**Figure 33. Structural analysis of apo-PB3 and the PLK4-PB3/STIL-CC complex**

PB3 adopts a canonical Polo-box fold. a) Ensemble of 20 NMR conformers with the lowest target function of free PLK4-PB3 (dark blue). b) X-ray structure of the PLK4-PB3/STIL-CC complex (light blue/green). c) Comparison of the free PLK4-PB3 (dark blue) to the PLK4-PB3 (light blue) in complex with STIL-CC by structural superposition (STIL-CC not shown for clarity). d) Close-up views of the binding interface of the PLK4-PB3/STIL-CC complex. Key residues contributing to the interaction between PLK4-PB3 (blue) and STIL-CC (green) are indicated. These data and illustrations are courtesy of S. Imseng and R. Böhm. (Adapted from Arquint et al., 2015)

The above-described binding mode of the PLK4-PB3/STIL-CC interaction substantiates the results obtained with the b/c/f mutants of STIL-CC (Table 2, Figure 32), which showed that the respective alanine substitutions do not disturb PB3 binding. Interestingly, the fact that STIL-CC interacts with PB3 via hydrophobic residues at positions a and d of the CC heptads leads to the prediction that STIL might change its

oligomeric state upon binding to PLK4, as these hydrophobic residues that mediate PB3 binding are expected to mediate also the self-association (i.e., oligomerization) of STIL.

#### 4.3.11 Structure-guided mutational analysis of the PLK4/STIL-CC interaction

Based on the structural analysis of the PLK4-PB3/STIL-CC complex, we designed seven STIL mutants (M1 to M7) to assess the *in vivo* relevance of the PLK4/STIL-CC interaction. In the first mutant (M1), L733 and L743 were substituted with two large residues (L733Y and L743Y). In the second mutant M2 and in the mutants M4 to M7 we replaced hydrophobic amino acids (at the positions a and d of the coiled-coil heptads) with charged residues. In the mutant M3, we introduced the mutations Q737E and Q739K in order to abolish hydrogen bond formation (Figure 34a). To examine the effect of these mutations on PLK4 binding, we co-expressed HA-S-EGFP-tagged mutants of STIL-CC with either FLAG-tagged PLK4-L2-PB3 (residues 814-970) or the N-terminal part of PLK4 (residues 1-570) in HEK293T cells. We subjected the cell extracts to GFP-immunoprecipitation experiments and Western blot analysis, and found that all mutants except for M3 were unable to bind to PLK4-L2-PB3 (Figure 34b). Thus, the residues L733, L736, I740, and L743 are indeed crucial for STIL binding to PB3, as predicted (Figure 33). In the case of the mutant M3 (Q737E, Q739K), the disruption of hydrogen bond formation drastically reduced PB3 binding but still allowed the interaction to occur to some extent. Interestingly, all STIL-CC mutants (M1-M7) were able to bind the N-terminal part of PLK4 (encompassing residues 1-570) (Figure 34c), suggesting that STIL-CC binds to the two PLK4 regions (PB3 versus L1) in different manners and may associate with both regions simultaneously.

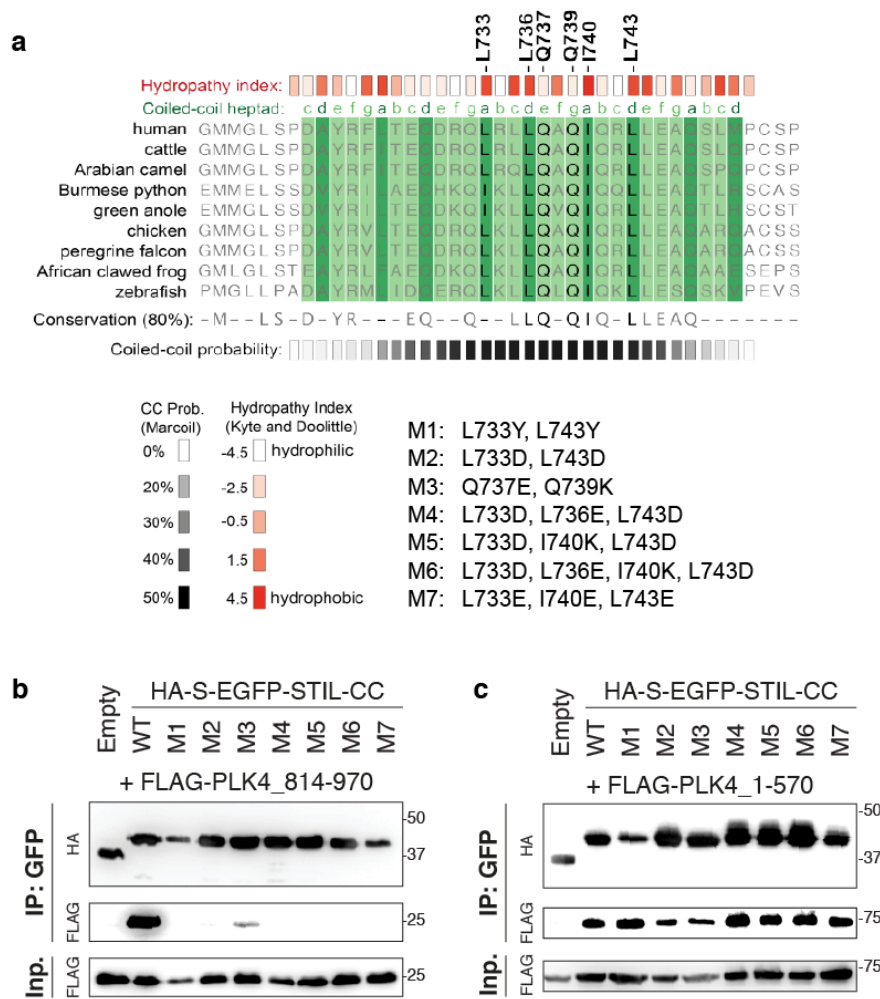


**Figure 34. Analysis of structure-based STIL-CC mutants**

a) Multiple sequence alignment of the STIL-CC region (ClustalW). Hydropathy index (Kyte-Doolittle) is depicted in red. Coiled-coil probability (according to MARCOIL prediction) is shown in black below the sequence alignment. The amino acid positions in the predicted heptad repeats are depicted in green on top of the alignment (a-g; a and d are hydrophobic residues). Residues that directly participate in the interaction with PLK4-PB3 are denoted on top. b-c) HEK293T cells were co-transfected with control, WT or mutant versions (M1-M7) of HA-S-EGFP-tagged STIL-CC and with either PLK4-L2-PB3 (residues 814-970) or N-terminal PLK4 (residues 1-570). GFP-immunoprecipitations were carried out and analyzed by Western blotting with the indicated antibodies. (Adapted from Arquint et al., 2015)

In addition to the co-immunoprecipitation experiments with the STIL mutants M1-M7, we analyzed the ability of these mutants to cause centriole amplification (i.e., centriole overduplication) upon overexpression in cells. To this end, we transfected U2OS cells with constructs of EGFP-tagged WT or mutant full-length STIL proteins (M1-M7). After overexpression for 48 hours, we analyzed the cells by immunofluorescence microscopy and determined the number of cells that contained more than four centrioles

(indicative of centriole amplification) (Figure 35a,b). Overexpression of STIL-WT resulted in centriole amplification in 54 % of cells, roughly half of them displaying a rosette-like centriole arrangement. By contrast, in the case of the STIL mutants M1 and M2 as well as M4 to M7, centriole amplification occurred only at background levels (i.e., in 11-14 % of cells). Interestingly, the STIL mutant M3 produced centriole amplification in 30 % of cells (7 % of cells exhibited a rosette-like centriole arrangement) (Figure 35a,b), reflecting the residual ability to bind PLK4-PB3 (Figure 34b). Taken together, the hydrophobic residues L733, L736, I740, and L743 within the STIL-CC motif are essential for the functionality of STIL in centriole amplification, most likely due to the importance of these residues for PLK4-PB3 binding (Figure 34b).

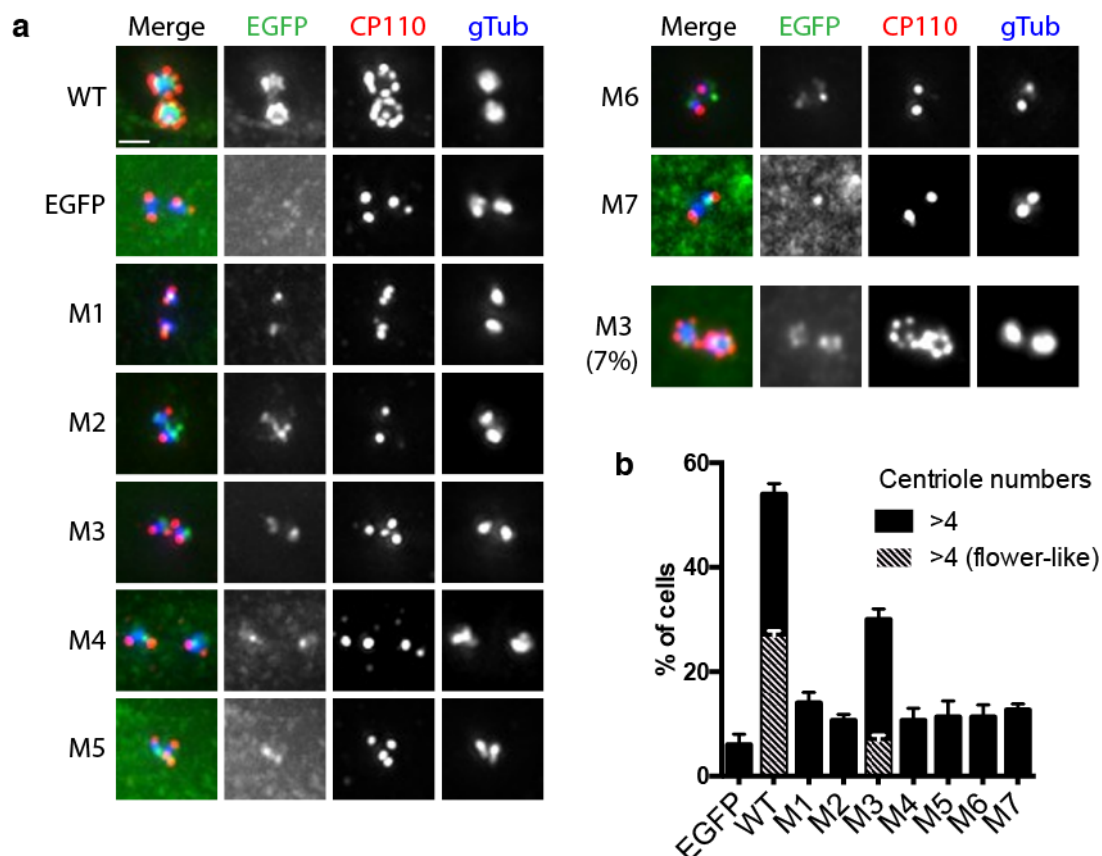


**Figure 35. Functional evaluation of structure-based STIL mutants**

a) To analyze centriole amplification, EGFP-tagged STIL-WT and mutant versions (M1-M7) were overexpressed in U2OS cells for 48 hours (EGFP was analyzed for control). Cells were fixed and stained with antibodies against CP110 (to mark centrioles) and  $\gamma$ -tubulin (to mark centrosomes) (gTub). Centriole amplification was quantified by immunofluorescence microscopy. Scale bar: 1  $\mu$ m b) Quantification of centriole amplification (percentage of transfected cells with >4 centrioles) (three independent experiments, 50 cells each). (Adapted from Arquint et al., 2015)

To test the above-mentioned assumption that STIL-CC might bind simultaneously to PB3 and L1 of PLK4, we performed a competitive binding assay. We co-immunoprecipitated GFP-STIL-CC and FLAG-tagged versions of PLK4 (residues 1-570 or residues 265-570, both containing the L1 region). Then we incubated the bead-bound complexes with bacterially purified, recombinant PB3 (in excess) or with buffer alone. The precipitates were washed and analyzed by immunoblotting (Figure 36). Equal amounts of the PLK4 proteins were bound to STIL-CC regardless of whether PB3 had been mixed with the complexes or not, indicating that PB3 does not interfere with the STIL-CC/PLK4-L1 interaction. This finding corroborates the assumption that STIL-CC probably binds to PB3 and L1 of PLK4 in different manners.

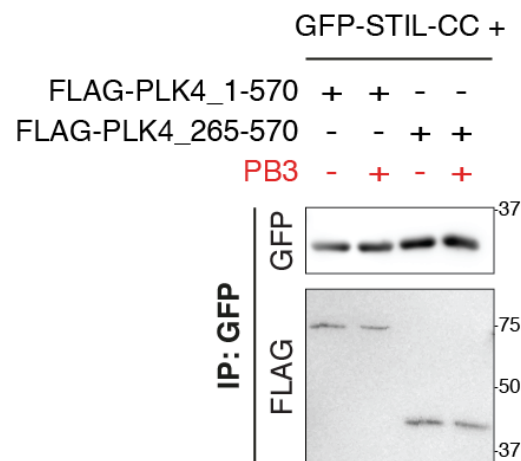


**Figure 36. PB3 appears not to interfere with the STIL-CC/PLK4-L1 interaction**

The indicated FLAG-tagged PLK4 constructs and GFP-STIL-CC were co-expressed in HEK293T cells. Cell extracts were subjected to anti-GFP co-immunoprecipiations and beads were washed and resuspended in lysis buffer in the presence or absence of bacterially purified recombinant PB3 (13  $\mu$ g) (+/- PB3, indicated in red). After 30 min at 37 °C (shaking at 1100 rpm), beads were washed and proteins were analyzed by Western blotting with anti-GFP and -FLAG antibodies.

#### 4.3.12 Analysis of PLK4 self-interactions

Our finding that STIL interacts with two separate regions within PLK4 raises the interesting prospect that STIL might regulate a possible intramolecular interaction between these two regions of PLK4. We therefore tested whether PB3 is able to interact with the N-terminal part of PLK4, spanning residues 1-570. To do so, FLAG-tagged PLK4 fragments and GFP-PB3 were co-expressed in HEK293T cells and the cell

extracts were subjected to anti-GFP co-immunoprecipitations. As revealed by Western blot analysis, PB3 brought down the PLK4 fragments comprising either the kinase domain and the linker L1 (residues 1-570) or the linker L1 alone (residues 265-570). The kinase domain itself (residues 1-271) was not brought down by PB3 (Figure 37). Thus, it is plausible that STIL might modulate a possible intramolecular interaction between PB3 and L1 of PLK4.

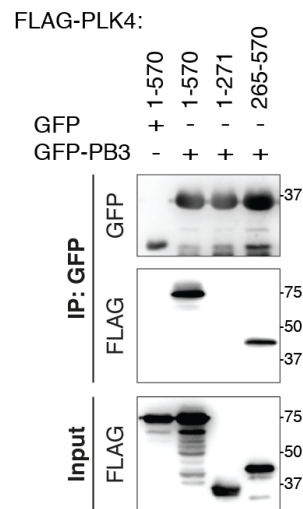


**Figure 37. Analysis of PLK4 self-interactions**

A putative interaction between PLK4-PB3 and the N-terminal part of PLK4 (residues 1-570) was analyzed. The indicated constructs were co-expressed in HEK293T cells. Cells were lysed and processed for anti-GFP co-immunoprecipitations. The precipitates were analyzed by immunoblotting with anti-FLAG and anti-GFP antibodies.

## 5 DISCUSSION

### 5.1 PLK4 interacts with Cep192 and STIL

Here we have examined the interactions of PLK4 with Cep192 and STIL in the context of centriole duplication in human cells. PLK4, the master regulator of centriole duplication, is unique among the PLK family members as it comprises three rather than two PBs within its C-terminal part (PB1-PB3) (Slevin et al., 2012). The first two PBs, PB1 and PB2 (formerly referred to as CPB), mediate recognition of the previously described binding partner Cep152/Asterless (Cizmecioglu et al., 2010; Dzhindzhev et al., 2010; Hatch et al., 2010). With regard to PB3, however, no binding partner has been described previously. Also, it has been unknown whether additional PB1-PB2 binding partner(s) might assist Cep152 in its function in centriole duplication. We now show that Cep192 directly interacts with PB1-PB2 in a similar manner as Cep152, enabling cooperation of Cep192 with Cep152 in PLK4 recruitment and centriole duplication (Sonnen et al., 2013). Furthermore, we identify STIL as the first known binding partner of PLK4-PB3. Based on structural and functional analyses of the PB3 binding mode and the identification of a second STIL-binding site within the PLK4-L1 region, we propose that STIL might regulate PLK4 stability and catalytic activity (see § 5.3-5.4). Importantly, our results largely confirm parallel, independent studies that concur to establish a central function for these interactions in centriole formation (Dzhindzhev et al., 2014; Firat-Karalar et al., 2014; Kim et al., 2013; Kratz et al., 2015; Moyer et al., 2015; Ohta et al., 2014; Park et al., 2014).

Recent genetic studies have linked mutations in PLK4, STIL, and Cep152 to microcephaly and dwarfism, highlighting a key role for these proteins in (neuro)development (Guernsey et al., 2010; Kalay et al., 2010; Kumar et al., 2009; Martin et al., 2014; Shaheen et al., 2014). Given the functional cooperation of Cep152 with Cep192 (Sonnen et al., 2013), mutations in Cep192 might affect human development in a similar manner as described for Cep152 (Guernsey et al., 2010; Kalay et al., 2010). Notably, in the case of PLK4, the disease-causing mutations have been located to PB3 and the linker L1 region (Martin et al., 2014; Shaheen et al., 2014), coinciding with the two regions that we identify here to be critical for STIL binding. It

will be interesting to find out to what extent the centriole duplication defect observed in the corresponding patient cells might result from an impaired PLK4/STIL interaction (Martin et al., 2014; Shaheen et al., 2014).

## 5.2 Exploring the PLK4/Cep192 interaction

Cep192 has initially been identified in a proteomic analysis of purified human centrosomes (Andersen et al., 2003), and has been reported to be the homolog of *C. elegans* SPD-2 (Pelletier et al., 2004). However, its role in centriole duplication has remained controversial (Gomez-Ferrera et al., 2007; Zhu et al., 2008). Here we show that Cep192 participates in the regulation of centriole duplication through its ability to directly bind PLK4 (Sonnen et al., 2013). Specifically, we demonstrate that Cep192 binds the PB1-PB2 domain of PLK4 via a short region within its N-terminus (encompassing residues 190-240), which comprises conserved patches of negatively charged amino acids (Figure 12a,c). Interestingly, the previously identified PB1-PB2 binding partner Cep152 also contains stretches of negatively charged (acidic) residues within its PLK4-binding region (amino acids 1-46) (Figure 12b,c), indicative of a similar binding mode. Deletion of the acidic region from *Drosophila* Asterless has previously been reported to abrogate binding to PLK4 (Dzhinzhev et al., 2010). Likewise, removal of the acidic region from Cep192 impairs PLK4 binding (Sonnen et al., 2013). We also show that two mutants of Cep192, M1 (D218A/D219A/E220A) and M2 (D214A/D215A/D216A), display reduced PLK4 binding affinity, albeit the effect is conspicuously weak compared to a parallel study that shows severely impaired PLK4 binding with the Cep192 double mutant D214A/D216A (Kim et al., 2013) (Figure 14). However, this disparity is probably explained by different washing conditions after immunoprecipitations. Importantly, we show that overexpression of the minimal PLK4-binding regions of both Cep192 and Cep152 causes a remarkable loss of PLK4 from centrosomes (Figure 13), corroborating the importance of the acidic residues for PLK4 binding and confirming other studies (Hatch et al., 2010; Kim et al., 2013). Collectively, our results lead to the prediction that PLK4 is recruited to centrioles by electrostatic interactions between positively charged residues of the PB1-PB2 domain (Slevin et al., 2012) and negatively charged residues on the centriolar docking proteins Cep152 and Cep192.

Recent crystal-structure analyses have confirmed the electrostatic interactions between the PB1-PB2 domain of PLK4 and the binding partners Cep192 and Cep152. Specifically, the structural analyses demonstrate that a basic patch running across the PB1-PB2 dimer binds peptides of Cep152 (1-60) and Cep192 (201-258) in opposite orientations and in a mutually exclusive manner (Park et al., 2014). Furthermore, Park and co-workers (2014) show that the Cep192- and Cep152-derived peptides interact with a lysine/arginine-enriched crater at the tip of the PB1 domain. Mutational analyses demonstrate that R684 in the lysine/arginine crater is essential for the binding of the Cep192-peptide whereas K711 is crucial for the interaction with the Cep152-peptide. K685, on the other hand, is important for binding to both Cep192- and Cep152-derived peptides (Park et al., 2014). In combination with biophysical analyses, the recent structural studies have additionally revealed that the PB1-PB2 domain forms an X-shaped end-to-end dimer (Levine and Holland, 2014; Park et al., 2014; Shimanovskaya et al., 2014), thus contradicting the previously reported side-by-side configuration (Slevin et al., 2012). In the X-shaped dimer, the PB2 domains bind end-to-end to each other and form a 12-stranded intermolecular  $\beta$ -sheet, while the PB1 domains are not directly associated with each other but are located on opposite sides of the intermolecular  $\beta$ -sheet. This X-shaped arrangement is now thought to represent the native, biologically relevant conformation, as the corresponding intermolecular interface is the only one that is present in all of the PB1-PB2 crystal structures resolved so far (Levine and Holland, 2014).

What is the functional relevance of Cep192 (and Cep152) binding to the PB1-PB2 domain of PLK4? In *Drosophila*, binding of Asterless (Cep152 ortholog (Blachon et al., 2008)) to the PB1-PB2 domain is crucial for PLK4 centriolar recruitment (Dzhinzhev et al., 2010). A possible analogous role for human Cep152 had initially been unclear (Cizmecioglu et al., 2010; Hatch et al., 2010), and regarding Cep192, a role in PLK4 recruitment had not been investigated. Meanwhile, RNAi-based depletion experiments have demonstrated that Cep152 and Cep192 cooperate in the recruitment of PLK4 to centrosomes, and hence both proteins are regarded as important for centriole duplication (Kim et al., 2013; Sonnen et al., 2013). While Cep192 alone is critical for PLK4 recruitment, a function for Cep152 in PLK4 recruitment becomes only detectable when Cep192 is depleted. Co-depletion of both Cep192 and Cep152 then leads to complete

loss of PLK4 from centrioles (Sonnen et al., 2013). Importantly, add-back of the corresponding proteins into Cep192- or Cep152-depleted cells restores centrosomal PLK4 levels back to normal, whereas the PLK4-binding deficient mutants of Cep192 and Cep152 cannot rescue the depletion phenotypes (Kim et al., 2013). Hence, PLK4 recruitment to centrosomes clearly depends on the interactions of Cep192 and Cep152 with the PB1-PB2 domain. Consistent with this view, the PB1-PB2 domain itself is both sufficient and necessary for robust centrosomal localization (Figure 10) (Habadanck et al., 2005; Slevin et al., 2012). In this context it is interesting to note that *Drosophila* SPD-2 lacks the acidic patches within its N-terminal region, in contrast to the other analyzed Cep192 family members (Figure 12), explaining why Asterless is essential for PLK4 centriolar recruitment in flies (Dzhindzhev et al., 2010). In *C. elegans*, on the other hand, SPD-2 is pivotal for ZYG-1 recruitment since no Cep152/Asterless gene is present (Delattre et al., 2006; Hodges et al., 2010; Pelletier et al., 2006).

The detailed mechanisms describing how Cep192 and Cep152 cooperate to regulate centriole duplication are only beginning to emerge. A recent study proposes a hierarchically ordered series of events, starting in early G1 phase (Park et al., 2014). At this stage, PLK4 binds Cep192 at the proximal end of the centriole, forming a ring of about 440 nm in diameter (Ohta et al., 2014; Park et al., 2014). Then, Cep192 becomes involved in the recruitment of Cep152 (Kim et al., 2013; Sonnen et al., 2013). During this process, Cep152 is thought to snatch away PLK4 molecules from the Cep192 scaffold, an idea that is supported by the observed higher PLK4-binding affinity of Cep152 compared to Cep192 (Park et al., 2014). The switch from a Cep192- to a Cep152-bound state is thought to reposition PLK4 to the outer boundary of the newly forming Cep152 ring, yielding a larger PLK4 ring structure with a diameter of about 600 nm (Park et al., 2014). Finally, at the G1-S transition, the PLK4 ring transforms into a dot that colocalizes with SAS-6 and STIL staining (Ohta et al., 2014; Park et al., 2014; Sonnen et al., 2012). These temporally and spatially coordinated events imply that PLK4 activity and localization are tightly controlled to ensure correct procentriole assembly. As Cep192 and Cep152 appear not to affect PLK4 catalytic activity (Figure 16) (Hatch et al., 2010; Park et al., 2014), they might modulate PLK4 function in another way, e.g. by changing its bound state. And, *vice versa*, PLK4 might regulate the function of Cep192 and Cep152, e.g. through phosphorylation. In fact, both Cep192

and Cep152 have been found to be substrates of PLK4 (Hatch et al., 2010; Park et al., 2014) (Figure 16).

The remarkable differences in the exact centrosome localizations of Cep152, Cep192 and PLK4 suggest that additional factors are involved in the interplay of these three proteins. Whereas Cep192 is distributed along the entire centriole walls during interphase and expands into the PCM at the onset of mitosis, Cep152 remains confined to the proximal ends of centriole cylinders throughout the cell cycle (Figure 17). Compared to the ring-shaped arrangement of Cep152, the dot-like centriolar association of PLK4 shows an even more confined pattern (Ohta et al., 2014; Park et al., 2014; Sonnen et al., 2012). These differences in the centriole associations are probably regulated by posttranslational modifications, such as phosphorylations. In fact, a recent report on the PLK1-Cep192 relationship provides an example for such a regulation. There, it has been shown that phosphorylation of Cep192 by PLK1 at the G2/M transition enables the interactions of Cep192 with PCM components to promote centrosome maturation (Joukov et al., 2014). Likewise, phosphorylation-dependent mechanisms can be expected to fine-tune the protein-protein interactions during the early events of centriole duplication. Here, the Cep192-mediated centriolar recruitment of Cep152 (Kim et al., 2013; Sonnen et al., 2013) might be fine-tuned by phosphorylation to achieve the local restriction of Cep152 at the proximal end of the centrioles while Cep192 itself remains more widely distributed. Such a phosphorylation-dependent interaction between Cep192 and Cep152 might also explain why Sonnen and colleagues (2013) could detect an interaction between these two proteins in co-immunoprecipitation experiments, whereas Kim and co-workers (2013) could not detect the interaction. Instead, Kim and co-workers (2013) showed that Cep152 and Cep192 are both capable of self-association (i.e. oligomerization), suggesting additional regulatory mechanisms.

### 5.3 Exploring the PLK4/STIL interaction

Unlike Cep192 and Cep152, which interact with PLK4 through binding to the PB1-PB2 domain, STIL interacts with PLK4 by using two different binding sites: One binding site lies within PLK4's linker region L1 (between the kinase domain and PB1-PB2), whereas the other binding site is provided by PB3 (Figure 29). Interestingly, the short, conserved STIL-CC region (residues 720-751) is both necessary and sufficient to mediate this twofold interaction with PLK4. Most importantly, STIL-CC represents the first known binding partner of PLK4-PB3, which has prompted us to thoroughly characterize this novel binding mode via biophysical, structural and *in vivo* approaches.

The NMR and crystallographic analyses of free PLK4-PB3 and the PLK4-PB3/STIL-CC complex were performed by collaborators from the Maier and Hiller laboratories at the Biozentrum. Based on these structural analyses, we show that monomeric PB3 adopts a canonical Polo-box fold (Figure 33a-c). This structure aligns readily with the structures of PLK1-PB1 and PLK1-PB2 as well as with PLK4-PB1 and PLK4-PB2 (Figure 38a). Similarly, we would assume that the PB3 structure closely resembles that of murine PB3, considering the high sequence similarity (97 %) (Sievers et al., 2011). However, the previously reported murine PB3 structure substantially differs from the one presented here (Leung et al., 2002) (Figure 38b). The murine PB3 was shown to adopt a domain-swapped dimer conformation, in which the  $\alpha$ 1-helix is shorter than observed here in human PB3. The  $\beta$ -sheet comprises three strands from one monomer and two strands from the second. Another strand is formed by the region corresponding to the C-terminal half of the  $\alpha$ 1-helix in the human structure, which is swapped between the monomers in the murine structure. Thus, the reported arrangement of murine PB3 is contradicted by the solution and crystal structures presented here, both of which suggest that the native conformation of PB3 corresponds to a canonical Polo-box fold.

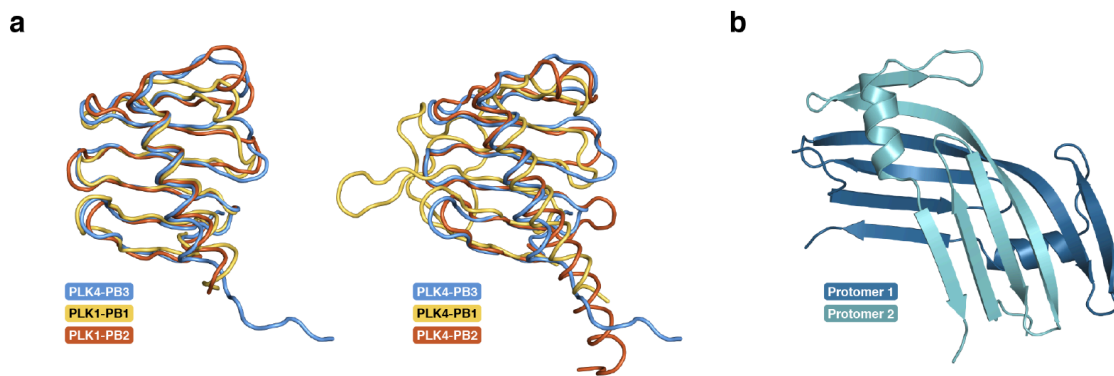


**Figure 38. Comparison of the PLK4-PB3 structure with previously determined PB structures**

a) Structural superposition of the fold of PLK4-PB3 (blue) with the folds of PB1 (1.7 Å rmsd, 72 C $\alpha$ ) and PB2 (1.3 Å rmsd, 79 C $\alpha$ ) of PLK1 (PDB accession code: 1Q4O, left) (Cheng et al., 2003) and with PB1 (2.5 Å rmsd, 66 C $\alpha$ ) and PB2 (1.4 Å rmsd, 68 C $\alpha$ ) of PLK4 (PDB accession code: 4N9J, right) (Park et al., 2014). b) Crystal structure of the domain-swapped dimer of murine PLK4-PB3 (Leung et al., 2002). This figure is courtesy of S. Imseng. (Reproduced from Arquint et al., 2015)

The PLK4-PB3/STIL-CC binding has nanomolar affinity and occurs in a direct manner with a 1:1 stoichiometry (Figure 29e). Crystal-structure analysis of the PLK4-PB3/STIL-CC complex has revealed a leucine zipper-type coiled-coil interaction. The binding is mediated by hydrophobic contacts of the STIL-CC helix to the  $\alpha$ 1-helix and central  $\beta$ -sheet of PB3. Key interacting amino acids on STIL are leucine and isoleucine residues (L733, L736, I740, L743, L744), which are oriented towards the hydrophobic surface of PB3. Interestingly, the PLK4-PB3/STIL-CC interaction reveals a novel binding mode compared to previously described Polo-box interactions (Figure 39a). In PLK1, the PBD generally binds to target proteins after their phosphorylation on Ser/Thr sites within a consensus motif (Ser-[pSer/pThr]-[Pro/X]) (Elia et al., 2003a), although phospho-independent binding has also been described, e.g. in the context of Map205 (Archambault et al., 2008; Xu et al., 2013) (Figure 39a). In the case of PLK4, the PB1-PB2 domain binds Cep192- and Cep152-derived peptides in a phospho-independent and mutually exclusive manner, through a binding interface that extends along both PB1 and PB2 (Park et al., 2014) (Figure 39a). Our data suggest that the PLK4-PB3/STIL-CC binding also occurs in a phospho-independent manner and, specifically, that the binding does not require phosphorylation by PLK4 (Figure 23). Ohta and co-workers (2014), in contrast, suggest that PLK4 kinase activity is required for the interaction between STIL and PLK4 (as judged based on yeast-two-hybrid assays), but because phosphorylation

of STIL itself did not appear to be critical, they propose that PLK4 autophosphorylation might be required for altering PLK4's oligomeric state to enable the interaction. Further experimentation will be necessary to clarify this issue. Strikingly, the binding of STIL-CC to PB3 closely resembles an intramolecular interaction within PLK1 (Figure 39b). In PLK1, PB2 binds to the Polo-cap (Pc), an N-terminal extension of PB1, which determines the relative orientation of PB1 and PB2 (Elia et al., 2003b). The Pc helix is shorter than the STIL-CC helix, but it forms a leucine-zipper interaction with the  $\alpha$ 1-helix of PLK1-PB2 that is very similar to the one formed by STIL-CC with the  $\alpha$ 1-helix of PLK4-PB3 (Figure 39b).

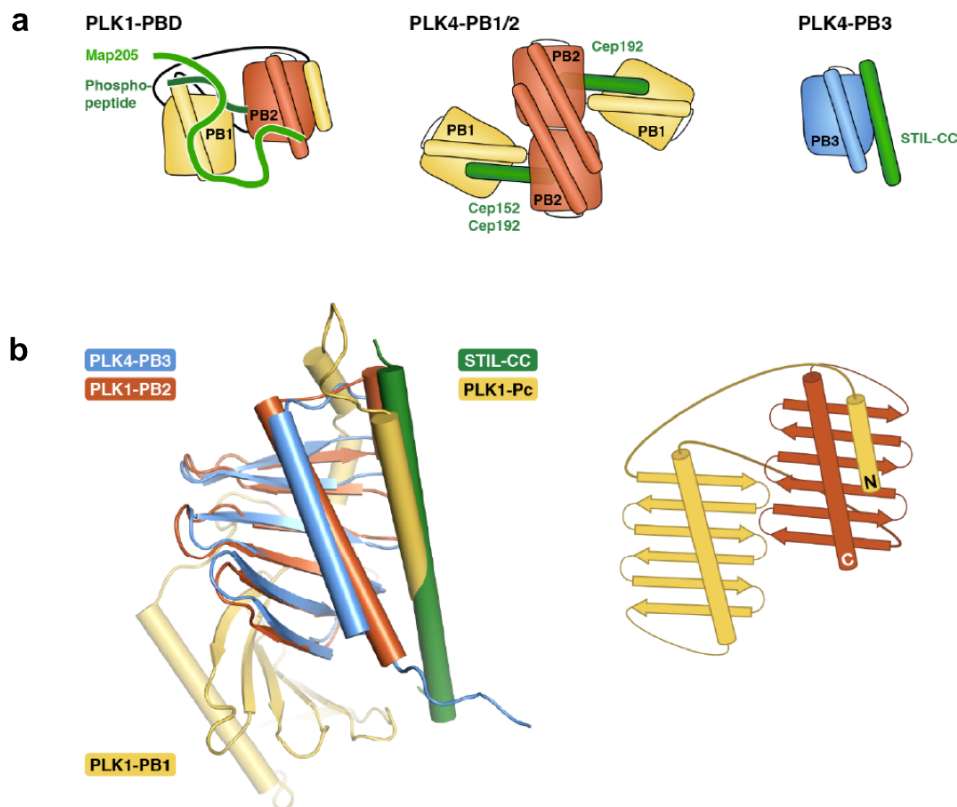


**Figure 39. Characterization of the PLK4-PB3/STIL-CC binding mode**

a) Schematic illustrations to compare the PLK4-PB3/STIL-CC binding mode (on the right) with previously observed binding modes of Polo-boxes (Park et al., 2014; Shimanovskaya et al., 2014; Xu et al., 2013; Cheng et al., 2003; Elia et al., 2003b). b) Binding of STIL-CC to PB3 closely resembles an intramolecular interaction within PLK1. On the left: Structural superposition of PLK4-PB3 (light blue) onto PB2 (orange) in the PLK1-PB1/2 structure. The bound STIL-CC peptide (green) occupies the same position on PLK4-PB3 as the Polo-cap helix (PLK1-Pc, yellow) in the PLK1-PB1/2 structure. On the right: Schematic representation of the relative orientation of PLK1-PB1 and PLK1-PB2 and the position of the PLK1-Pc (Elia et al., 2003b). These illustrations are courtesy of S. Imseng. (Reproduced from Arquint et al., 2015)

From the *in vivo* perspective, our data reveal a pivotal role for the PLK4/STIL interaction in centriole biogenesis, similar to conclusions drawn from other, independent studies (Dzhindzhev et al., 2014; Moyer et al., 2015; Ohta et al., 2014; Kratz et al., 2015). Surprisingly, however, the other studies show no involvement of PB3 in the PLK4/STIL interaction. Ohta and co-workers (2014) proposed that PB1 and PB2, but not PB3, are important for STIL binding, and Kratz and colleagues (2015) claimed that neither of the PBs is sufficient for the interaction. However, we have established the requirement for PB3 not only on a biophysical and structural basis but also on a functional level *in vivo*. For the *in vivo* validation of the PLK4/STIL-CC interaction, we have engineered a set of STIL-CC mutants by using structure-guided, site-directed mutagenesis to confirm the importance of the identified key residues for PB3 binding and centriole duplication. We show that the analyzed residues within STIL-CC (L733, L736, Q737, Q739, I740, L743) are indeed important for the interaction with PLK4-PB3 (Figure 34) and for centriole biogenesis (Figure 35). The inability of the STIL mutants to trigger centriole amplification could be explained by a possible failure in PLK4 activation and/or impaired SAS-6 recruitment (see below) – due to impaired PLK4-PB3 binding and/or a failure in STIL oligomerization. As the STIL-CC motif is essential for STIL oligomerization (Figure 27) (presumably tetramerization (Cottee et al., 2015)), we propose that PB3 binding to STIL-CC may influence the oligomeric state of STIL, possibly affecting protein-protein interactions downstream of STIL. In future experiments, it will be interesting to examine whether the mutations in STIL that abolish the PB3 interaction also compromise the self-interaction of STIL. Although the analyzed STIL mutants are not functional in centriole duplication, they are still able to localize to centrioles, presumably because the interaction with the L1 region of PLK4 is not compromised (Figure 34c). Only when the entire CC region is deleted from the STIL protein, centriole localization of STIL is drastically reduced (Figure 28a,c). Likewise, loss of PLK4 by RNAi-mediated depletion severely impairs STIL localization to centrioles (Figure 21a,c), indicating that the PLK4/STIL-CC interaction is crucial for STIL recruitment to centrosomes. Stable centriolar localization of STIL depends on further interactions involving the STAN domain and C-terminal region of STIL, as well as SAS-6 (Arquint and Nigg, 2014; Moyer et al., 2015).

It has previously been shown that STIL and SAS-6 largely depend on each other for robust centrosomal localization (Arquint et al., 2012; Tang et al., 2011; Vulprecht et al., 2012). We have observed in addition that both STIL and SAS-6 require the presence of PLK4 to localize to the centrosome (Figure 21) (Strnad et al., 2007; Tang et al., 2011). These interdependencies for centrosomal localization clearly hint at an intricate functional cooperation between STIL, SAS-6 and PLK4 in the early phase of procentriole assembly, most likely in cartwheel assembly. Recent evidence indicates that PLK4-mediated phosphorylation of residues in the STIL STAN domain facilitates the formation of STIL-SAS-6 complexes, which enables efficient centriolar targeting of STIL and SAS-6 and centriole assembly (Dzhindzhev et al., 2014; Moyer et al., 2015; Ohta et al., 2014; Kratz et al., 2015). In agreement with these findings, we show that PLK4 binds and phosphorylates STIL (Figure 22c; Arquint et al., 2015), which facilitates the interaction between STIL and SAS-6 (Figure 24).

While PLK4 clearly affects STIL (and SAS-6) centriolar localization and function, our data also imply that, conversely, STIL modulates the localization and function of PLK4. Specifically, we propose that STIL stabilizes PLK4 at the site of procentriole assembly (Figure 28d-g), in line with a recent report (Ohta et al., 2014). In addition, we suggest that STIL might relieve PLK4 autoinhibition and thereby trigger kinase activation (see also Klebba et al., 2015; Moyer et al., 2015). In *Drosophila*, PLK4 autoinhibition is relieved after homodimerization via a mechanism that is thought to require L1 autophosphorylation, PB3, and possibly another yet unknown binding partner (Klebba et al., 2015). The binding partner STIL represents a prime candidate for a regulator of PLK4 kinase activity because it is capable of binding both PB3 and L1, thereby possibly controlling the conformational state of PLK4 through regulating intramolecular interactions. Our mutational analyses suggest that STIL-CC is able to simultaneously interact with both PB3 and L1, as the STIL-CC mutants that are deficient in PB3 binding still can bind L1 (Figure 34). This notion is corroborated by the apparent absence of any predicted Polo-box folds or other domains enabling coiled-coil interactions within the L1 sequence, indicative of distinct binding modes for PB3/STIL-CC versus L1/STIL-CC. Furthermore, supporting the view that STIL may activate PLK4, we show that PLK4 protein levels are remarkably increased upon depletion of STIL (Figure 22a,b). This observation suggests that, in the absence of STIL, PLK4 is

inactive and thus protected from degradation via the SCF- $\beta$ TrCP proteasomal pathway (as this process requires PLK4 activity for *trans*-autophosphorylation in order to trigger  $\beta$ TrCP binding) (Guderian et al., 2010). On the other hand, once STIL is present, the STIL-CC interactions with PB3 and L1 of PLK4 might cause activation and, simultaneously, stabilization of the kinase, enabling accumulation of active PLK4 at the site of procentriole formation. Further experimentation is required to examine this intriguing idea in more detail. It will be most important to first determine the *in vivo* relevance of the L1/STIL-CC interaction and to clarify whether STIL-CC interacts simultaneously with both PB3 and L1.

As discussed above, the PB3 domain might regulate PLK4's catalytic activity, in contrast to the PB1-PB2 domain, which appears to mainly control PLK4 localization. In fact, whereas PB1-PB2 is pivotal for the centriolar localization of PLK4, the single PB3 domain has rather weak centrosome targeting ability (this study; Slevin et al., 2012). Accordingly, deletion of the PB1-PB2 domain abolishes PLK4 centriolar localization and functionality in centriole duplication, whereas removal of the single PB3 domain does not affect the capacity of PLK4 to drive centriole amplification upon overexpression in cells (Habadanck et al., 2005) (however, binding of truncated PLK4 to endogenous PLK4 might have accounted for functionality in these experiments). Another difference between PB1-PB2 and the PB3 domain concerns their ability to dimerize. Whereas the PB1-PB2 domain clearly participates in PLK4 dimerization, which promotes PLK4 *trans*-autophosphorylation (Klebba et al., 2015; Slevin et al., 2012), the *in vivo* relevance of a PB3-PB3 dimer is so far less clear. Although dimerization has been reported to occur in the case of murine and human PB3 (Leung et al., 2002; Park et al., 2014), a recent study on *Drosophila* PLK4 explicitly claims that PB3 does not dimerize (Klebba et al., 2015). Further experimentation is required to assess a possible function of PB3 dimerization/oligomerization.

#### **5.4 Speculative model for the initial steps of procentriole assembly**

In summary, our data suggest a speculative model for the initial steps of procentriole assembly (Figure 40). According to this model, PLK4 is first targeted to the proximal end of centrioles through interactions with the scaffold proteins Cep192 and Cep152.

The recruitment of PLK4 is mediated by electrostatic interactions between positively charged residues on the PB1-PB2 domain and acidic amino acids within the N-terminal regions of Cep152 and Cep192 (this study; Kim et al., 2013; Park et al., 2014; Shimanovskaya et al., 2014; Sonnen et al., 2013). At the site of procentriole assembly, PLK4 binds STIL and phosphorylates residues of the STIL STAN domain, thereby promoting STIL-SAS-6 complex formation, SAS-6 recruitment and cartwheel assembly (Dzhindzhev et al., 2014; Moyer et al., 2015; Ohta et al., 2014; Kratz et al., 2015). In parallel, PLK4-mediated phosphorylation of STIL might alter the oligomeric state of STIL and thus affect the capacity of STIL to bind other centriolar proteins. We speculate that binding of STIL to PB3 and L1 of PLK4 (via STIL-CC) relieves the autoinhibited state of PLK4 and thereby causes PLK4 activation and *trans*-autophosphorylation (see also Klebba et al., 2015; Moyer et al., 2015). Furthermore, we propose that STIL-bound PLK4 is protected against  $\beta$ TrCP-mediated degradation and thus stabilized at the site of procentriole formation (Figure 28d-g; Ohta et al., 2014). The stabilization of PLK4 might result from STIL binding to the L1 region and consequential shielding of the phosphorylated DSG motif from recognition by the SCF- $\beta$ TrCP E3 ubiquitin ligase complex (Guderian et al., 2010; Holland et al., 2010b). Concerning the observed increase in PLK4 levels upon depletion of STIL (Figure 22a,b), we suggest that, in the absence of STIL, PLK4 is inactive and hence unable to trigger its SCF- $\beta$ TrCP-mediated degradation, which leads to an increase in the abundance of PLK4. Taken together, this model provides a possible mechanism underlying the accumulation of active PLK4 at the site of procentriole formation.

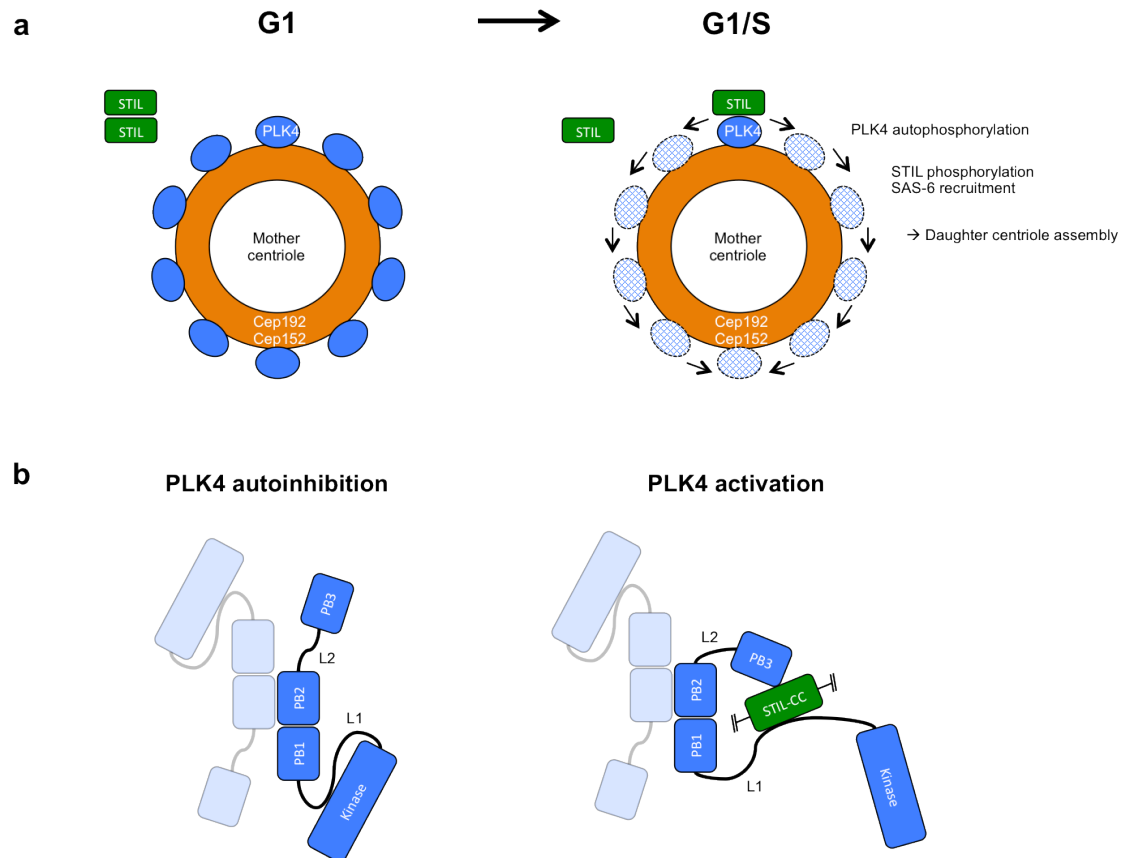


**Figure 40. Speculative model for the initial steps of procentriole assembly**

a) Schematic illustration of the centriolar events in G1 and G1/S phase. b) Close-up views of PLK4 at the respective stages. a-b) PLK4 (blue) is recruited to the proximal end of the mother centriole through binding to Cep192 and Cep152 (orange circle). PLK4 is intrinsically inactive, presumably due to autoinhibition by the linker L1 (Klebba et al., 2015). STIL (green) binding to PB3 and L1 of PLK4 (via STIL-CC) relieves the autoinhibition, resulting in PLK4 activation and autophosphorylation *in trans* (see also Moyer et al., 2015). The linker L1 is thought to be enough long and flexible so that the DSG motif can be properly positioned for phosphorylation (Levine and Holland, 2014). PLK4 phosphorylates residues of the STAN domain of STIL, thereby inducing SAS-6 recruitment and procentriole assembly (Dzhindzhev et al., 2014; Moyer et al., 2015; Ohta et al., 2014; Kratz et al., 2015). PLK4 is likely to phosphorylate additional substrates. Activated PLK4 also phosphorylates adjacent PLK4 molecules (illustrated by the arrows), inducing their  $\beta$ TrCP-mediated degradation (Guderian et al., 2010). STIL-bound PLK4 is protected against degradation and thus stabilized.

## 6 MATERIALS AND METHODS

### 6.1 Cell culture and transfections

HEK293T and U2OS cells were cultured at 37 °C and 5 % CO<sub>2</sub> in Dulbecco's modified Eagle's medium (DMEM), supplemented with 10 % heat-inactivated fetal calf serum (FCS, PAN Biotech, Aidenbach, Germany) and penicillin-streptomycin (50 U/ml, Life Technologies). The U2OS cell line for tetracycline-inducible expression of Myc-PLK4 has been described previously (Kleylein-Sohn et al., 2007). The other stable cell lines were generated according to manufacturer protocols (Invitrogen) using the Flp-In T-REx U2OS cells kindly provided by Stephen C. Blacklow (Harvard Medical School) (Malecki et al., 2006) (originally generated by Jeff Parvin (Department of Pathology, Brigham and Women's Hospital)). For selection of transgene integration, the cells were propagated in DMEM with 10 % tetracycline-free FCS (PAA), penicillin-streptomycin (50 U/ml), Hygromycin B (100 µg/ml), and Blasticidin (10 µg/ml) (all from Life Technologies). Transgene expression was induced by addition of 1 µg/ml tetracycline for 16-24 hours. PLK4, STIL, and βTrCP proteins were depleted using siRNA oligonucleotides described previously (Arquint et al., 2012; Guardavaccaro et al., 2003; Habedanck et al., 2005). Plasmids and siRNA oligonucleotides were transfected using TransIT-LT1 (Mirus Bio) and Oligofectamin (Invitrogen), respectively, according to the supplier's recommendations.

### 6.2 Antibodies

The following antibodies have been described previously: Rabbit anti-Cep152 (Cep152-C (R218) and Cep152-N (R242)) (Sonnen et al., 2012), rabbit anti-Centrin-3 (Thein et al., 2007), rabbit anti-CP110 and rabbit anti-Cep192 (R238) (Schmidt et al., 2009), mouse anti-CP110 (Arquint and Nigg, 2014), mouse anti-Myc (clone 9E10) (Evan et al., 1985), mouse anti-PLK4 (93-80-4) (Guderian et al., 2010), mouse anti-SAS-6, rabbit anti-Cep135, rabbit anti-PLK4 (R168) (all described in Kleylein-Sohn et al., 2007), and rabbit anti-STIL (Arquint et al., 2012). Antibodies against glutamylated tubulin (GT335; mouse) were kindly provided by B. Eddé (Montpellier, France) (Wolff

et al., 1992). Mouse anti-HA antibodies (12CA5) were a gift from R. Iggo (available from Abcam).

The following antibodies were purchased: Anti-Pericentrin, mouse anti- $\alpha$ -Tubulin (T9026), mouse anti-FLAG M2, rabbit anti-FLAG (F7425) (all from Sigma-Aldrich), rabbit anti-GFP (ab290), mouse anti- $\gamma$ -tubulin (TU-30), rabbit anti-STIL (all from Abcam), goat anti-GST (#27-4577-01, GE Healthcare Life Sciences), mouse anti-His (Qiagen), rabbit anti-c-Myc (A-14, sc-789; Santa Cruz Biotechnology), mouse anti-PLK4 MABC544, clone 6H5 (Merck Millipore).

For immunofluorescence microscopy stainings, Alexa-555-, Alexa-488-, Alexa-647-labeled secondary anti-mouse and anti-rabbit antibodies were used (all from Life Technologies, Carlsbad, CA, USA). Whenever required, antibodies were directly labeled with Alexa-555, Alexa-488 and Alexa-647 fluorophores using an Antibody Labeling Kit (Molecular Probes, Life Technologies).

For Western blot analysis, the following HRP-conjugated antibodies were used: goat anti-mouse (170-6516) and goat anti-rabbit (170-6515, both from Bio-Rad Laboratories), and donkey anti-goat (sc-2020; Santa Cruz Biotechnology).

### **6.3 Plasmids and cloning**

Cloning of the following plasmids has been described previously: Myc-PLK4-WT (JW153 and HR9) (Habedanck et al., 2005), Myc-PLK4-ND, S285A/T289A (JW185) and Myc-PLK4-KD, D154A (JW155) (both described in Guderian et al., 2010), FLAG-STIL (CA37) (Arquint et al., 2012), FLAG-Cep152 1-220 (KFM69), FLAG-Cep192 1-330 (KFM117), FLAG-Cep192 (KFM114) (all described in Sonnen et al., 2013), Myc-Aurora A (EC108). Myc-PLK1 and Myc-SAS-6 (GU104) were kindly provided by A. Santamaria and G. Guderian, respectively. For generation of stable cell lines, we used the Flp-Recombinase expression vector pOG44 (COM273) (Life Technologies) and the pgLAP1 vector (Addgene plasmid #19702).

All other plasmids were cloned via the Gateway system (Life Technologies) using the pENTR/D-TOPO cloning kit (Life Technologies). Inserts for the entry vectors were generated by PCR with the Pfu Ultra II Fusion DNA polymerase (Agilent Technologies) and appropriate primers (Sigma-Aldrich) (Table 3). Plasmid purifications and DNA extractions from agarose gels were performed using the corresponding kits (Qiagen) as instructed by the supplier. The inserts in the entry vectors were verified by sequencing (Microsynth) and shuttled into the appropriate destination vectors (Table 4). Mutations in the Cep192 and STIL constructs were generated using the QuikChange II XL Site-Directed Mutagenesis Kit (Agilent Technologies) and the respective entry vectors and appropriate primers (Table 5).

**Table 3. Entry vectors generated via pENTR/D-TOPO cloning** (Entry vectors generated via site-directed mutagenesis are shown in Table 5)  
Blunt-ended PCR products were ligated into the pENTR/D-TOPO vector (Invitrogen). Insert numberings indicate amino acid positions (FL, full length; CC, coiled-coil).

Entry vector	Insert	Template DNA	Forward Primer	Reverse Primer
AG33	Cep192 1-330 (no stop codon)	KFM114	caccgaagattttcgaggatagcagaa	ttaccagaggaaaatggaacataccatc
AG38	Cep192 1-110	KFM114	caccgaagattttcgaggatagcagaa	ttaacgttgactttccacatagctcttttcta
AG39	Cep192 FL	KFM114	caccgaagattttcgaggatagcagaa	ttaatttttccaagagctcacca
AG41	Cep192 1-330	KFM114	caccgaagattttcgaggatagcagaa	ttaaccagaggaaaatggaacataccatc
AG42	Cep192 110-330	KFM114	cacctgtcaaatgctctcagcaaacagt	ttaaccagaggaaaatggaacataccatc
AG44	Cep192 1-270	KFM114	caccgaagattttcgaggatagcagaa	ttataagctaccgttttcattgctgt
AG47	Cep192 1-220	KFM114	caccgaagattttcgaggatagcagaa	ttaatcatcatcaatacatcatcagaagaatctt
AG78	Cep192 190-330	KFM114	caccagtgcactaagccacactagctt	ttaaccagaggaaaatggaacataccatc
AG84	Cep192 1-240	KFM114	caccgaagattttcgaggatagcagaa	ttatattcctggaattgccagttg
AG95	PLK4 570-820	JW153	caccagagcaagactaggggatg	tcaaggaggaggatgataaggccta
AG96	PLK4 570-708	JW153	caccagagcaagactaggggatg	tcactgtgaaaataagtgatttgggagatt
AG97	PLK4 677-820	JW153	caccaattaccagaaaaatactggcgaaaata	tcaaggaggaggatgataaggccta
AG98	PLK4 880-970	JW153	cacctgtctcctaaatcagcacaactttt	tcaatgaaaattaggagtcggattaga
AG99	PLK4 1-570	JW153	caccatggcgacctgcatcgggg	tcactgttcagaaagaggatctgagc
AG101	PLK4 814-970	JW153	caccaaggccttatcactctcctt	tcaatgaaaattaggagtcggattaga
AG102	PLK4 570-970	JW153	caccagagcaagactaggggatg	tcaatgaaaattaggagtcggattaga
AG104	Cep192 1-110 (no stop codon)	KFM114	caccgaagattttcgaggatagcagaa	ttaacgttgactttccacatagctcttttcta
AG108	Cep192 220-330	KFM114	caccgaaatgtttatgatgatcattggag	ttaaccagaggaaaatggaacataccatc
AG109	Cep192 190-240	KFM114	caccagtgcactaagccacactagctt	ttatattcctggaattgccagttg
AG129	Cep152 1-220	KFM62	cacctcattagactttggcagtggtggc	ttagccttccaatgtgtcacttct
AG130	Cep152 1-46	KFM62	cacctcattagactttggcagtggtggc	ttagaggctgcatccagcatgctc
AG137	Cep152 46-220	KFM62	cacctcctccagagctccagtat	ttagccttccaatgtgtcacttct
AG155	PLK4 1-271	JW153	caccgacacctgcatcgggga	ttatgtgaagaatttcgggacataaaa
AG204	PLK4 265-570	JW153	caccatgtcccgaattctcaaaaaaag	ttactgttcagaaagaggatctgagc
AG205	PLK4 570-880	JW153	caccagagcaagactaggggatg	ttaaagacaatcttttagactattagaaga
AG245	PLK4 1-570 (S285A/T289A)	JW185	caccatggcgacctgcatcgggg	tcactgttcagaaagaggatctgagc
CA07	STIL FL 1-1287	cDNA STIL Imagen, clone IRCMp5012H1125D	caccgagcctatatatccttttg	ttaaataaatttggtaactgtctc
CA262	STIL-CC 720-751	CA07	caccagatgcatatcggttctc	ttaggatcagagactgtgct
CA307	PLK4 880-970	JW153	caccgagaatctgtattccagggtgtctcctaaatcagcacaactttt	tcaatgaaaattaggagtcggattagaaaaca
CA78	PLK4 FL (with stop codon)	x	<i>Kindly provided by C. Arquint</i>	
LC16	PLK4 FL (no stop codon)	x	<i>Obtained from the CCSB Human ORFeome Collection (hORFeome V7.1)</i>	

**Table 4. Expression vectors used in this study**

The epitope tags are N-terminal unless otherwise stated (FL, full length; CC, coiled-coil). Insert numberings indicate amino acid positions. The EGFP tag is interchangeably referred to as EGFP or GFP in this study (vector COM201).

Expression vector	Entry vector	Insert	Tag	Destination Vector	
AG48	AG47	Cep192 1-220	EGFP	COM201	pDEST_pcDNA3.1(-)Puro/EGFP-C1
AG49	AG39	Cep192 FL	EGFP	COM201	pDEST_pcDNA3.1(-)Puro/EGFP-C1
AG49 M1	AG39 M1	Cep192-M1 (D218A, D219A, E220A)	EGFP	COM201	pDEST_pcDNA3.1(-)Puro/EGFP-C1
AG49 M2	AG39 M2	Cep192-M2 (D214A, D215A, D216A)	EGFP	COM201	pDEST_pcDNA3.1(-)Puro/EGFP-C1
AG50	AG33	Cep192 1-330	GST	COM183	pDEST-15 (GibcoBRL)
AG51	AG33	Cep192 1-330	N-terminal His-Nus-Tag, C-terminal Strep-Tag II	pET-57-DEST	Gateway Nova pET-57-DEST Vector (Novagen)
AG58	AG41	Cep192 1-330	EGFP	COM201	pDEST_pcDNA3.1(-)Puro/EGFP-C1
AG59	AG42	Cep192 110-330	EGFP	COM201	pDEST_pcDNA3.1(-)Puro/EGFP-C1
AG61	AG44	Cep192 1-270	EGFP	COM201	pDEST_pcDNA3.1(-)Puro/EGFP-C1
AG64	AG38	Cep192 1-110	EGFP	COM201	pDEST_pcDNA3.1(-)Puro/EGFP-C1
AG76	LC16	PLK4 FL (no STOP codon)	GST	COM183	pDEST-15 (GibcoBRL)
AG85	AG41	Cep192 1-330	3xFLAG	COM295	pDEST_pcDNA3.1_N3xFLAG
AG86	AG41	Cep192 1-330	GST	COM183	pDEST-15 (GibcoBRL)
AG88	AG78	Cep192 190-330	EGFP	COM201	pDEST_pcDNA3.1(-)Puro/EGFP-C1
AG94	AG84	Cep192 1-240	EGFP	COM201	pDEST_pcDNA3.1(-)Puro/EGFP-C1
AG105	AG104	Cep192 1-110	N-terminal His-Nus-Tag, C-terminal Strep-Tag II	pET-57-DEST	Gateway Nova pET-57-DEST Vector (Novagen)
AG111	AG95	PLK4 570-820	GST	COM183	pDEST-15 (GibcoBRL)
AG114	AG95	PLK4 570-820	EGFP	COM201	pDEST_pcDNA3.1(-)Puro/EGFP-C1
AG115	AG96	PLK4 570-708	EGFP	COM201	pDEST_pcDNA3.1(-)Puro/EGFP-C1
AG116	AG97	PLK4 677-820	EGFP	COM201	pDEST_pcDNA3.1(-)Puro/EGFP-C1
AG117	AG99	PLK4 1-570	EGFP	COM201	pDEST_pcDNA3.1(-)Puro/EGFP-C1
AG118	AG101	PLK4 814-970	EGFP	COM201	pDEST_pcDNA3.1(-)Puro/EGFP-C1
AG119	AG102	PLK4 570-970	EGFP	COM201	pDEST_pcDNA3.1(-)Puro/EGFP-C1
AG120	LC16	PLK4 FL (no STOP codon)	EGFP	COM201	pDEST_pcDNA3.1(-)Puro/EGFP-C1
AG121	AG95	PLK4 570-820	EGFP/TEV/S-Peptide	COM301	pgLAP1 (Addgene 19702)

Expression vector	Entry vector	Insert	Tag	Destination Vector	
AG122	AG99	PLK4 1-570	EGFP/TEV/S-Peptide	COM301	pgLAP1 (Addgene 19702)
AG123	AG101	PLK4 814-970	EGFP/TEV/S-Peptide	COM301	pgLAP1 (Addgene 19702)
AG124	AG102	PLK4 570-970	EGFP/TEV/S-Peptide	COM301	pgLAP1 (Addgene 19702)
AG127	AG108	Cep192 220-330	EGFP	COM201	pDEST_pcDNA3.1(-)Puro/EGFP-C1
AG128	AG109	Cep192 190-240	EGFP	COM201	pDEST_pcDNA3.1(-)Puro/EGFP-C1
AG131	AG129	Cep152 1-220	EGFP	COM201	pDEST_pcDNA3.1(-)Puro/EGFP-C1
AG132	AG130	Cep152 1-46	EGFP	COM201	pDEST_pcDNA3.1(-)Puro/EGFP-C1
AG138	AG137	Cep152 46-220	EGFP	COM201	pDEST_pcDNA3.1(-)Puro/EGFP-C1
AG139	AG98	PLK4 880-970	EGFP	COM201	pDEST_pcDNA3.1(-)Puro/EGFP-C1
AG171	AG99	PLK4 1-570	3xFLAG	COM295	pDEST_pcDNA3.1_N3xFLAG
AG172	AG102	PLK4 570-970	3xFLAG	COM295	pDEST_pcDNA3.1_N3xFLAG
AG173	AG95	PLK4 570-820	3xFLAG	COM295	pDEST_pcDNA3.1_N3xFLAG
AG176	AG101	PLK4 814-970	3xFLAG	COM295	pDEST_pcDNA3.1_N3xFLAG
AG177	AG98	PLK4 880-970	3xFLAG	COM295	pDEST_pcDNA3.1_N3xFLAG
AG178	CA78	PLK4 FL (with STOP codon)	3xFLAG	COM295	pDEST_pcDNA3.1_N3xFLAG
AG195	AG155	PLK4 1-271	3xFLAG	COM295	pDEST_pcDNA3.1_N3xFLAG
AG211	AG204	PLK4 265-570	3xFLAG	COM295	pDEST_pcDNA3.1_N3xFLAG
AG212	AG205	PLK4 570-880	3xFLAG	COM295	pDEST_pcDNA3.1_N3xFLAG
AG250	AG245	PLK4 1-570 (S285A/T289A)	3xFLAG	COM295	pDEST_pcDNA3.1_N3xFLAG
AG261	AG255	STIL FL L733Y_L743Y	EGFP	COM201	pDEST_pcDNA3.1(-)Puro/EGFP-C1
AG262	AG256	STIL FL L733D_L743D	EGFP	COM201	pDEST_pcDNA3.1(-)Puro/EGFP-C1
AG263	AG257	STIL FL Q737E_Q739K	EGFP	COM201	pDEST_pcDNA3.1(-)Puro/EGFP-C1
AG293	AG252	STIL-CC_L733Y_L743Y	HA-Strep-EGFP	COM299	pDEST_pcDNA3.1_N1xHA/StrepIII/EGFP
AG294	AG253	STIL-CC_L733D_L743D	HA-Strep-EGFP	COM299	pDEST_pcDNA3.1_N1xHA/StrepIII/EGFP
AG295	AG254	STIL-CC_Q737E_Q739K	HA-Strep-EGFP	COM299	pDEST_pcDNA3.1_N1xHA/StrepIII/EGFP
AG316	AG304	STIL-CC_L733D_L736E_L743D	HA-Strep-EGFP	COM299	pDEST_pcDNA3.1_N1xHA/StrepIII/EGFP
AG317	AG305	STIL-CC_L733D_I740K_L743D	HA-Strep-EGFP	COM299	pDEST_pcDNA3.1_N1xHA/StrepIII/EGFP
AG318	AG306	STIL-CC_L733D_L736E_I740K_L743D	HA-Strep-EGFP	COM299	pDEST_pcDNA3.1_N1xHA/StrepIII/EGFP

Expression vector	Entry vector	Insert	Tag	Destination Vector	
AG319	AG307	STIL-CC_L733E_I740E_L743E	HA-Strep-EGFP	COM299	pDEST_pcDNA3.1_N1xHA/StrepIII/EGFP
AG320	AG308	STIL FL L733D_L736E_L743D	EGFP	COM201	pDEST_pcDNA3.1(-)Puro/EGFP-C1
AG321	AG309	STIL FL L733D_I740K_L743D	EGFP	COM201	pDEST_pcDNA3.1(-)Puro/EGFP-C1
AG322	AG310	STIL FL L733D_L736E_I740K_L743D	EGFP	COM201	pDEST_pcDNA3.1(-)Puro/EGFP-C1
AG323	AG311	STIL FL L733E_I740E_L743E	EGFP	COM201	pDEST_pcDNA3.1(-)Puro/EGFP-C1
CA37	CA07	STIL FL 1-1287	3xFLAG	COM295	pDEST_pcDNA3.1_N3xFLAG
CA56	CA262	STIL-CC 720-751	EGFP	COM201	pDEST_pcDNA3.1(-)Puro/EGFP-C1
CA62	CA07	STIL FL 1-1287	EGFP	COM201	pDEST_pcDNA3.1(-)Puro/EGFP-C1
CA316	CA262	STIL-CC 720-751	3xFLAG-EGFP	COM307	pDEST_pcDNA3.1_N_3xFLAG_EGFP
CA317	CA339	STIL-CC_H1 (P720A, D721A, R724A)	3xFLAG-EGFP	COM307	pDEST_pcDNA3.1_N_3xFLAG_EGFP
CA318	CA340	STIL-CC_H2 (T727A, E728A, R731A)	3xFLAG-EGFP	COM307	pDEST_pcDNA3.1_N_3xFLAG_EGFP
CA319	CA341	STIL-CC_H3 (R734A, L735A)	3xFLAG-EGFP	COM307	pDEST_pcDNA3.1_N_3xFLAG_EGFP
CA320	CA342	STIL-CC_H4 (Q741A, R742A, E745A)	3xFLAG-EGFP	COM307	pDEST_pcDNA3.1_N_3xFLAG_EGFP
CA321	CA343	STIL-CC_H5 (S748A, L749A)	3xFLAG-EGFP	COM307	pDEST_pcDNA3.1_N_3xFLAG_EGFP
CA322	CA262	STIL-CC 720-751	HA-Strep-EGFP	COM299	pDEST_pcDNA3.1_N1xHA/StrepIII/EGFP
CA323	CA339	STIL-CC_H1 (P720A, D721A, R724A)	HA-Strep-EGFP	COM299	pDEST_pcDNA3.1_N1xHA/StrepIII/EGFP
CA324	CA340	STIL-CC_H2 (T727A, E728A, R731A)	HA-Strep-EGFP	COM299	pDEST_pcDNA3.1_N1xHA/StrepIII/EGFP
CA325	CA341	STIL-CC_H3 (R734A, L735A)	HA-Strep-EGFP	COM299	pDEST_pcDNA3.1_N1xHA/StrepIII/EGFP
CA326	CA342	STIL-CC_H4 (Q741A, R742A, E745A)	HA-Strep-EGFP	COM299	pDEST_pcDNA3.1_N1xHA/StrepIII/EGFP
CA327	CA343	STIL-CC_H5 (S748A, L749A)	HA-Strep-EGFP	COM299	pDEST_pcDNA3.1_N1xHA/StrepIII/EGFP
CA354	CA307	PLK4 880-970	HA-Strep-EGFP	COM299	pDEST_pcDNA3.1_N1xHA/StrepIII/EGFP

**Table 5. Entry vectors generated via site-directed mutagenesis**

Entry vector	Insert	Template DNA	Forward Primers	Reverse Primers
AG39 M1	Cep192-M1 (D218A, D219A, E220A)	AG39	ggaagattctctgatgatgatattgctgctgcaatgtttatgatgatcattggagg	cctccaaatgatcatcataaaacattgagcagcagaatcatcatcagaagaatctcc
AG39 M2	Cep192-M2 (D214A, D215A, D216A)	AG39	ccgacaagcttgaagattctctgctgctgctattgatgatgaaatgtttatgat	atcataaaacattcatcatcaatagcagcagcagaagaatctccaagcttgcgg
AG252	STIL-CC L733Y_L743Y	CA262	1) cctcacagaacaagacagacagtagactacttcaggcacagattc 2) acttcaggcacagattcagcgttatttgaagcacagtctc	1) gaatctgtgcctgaagtagtctatactgtctgtcttctgtgagg 2) gagactgtgcttccaaataacgctgaatctgtgcctgaagt
AG253	STIL-CC L733D_L743D	CA262	1) ctcacagaacaagacagacagtagactacttcaggcacagatt 2) cttcaggcacagattcagcgtgatttgaagcacagtctctgatg	1) aatctgtgcctgaagtagtctatcctgtctgtcttctgtgag 2) catcagagactgtgcttccaaatcacgctgaatctgtgcctgaag
AG254	STIL-CC Q737E_Q739K	CA262	agacagacagctaagactacttgaggcaaagattcagcgttt	aaacgctgaatcttgcctcaagtagtcttagctgtctgtct
AG255	STIL FL L733Y_L743Y	CA07	1) cctcacagaacaagacagacagtagactacttcaggcacagattc 2) acttcaggcacagattcagcgttatttgaagcacagtctc	gaatctgtgcctgaagtagtctatactgtctgtcttctgtgagg gagactgtgcttccaaataacgctgaatctgtgcctgaagt
AG256	STIL FL L733D_L743D	CA07	1) ctcacagaacaagacagacagtagactacttcaggcacagatt 2) cttcaggcacagattcagcgtgatttgaagcacagtctctgatg	1) aatctgtgcctgaagtagtctatcctgtctgtcttctgtgag 2) catcagagactgtgcttccaaatcacgctgaatctgtgcctgaag
AG257	STIL FL Q737E_Q739K	CA07	agacagacagctaagactacttgaggcaaagattcagcgttt	aaacgctgaatcttgcctcaagtagtcttagctgtctgtct
AG299	STIL-CC L733E	CA262	ctcacagaacaagacagacagtagactacttcaggcacagatt	aatctgtgcctgaagtagtctctctgtctgtcttctgtgag
AG303	STIL FL L733E	CA07	ctcacagaacaagacagacagtagactacttcaggcacagatt	aatctgtgcctgaagtagtctctctgtctgtcttctgtgag
AG304	STIL-CC L733D_L736E_L743D	AG253	acagaacaagacagacagtagactagagcaggcacagattcagc	gctgaatctgtgcctgctctagtctatcctgtctgtcttctgt
AG305	STIL-CC L733D_I740K_L743D	AG253	agactacttcaggcacagaagcagcgtgatttgaagcac	gtgcttccaaatcacgctgcttctgtgcctgaagtagtct
AG306	STIL-CC L733D_L736E_I740K_L743D	AG253	cagaacaagacagacagtagactagagcaggcacagaagcagcgtgatttgaagc	gcttccaaatcacgctgcttctgtgcctgctctagtctatcctgtctgttctgt
AG307	STIL-CC L733E_I740E_L743E	AG299	ggagagactacttcaggcacaggagcagcgtgatttgaagcacagtctctgatg	catcagagactgtgcttccaaatcacgctgctctgtgcctgaagtagtctcc
AG308	STIL FL L733D_L736E_L743D	AG256	acagaacaagacagacagtagactagagcaggcacagattcagc	gctgaatctgtgcctgctctagtctatcctgtctgtcttctgt
AG309	STIL FL L733D_I740K_L743D	AG256	agactacttcaggcacagaagcagcgtgatttgaagcac	gtgcttccaaatcacgctgcttctgtgcctgaagtagtct
AG310	STIL FL L733D_L736E_I740K_L743D	AG256	cagaacaagacagacagtagactagagcaggcacagaagcagcgtgatttgaagc	gcttccaaatcacgctgcttctgtgcctgctctagtctatcctgtctgttctgt
AG311	STIL FL L733E_I740E_L743E	AG303	ggagagactacttcaggcacaggagcagcgtgatttgaagcacagtctctgatg	catcagagactgtgcttccaaatcacgctgctctgtgcctgaagtagtctcc
CA339	STIL-CC_H1 (P720A, D721A, R724A)	CA262	tggaatgatgggactatctgcagctgcatatgcttctcacagaacaagac	gtcttctgtgaggaaacgcatatgagctgagatagccatattcca
CA340	STIL-CC_H2 (T727A, E728A, R731A)	CA262	cagatgcatatcgggtcctgcagcacaagacgcacagctaaactacttcagg	cctgaagtagtcttagctgtgcttctgtgcgaggaaccgatagctctg
CA341	STIL-CC_H3 (R734A, L735A)	CA262	ggttctcacagaacaagacagacagctagcagcacttcaggcacagattc	gaatctgtgcctgaagtagtcttagctgtctgtcttctgtgaggaaacc
CA342	STIL-CC_H4 (Q741A, R742A, E745A)	CA262	cagctaagactacttcaggcacagattcgggttggcagcacagtctctga	tcagagactgtgcttccaaacaaagccgaatctgtgcctgaagtagtcttagctg
CA343	STIL-CC_H5 (S748A, L749A)	CA262	ccacccttttagggcatcgcagcctgtgcttccaaacaaacg	cgtttgggaagcacaggctgcgatgcctaaagggtgg

## 6.4 Cell extracts, immunoprecipitations, and Western blotting

At 24-36 hours post-transfection, HEK293T cells were washed with PBS and lysed on ice for 30 minutes in lysis buffer containing 50 mM Tris-HCl (pH 7.4), 150 mM NaCl, 0.5 % IgePal CA630, 25 mM  $\beta$ -Glycerophosphate, 1mM Na-Vanadate, 50mM NaF, 100 nM Okadaic acid, 2mU Pefabloc SC-Protease Inhibitor (Roth), Complete Mini Protease Inhibitor (EDTA-free) (Roche). Lysates were cleared by centrifugation for 15 minutes at 13'000xg, 4 °C. For immunoprecipitations, cell extracts (2-5 mg total protein) were incubated for 2 hours at 4 °C with appropriate beads (anti-FLAG M2 Affinity Gel (Sigma-Aldrich), GFP-Trap agarose (ChromoTek), Affi-Prep protein A matrix (Bio-Rad Laboratories) crosslinked with anti-Myc 9E10 antibodies or S-protein Agarose beads (Novagen)). Immunocomplexes bound to beads were washed 4-6 times with wash buffer (50 mM Tris-HCl pH 7.4, 150-500 mM NaCl, 0.5-1 % IgePal CA630). Proteins were eluted by boiling for 5 minutes in Laemmli buffer (0.025 M Tris, 0.192 M Glycine, 0.1 % SDS) and analyzed by Western blotting. Chemiluminescence signal was detected using the SuperSignal Femto detection kit at appropriate dilutions in PBS (1:10 – 1:1) (Thermo Scientific) and LAS3000 (GE Healthcare). Mass spectrometry analysis of protein elutions was performed according to standard protocols as described previously (Mazé et al., 2014).

## 6.5 Recombinant protein purification and biochemical assays

Recombinant protein expression was induced in BL21 DE3 *E. coli* by addition of 1 mM IPTG for 18 hours at 16 °C. GST-fusion proteins were purified using Glutathione Sepharose 4B beads (GE Healthcare) and proteins expressed from the pET-57-DEST vector (Novagen) were isolated with Strep-Tactin Superflow beads (IBA GmbH, Germany), according to the manufacturer's recommendations.

GST-pulldowns were carried out by incubating the proteins for 2 hours at 4 °C in lysis buffer (supplemented with 1 mM DTT and 2  $\mu$ g/ml BSA), followed by incubation for 1 hour at 4 °C with Glutathione Sepharose 4B beads (GE Healthcare). Beads were washed four times for 5 minutes with wash buffer (50 mM Tris-HCl pH 7.4, 500 mM

NaCl, 1 % Igepal CA630). Proteins were eluted by boiling for 5 minutes in Laemmli buffer and resolved by SDS-PAGE, followed by detection via Coomassie Blue staining and immunoblotting.

For anti-Myc *in vitro* binding experiments, Myc-PLK4-WT and -KD were expressed in HEK293T cells or, alternatively, Myc-PLK4 was translated *in vitro* using the TNT-T7 quick coupled transcription/translation system (Promega) according to the manufacturer's protocol. Myc-PLK4 protein was isolated by anti-Myc immunoprecipitation in lysis buffer. Beads were washed and resuspended in lysis buffer supplemented with bacterially purified GST-Cep192 1-330 (approx. 2  $\mu$ g). After incubation for 90 minutes at 4°C, beads were washed four times with wash buffer (50 mM Tris-HCl pH 7.4, 150 mM NaCl, 0.5 % IgePal CA630). Bound proteins were eluted by boiling for 5 minutes in Laemmli buffer and analyzed by Western blotting.

*In vitro* kinase assays were carried out at 30 °C in the presence of  $\gamma$ -[<sup>32</sup>P]-ATP in kinase buffer (50 mM HEPES pH 7.0, 100 mM NaCl, 10 mM MgCl<sub>2</sub>, 5 % glycerol, 1 mM DTT). Reactions were stopped after 30 minutes by addition of Laemmli buffer. Samples were analyzed by autoradiography and Western blotting.

## 6.6 Immunofluorescence microscopy

Cells were fixed in methanol for 5 minutes at -20 °C. The staining procedure for immunofluorescence microscopy has been described before (Meraldi et al., 1999). We used a DeltaVision microscope on a Nikon TE200 base (Applied Precision), equipped with a Plan Apochromat 60x 1.42 and an APOPLAN 100x 1.4 N.A. oil-immersion objective (Olympus), and a CoolSNAP HQ2 camera (Photometrics). Serial optical sections were acquired 0.2  $\mu$ m apart along the z-axis. Image processing was done using Softworx (Applied Precision). For quantifications of STIL and PLK4 protein levels, signal intensities were measured with ImageJ and background signal intensity was subtracted. Identical image acquisition and processing settings were applied whenever measurements were compared. 3D-structured illumination microscopy was conducted using a DeltaVision OMX-Blaze microscope (as described in Sonnen et al., 2013).

## **6.7 Miscellaneous**

Coiled-coil domains in the STIL protein were scored using the COILS program ([http://www.ch.embnet.org/software/COILS\\_form.html](http://www.ch.embnet.org/software/COILS_form.html)) (Lupas et al., 1991). Protein sequence alignments were done using the software CLC Main Workbench 6.7.1 or ClustalW ([www.clustal.org](http://www.clustal.org)).

## 7 ABBREVIATIONS

All units are abbreviated according to the International Unit System.

ATP: adenosine 5'-triphosphate

$\beta$ TrCP:  $\beta$ -transducin repeat containing protein

BSA: bovine serum albumin

CC: coiled-coil

CDK: Cyclin-dependent kinase

Cep/CP: centrosomal protein

*C. elegans*: *Caenorhabditis elegans*

CP110: centrosomal protein of 110 kDa

CPAP: centrosomal P4.1-associated protein

DAPI: 4',6-diamidino-2-phenylindole

DNA: deoxyribonucleic acid

DTT: dithiothreitol

*E. coli*: *Escherichia coli*

EDTA: ethylenedinitrilotetraacetic acid

EGFP: enhanced green fluorescent protein (interchangeably referred to as GFP)

FBXW5: F-box/WD repeat-containing protein 5

FCS: fetal calf serum

GCP: gamma complex protein

GFP: (enhanced) green fluorescent protein (interchangeably referred to as EGFP)

$\gamma$ -TuRC: gamma tubulin ring complex

HCl: hydrochloric acid

HEK: human embryonic kidney

HEPES: N-2-hydroxyethylpiperazine-N'-2-ethane sulfonic acid

IP: immunoprecipitation

IPTG: isopropyl-beta-D-thiogalactopyranoside

kDa: kiloDalton

KD: kinase-dead

Mst2: mammalian sterile 20-like kinase 2

MTOC: microtubule-organizing centre

ND: non-degradable

Nedd1: neural precursor cell expressed developmentally down-regulated protein 1

Nek2A: NIMA (never in mitosis A)-related kinase 2A

PBD: polo-box domain

PBS: phosphate-buffered saline

PCM: pericentriolar material

PCR: polymerase chain reaction

PLK1: Polo-like kinase 1

PLK4: Polo-like kinase 4

SAS: spindle assembly abnormal

SDS-PAGE: sodium dodecylsulfate polyacrylamid gel-electrophoresis

SEM: standard error of the mean

3D-SIM: Three-dimensional structured illumination microscopy

siRNA: small interference ribonucleic acid

STAN: STIL/Ana2 motif

STIL: SCL/TAL1 interrupting locus protein

WB: Western Blot

WD: WD repeat

WT: wild-type

ZYG-1: zygote defective protein 1

## 8 REFERENCES

Acilan, C., and Saunders, W.S. (2008). A tale of too many centrosomes. *Cell* *134*, 572–575.

Alkuraya, F.S., Cai, X., Emery, C., Mochida, G.H., Al-Dosari, M.S., Felie, J.M., Hill, R.S., Barry, B.J., Partlow, J.N., Gascon, G.G., et al. (2011). ScienceDirect.com - The American Journal of Human Genetics - Human Mutations in NDE1 Cause Extreme Microcephaly with Lissencephaly. *The American Journal of Human Genetics* *88*, 12–12.

Andersen, J.S., Wilkinson, C.J., Mayor, T., Mortensen, P., Nigg, E.A., and Mann, M. (2003). Proteomic characterization of the human centrosome by protein correlation profiling. *Nature* *426*, 570–574.

Aplan, P.D., Lombardi, D.P., and Kirsch, I.R. (1991). Structural characterization of SIL, a gene frequently disrupted in T-cell acute lymphoblastic leukemia. *Molecular and Cellular Biology* *11*, 5462–5469.

Aplan, P., Lombardi, D., Ginsberg, A., Cossman, J., Bertness, V., and Kirsch, I. (1990). Disruption of the human SCL locus by “illegitimate” V-(D)-J recombinase activity. *Science* *250*, 1426–1429.

Archambault, V., and Glover, D.M. (2009). Polo-like kinases: conservation and divergence in their functions and regulation. *Nature Publishing Group* *10*, 265–275.

Archambault, V., D’Avino, P.P., Deery, M.J., Lilley, K.S., and Glover, D.M. (2008). Sequestration of Polo kinase to microtubules by phosphopriming-independent binding to Map205 is relieved by phosphorylation at a CDK site in mitosis. *Genes & Development* *22*, 2707–2720.

Arquint, C., and Nigg, E.A. (2014). STIL microcephaly mutations interfere with APC/C-mediated degradation and cause centriole amplification. *Curr. Biol.* *24*, 351–360.

Arquint, C.C., Sonnen, K.F.K., Stierhof, Y.-D.Y., and Nigg, E.A.E. (2012). Cell-cycle-regulated expression of STIL controls centriole number in human cells. *Journal of Cell Science* *125*, 1342–1352.

Arquint, C., Gabryjonczyk, A.-M., and Nigg, E.A. (2014). Centrosomes as signalling centres. *Philos. Trans. R. Soc. Lond., B, Biol. Sci.* *369*.

Arquint, C., Gabryjonczyk, A.-M., Imseng, S., Böhm, R., Sauer, E., Hiller, S., Nigg, E.A., and Maier, T. (2015). STIL binding to Polo-box 3 of PLK4 regulates centriole duplication. *eLife* *4*.

Azimzadeh, J., Wong, M.L., Downhour, D.M., Alvarado, A.S., and Marshall, W.F. (2012). Centrosome Loss in the Evolution of Planarians. *Science* *335*, 461–463.

- Azimzadeh, J., and Bornens, M. (2007). Structure and duplication of the centrosome. *Journal of Cell Science* *120*, 2139–2142.
- Azimzadeh, J., and Marshall, W.F. (2010). Building the centriole. *Curr. Biol.* *20*, R816–R825.
- Bahe, S., Stierhof, Y.-D., Wilkinson, C.J., Leiss, F., and Nigg, E.A. (2005). Rootletin forms centriole-associated filaments and functions in centrosome cohesion. *J Cell Biol* *171*, 27–33.
- Bahtz, R., Seidler, J., Arnold, M., Haselmann-Weiss, U., Antony, C., Lehmann, W.D., and Hoffmann, I. (2012). GCP6 is a substrate of Plk4 and required for centriole duplication. *Journal of Cell Science* *125*, 486–496.
- Bakircioglu, M., Carvalho, O.P., Khurshid, M., Cox, J.J., Tüysüz, B., Barak, T., Yilmaz, S., Caglayan, O., Dincer, A., Nicholas, A.K., et al. (2011). The essential role of centrosomal NDE1 in human cerebral cortex neurogenesis. *The American Journal of Human Genetics* *88*, 523–535.
- Balczon, R., Bao, L., Zimmer, W.E., Brown, K., Zinkowski, R.P., and Brinkley, B.R. (1995). Dissociation of centrosome replication events from cycles of DNA synthesis and mitotic division in hydroxyurea-arrested Chinese hamster ovary cells. *J Cell Biol* *130*, 105–115.
- Barr, F.A., Silljé, H.H., and Nigg, E.A. (2004). Polo-like kinases and the orchestration of cell division. *Nat. Rev. Mol. Cell Biol.* *5*, 429–441.
- Barrera, J.A., Kao, L.-R., Hammer, R.E., Seemann, J., Fuchs, J.L., and Megraw, T.L. (2010). CDK5RAP2 regulates centriole engagement and cohesion in mice. *Developmental Cell* *18*, 913–926.
- Basto, R., Brunk, K., Vinadogrova, T., Peel, N., Franz, A., Khodjakov, A., and Raff, J.W. (2008). Centrosome Amplification Can Initiate Tumorigenesis in Flies. *Cell* *133*, 1032–1042.
- Basto, R., Lau, J., Vinogradova, T., Gardiol, A., Woods, C.G., Khodjakov, A., and Raff, J.W. (2006). Flies without Centrioles. *Cell* *125*, 1375–1386.
- Berdnik, D., and Knoblich, J.A. (2002). *Drosophila* Aurora-A Is Required for Centrosome Maturation and Actin-Dependent Asymmetric Protein Localization during Mitosis. *Current Biology* *12*, 640–647.
- Bettencourt-Dias, M., and Glover, D.M. (2007). Centrosome biogenesis and function: centrosomics brings new understanding. *Nature Reviews Molecular Cell* ....
- Bettencourt-Dias, M., Rodrigues-Martins, A., Carpenter, L., Riparbelli, M., Lehmann, L., Gatt, M.K., Carmo, N., Balloux, F., Callaini, G., and Glover, D.M. (2005). SAK/PLK4 is required for centriole duplication and flagella development. *Curr. Biol.* *15*, 2199–2207.
- Bettencourt-Dias, M., Hildebrandt, F., Pellman, D., Woods, G., and Godinho, S.A.

- (2011). Centrosomes and cilia in human disease. *Trends in Genetics* 27, 307–315.
- Blachon, S., Gopalakrishnan, J., Omori, Y., Polyanovsky, A., Church, A., Nicastro, D., Malicki, J., and Avidor-Reiss, T. (2008). *Drosophila* asterless and Vertebrate Cep152 Are Orthologs Essential for Centriole Duplication. *Genetics* 180, 2081–2094.
- Blagden, S.P., and Glover, D.M. (2003). Polar expeditions--provisioning the centrosome for mitosis. *Nature Cell Biology* 5, 505–511.
- Blow, J.J., and Dutta, A. (2005). Preventing re-replication of chromosomal DNA. *Nature Publishing Group* 6, 476–486.
- Bobinnec, Y. (1998). Centriole Disassembly In Vivo and Its Effect on Centrosome Structure and Function in Vertebrate Cells. *The Journal of Cell Biology* 143, 1575–1589.
- Bornens, M. (2012). The Centrosome in Cells and Organisms. *Science* 335, 422–426.
- Boveri, T. (1887). Ueber die Befruchtung der Eier von *Ascaris megalocephala*. *Sitzungsberichte Der Gesellschaft Für Morphologie Und Physiologie in München* 3, 394–443.
- Boveri, T. (1914). Zur Frage der Entstehung maligner Tumore. (English Translation: *The Origin of malignant Tumors*, Williams and Wilkins, Baltimore, Maryland, 1929).
- Cao, L.G., and Wang, Y.L. (1996). Signals from the spindle midzone are required for the stimulation of cytokinesis in cultured epithelial cells. *Molecular Biology of the Cell* 7, 225–232.
- Chan, J.Y. (2011). A Clinical Overview of Centrosome Amplification in Human Cancers. *International Journal of Biological Sciences* 7, 1122.
- Chang, J., Cizmecioglu, O., Hoffmann, I., and Rhee, K. (2010). PLK2 phosphorylation is critical for CPAP function in procentriole formation during the centrosome cycle. *The EMBO Journal* 29, 2395–2406.
- Cheng, K.-Y.K., Lowe, E.D.E., Sinclair, J.J., Nigg, E.A.E., and Johnson, L.N.L. (2003). The crystal structure of the human polo-like kinase-1 polo box domain and its phosphopeptide complex. *Embo J* 22, 5757–5768.
- Cizmecioglu, O., Arnold, M., Bahtz, R., Settele, F., Ehret, L., Haselmann-Weiß, U., Antony, C., and Hoffmann, I. (2010). Cep152 acts as a scaffold for recruitment of Plk4 and CPAP to the centrosome. *The Journal of Cell Biology* 191, 731–739.
- Cottee, M.A., Muschalik, N., Johnson, S., Leveson, J., Raff, J.W., and Lea, S.M. (2015). The homo-oligomerisation of both Sas-6 and Ana2 is required for efficient centriole assembly in flies. *eLife* 4, e07236.
- Cunha-Ferreira, I., Bento, I., Pimenta-Marques, A., Jana, S.C., Lince-Faria, M., Duarte, P., Borrego-Pinto, J., Gilberto, S., Amado, T., Brito, D., et al. (2013). Regulation of autophosphorylation controls PLK4 self-destruction and centriole number. *Curr. Biol.*

23, 2245–2254.

Cunha-Ferreira, I., Rodrigues-Martins, A., Bento, I., Riparbelli, M., Zhang, W., Laue, E., Callaini, G., Glover, D.M., and Bettencourt-Dias, M. (2009). The SCF/Slimb ubiquitin ligase limits centrosome amplification through degradation of SAK/PLK4. *Curr. Biol.* *19*, 43–49.

Dammermann, A., Maddox, P.S., Desai, A., and Oegema, K. (2008). SAS-4 is recruited to a dynamic structure in newly forming centrioles that is stabilized by the gamma-tubulin-mediated addition of centriolar microtubules. *The Journal of Cell Biology* *180*, 771–785.

Dammermann, A., Müller-Reichert, T., Pelletier, L., Habermann, B., Desai, A., and Oegema, K. (2004). Centriole assembly requires both centriolar and pericentriolar material proteins. *Developmental Cell* *7*, 815–829.

Delattre, M. (2004). The arithmetic of centrosome biogenesis. *Journal of Cell Science* *117*, 1619–1630.

Delattre, M., Canard, C., and Gönczy, P. (2006). Sequential protein recruitment in *C. elegans* centriole formation. *Curr. Biol.* *16*, 1844–1849.

Delattre, M., Leidel, S., Wani, K., Baumer, K., Bamat, J., Schnabel, H., Feichtinger, R., Schnabel, R., and Gönczy, P. (2004). Centriolar SAS-5 is required for centrosome duplication in *C. elegans*. *Nature Cell Biology* *6*, 656–664.

Dix, C.I., and Raff, J.W. (2007). *Drosophila* Spd-2 recruits PCM to the sperm centriole, but is dispensable for centriole duplication. *Current Biology* *17*, 1759–1764.

Dodson, H., Bourke, E., Jeffers, L.J., Vagnarelli, P., Sonoda, E., Takeda, S., Earnshaw, W.C., Merdes, A., and Morrison, C. (2004). Centrosome amplification induced by DNA damage occurs during a prolonged G2 phase and involves ATM. *Embo J* *23*, 3864–3873.

Doxsey, S., McCollum, D., and Theurkauf, W. (2005). Centrosomes in cellular regulation. *Annu. Rev. Cell Dev. Biol.* *21*, 411–434.

Duncan, T., and Wakefield, J.G. (2011). 50 ways to build a spindle: the complexity of microtubule generation during mitosis. *Chromosome Res* *19*, 321–333.

Dzhindzhev, N.S., Tzolovsky, G., Lipinszki, Z., Schneider, S., Lattao, R., Fu, J., Debski, J., Dadlez, M., and Glover, D.M. (2014). Plk4 phosphorylates Ana2 to trigger Sas6 recruitment and procentriole formation. *Curr. Biol.* *24*, 2526–2532.

Dzhindzhev, N.S., Yu, Q.D., Weiskopf, K., Tzolovsky, G., Cunha-Ferreira, I., Riparbelli, M., Rodrigues-Martins, A., Bettencourt-Dias, M., Callaini, G., and Glover, D.M. (2010). Asterless is a scaffold for the onset of centriole assembly. *Nature* *467*, 714–718.

Eckerdt, F., Yamamoto, T.M., Lewellyn, A.L., and Maller, J.L. (2011). Identification of a polo-like kinase 4-dependent pathway for de novo centriole formation. *Curr. Biol.* *21*,

428–432.

Elia, A.E.H., Cantley, L.C., and Yaffe, M.B. (2003a). Proteomic screen finds pSer/pThr-binding domain localizing Plk1 to mitotic substrates. *Science* *299*, 1228–1231.

Elia, A.E.H., Rellos, P., Haire, L.F., Chao, J.W., Ivins, F.J., Hoepker, K., Mohammad, D., Cantley, L.C., Smerdon, S.J., and Yaffe, M.B. (2003b). The molecular basis for phosphodependent substrate targeting and regulation of Plks by the Polo-box domain. *Cell* *115*, 83–95.

Elliott Robbins, G.J.A.M. (1968). THE CENTRIOLE CYCLE IN SYNCHRONIZED HELA CELLS. *The Journal of Cell Biology* *36*, 329.

Evan, G.I., Lewis, G.K., Ramsay, G., and Bishop, J.M. (1985). Isolation of monoclonal antibodies specific for human c-myc proto-oncogene product. *Molecular and Cellular Biology* *5*, 3610–3616.

Feng, Y., and Walsh, C.A. (2004). Mitotic Spindle Regulation by Nde1 Controls Cerebral Cortical Size. *Neuron* *44*, 279–293.

Firat-Karalar, E.N., Rauniyar, N., Yates, J.R., III, and Stearns, T. (2014). Proximity Interactions among Centrosome Components Identify Regulators of Centriole Duplication. *Current Biology* *24*, 664–670.

Fong, C.S., Kim, M., Yang, T.T., Liao, J.-C., and Tsou, M.-F.B. (2014). SAS-6 assembly templated by the lumen of cartwheel-less centrioles precedes centriole duplication. *Developmental Cell* *30*, 238–245.

Fry, A.M. (1998). C-Nap1, a Novel Centrosomal Coiled-Coil Protein and Candidate Substrate of the Cell Cycle-regulated Protein Kinase Nek2. *The Journal of Cell Biology* *141*, 1563–1574.

Fu, J., and Glover, D.M. (2012). Structured illumination of the interface between centriole and peri-centriolar material. *Open Biology* *2*, 120104–120104.

Gadde, S., and Heald, R. (2004). Mechanisms and Molecules of the Mitotic Spindle. *Current Biology* *14*, R797–R805.

Ganem, N.J., Godinho, S.A., and Pellman, D. (2009). A mechanism linking extra centrosomes to chromosomal instability. *Nature* *460*, 278–282.

Giansanti, M.G., Bucciarelli, E., Bonaccorsi, S., and Gatti, M. (2008). *Drosophila* SPD-2 Is an Essential Centriole Component Required for PCM Recruitment and Astral-Microtubule Nucleation. *Current Biology* *18*, 303–309.

Godinho, S.A., Kwon, M., and Pellman, D. (2009). Centrosomes and cancer: how cancer cells divide with too many centrosomes. *Cancer Metastasis Rev* *28*, 85–98.

Goetz, S.C., and Anderson, K.V. (2010). The primary cilium: a signalling centre during vertebrate development. *Nat Rev Genet* *11*, 331–344.

- Gomez-Ferreria, M.A., Bashkurov, M., Mullin, M., Gingras, A.-C., and Pelletier, L. (2012). CEP192 interacts physically and functionally with the K63-deubiquitinase CYLD to promote mitotic spindle assembly. *Cc 11*, 3555–3558.
- Gomez-Ferreria, M.A., Rath, U., Buster, D.W., Chanda, S.K., Caldwell, J.S., Rines, D.R., and Sharp, D.J. (2007). Human Cep192 Is Required for Mitotic Centrosome and Spindle Assembly. *Current Biology 17*, 1960–1966.
- Gönczy, P. (2012). Towards a molecular architecture of centriole assembly. *Nature Publishing Group 13*, 425–435.
- Graser, S., Stierhof, Y.D., Lavoie, S.B., Gassner, O.S., Lamla, S., Le Clech, M., and Nigg, E.A. (2007a). Cep164, a novel centriole appendage protein required for primary cilium formation. *The Journal of Cell Biology 179*, 321–330.
- Graser, S., Stierhof, Y.-D., and Nigg, E.A. (2007b). Cep68 and Cep215 (Cdk5rap2) are required for centrosome cohesion. *Journal of Cell Science 120*, 4321–4331.
- Guardavaccaro, D., Kudo, Y., Boulaire, J., Barchi, M., Busino, L., Donzelli, M., Margottin-Goguet, F., Jackson, P.K., Yamasaki, L., and Pagano, M. (2003). Control of meiotic and mitotic progression by the F box protein beta-Trcp1 in vivo. *Developmental Cell 4*, 799–812.
- Guderian, G., Westendorf, J., Uldschmid, A., and Nigg, E.A. (2010). Plk4 trans-autophosphorylation regulates centriole number by controlling betaTrCP-mediated degradation. *Journal of Cell Science 123*, 2163–2169.
- Guernsey, D.L., Jiang, H., Hussin, J., Arnold, M., Bouyakdan, K., Perry, S., Babineau-Sturk, T., Beis, J., Dumas, N., Evans, S.C., et al. (2010). Mutations in centrosomal protein CEP152 in primary microcephaly families linked to MCPH4. *Am. J. Hum. Genet. 87*, 40–51.
- Guichard, P., Hachet, V., Majubu, N., Neves, A., Demurtas, D., Olieric, N., Flückiger, I., Yamada, A., Kihara, K., Nishida, Y., et al. (2013). Native Architecture of the Centriole Proximal Region Reveals Features Underlying Its 9-Fold Radial Symmetry. *Curr. Biol. 23*, 1620–1628.
- Habedanck, R., Stierhof, Y.-D., Wilkinson, C.J., and Nigg, E.A. (2005). The Polo kinase Plk4 functions in centriole duplication. *Nature Cell Biology 7*, 1140–1146.
- Haren, L., Stearns, T., and Lüders, J. (2009). Plk1-Dependent Recruitment of  $\gamma$ -Tubulin Complexes to Mitotic Centrosomes Involves Multiple PCM Components. *PLoS ONE 4*, e5976.
- Hatch, E.M., Kulukian, A., Holland, A.J., Cleveland, D.W., and Stearns, T. (2010). Cep152 interacts with Plk4 and is required for centriole duplication. *The Journal of Cell Biology 191*, 721–729.
- Heald, R., Tournebise, R., Blank, T., Sandaltzopoulos, R., Becker, P., Hyman, A., and Karsenti, E. (1996). Self-organization of microtubules into bipolar spindles around artificial chromosomes in *Xenopus* egg extracts. *Nature 382*, 420–425.

- Hilbert, M., Erat, M.C., Hachet, V., Guichard, P., Blank, I.D., Flückiger, I., Slater, L., Lowe, E.D., Hatzopoulos, G.N., Steinmetz, M.O., et al. (2013). *Caenorhabditis elegans* centriolar protein SAS-6 forms a spiral that is consistent with imparting a ninefold symmetry. *Proceedings of the National Academy of Sciences* *110*, 11373–11378.
- Hinchcliffe, E.H. (2001). Requirement of a Centrosomal Activity for Cell Cycle Progression Through G1 into S Phase. *Science* *291*, 1547–1550.
- Hirono, M. (2014). Cartwheel assembly. *Philos. Trans. R. Soc. Lond., B, Biol. Sci.* *369*.
- Hodges, M.E., Scheumann, N., Wickstead, B., Langdale, J.A., and Gull, K. (2010). Reconstructing the evolutionary history of the centriole from protein components. *Journal of Cell Science* *123*, 1407–1413.
- Holland, A.J., Lan, W., and Cleveland, D.W. (2010a). Centriole duplication: A lesson in self-control. *Cc* *9*, 2731–2736.
- Holland, A.J., Lan, W., Niessen, S., Hoover, H., and Cleveland, D.W. (2010b). Polo-like kinase 4 kinase activity limits centrosome overduplication by autoregulating its own stability. *J Cell Biol* *188*, 191–198.
- Inanc, B., Dodson, H., and Morrison, C.G. (2010). A centrosome-autonomous signal that involves centriole disengagement permits centrosome duplication in G2 phase after DNA damage. *Molecular Biology of the Cell* *21*, 3866–3877.
- Ishikawa, H., and Marshall, W.F. (2011). Ciliogenesis: building the cell's antenna. *Nature Publishing Group* *12*, 222–234.
- Izraeli, S., Lowe, L.A., Bertness, V.L., Good, D.J., Dorward, D.W., Kirsch, I.R., and Kuehn, M.R. (1999). The *SIL* gene is required for mouse embryonic axial development and left-right specification. *Nature* *399*, 691–694.
- Jakobsen, L., Vanselow, K., Skogs, M., Toyoda, Y., Lundberg, E., Poser, I., Falkenby, L.G., Bennetzen, M., Westendorf, J., Nigg, E.A., et al. (2011). Novel asymmetrically localizing components of human centrosomes identified by complementary proteomics methods. *The EMBO Journal* *30*, 1520–1535.
- Jord, A.I., Lemaître, A.-I., Delgehyr, N., Faucourt, M., Spassky, N., and Meunier, A. (2014). Centriole amplification by mother and daughter centrioles differs in multiciliated cells. *Nature* *516*, 104–107.
- Joukov, V., De Nicolo, A., Rodriguez, A., Walter, J.C., and Livingston, D.M. (2010). Centrosomal protein of 192 kDa (Cep192) promotes centrosome-driven spindle assembly by engaging in organelle-specific Aurora A activation. *Proceedings of the National Academy of Sciences* *107*, 21022–21027.
- Joukov, V., Walter, J.C., and De Nicolo, A. (2014). The Cep192-Organized Aurora A-Plk1 Cascade Is Essential for Centrosome Cycle and Bipolar Spindle Assembly. *Molecular Cell* *55*, 578–591.
- Kalab, P., and Heald, R. (2008). The RanGTP gradient - a GPS for the mitotic spindle.

Journal of Cell Science *121*, 1577–1586.

Kalay, E., Yigit, G., Aslan, Y., Brown, K.E., Pohl, E., Bicknell, L.S., Kayserili, H., Li, Y., Tüysüz, B., Nürnberg, G., et al. (2010). CEP152 is a genome maintenance protein disrupted in Seckel syndrome. *Nature Genetics* *43*, 23–26.

Kaltschmidt, J.A., Davidson, C.M., Brown, N.H., and Brand, A.H. (2000). Rotation and asymmetry of the mitotic spindle direct asymmetric cell division in the developing central nervous system. *Nature Cell Biology* *2*, 7–12.

Kemp, C.A., Kopish, K.R., Zipperlen, P., Ahringer, J., and O'Connell, K.F. (2004). Centrosome maturation and duplication in *C. elegans* require the coiled-coil protein SPD-2. *Developmental Cell* *6*, 511–523.

Khodjakov, A., and Rieder, C.L. (2001). Centrosomes enhance the fidelity of cytokinesis in vertebrates and are required for cell cycle progression. *J Cell Biol* *153*, 237–242.

Khodjakov, A., Cole, R.W., Oakley, B.R., and Rieder, C.L. (2000). Centrosome-independent mitotic spindle formation in vertebrates. *Curr. Biol.* *10*, 59–67.

Khodjakov, A., Rieder, C.L., Sluder, G., Cassels, G., Sibon, O., and Wang, C.-L. (2002). De novo formation of centrosomes in vertebrate cells arrested during S phase. *J Cell Biol* *158*, 1171–1181.

Kim, S., and Dynlacht, B.D. (2013). Assembling a primary cilium. *Current Opinion in Cell Biology* *25*, 506–511.

Kim, T.-S., Park, J.-E., Shukla, A., Choi, S., Murugan, R.N., Lee, J.H., Ahn, M., Rhee, K., Bang, J.K., Kim, B.Y., et al. (2013). Hierarchical recruitment of Plk4 and regulation of centriole biogenesis by two centrosomal scaffolds, Cep192 and Cep152. *Proc Natl Acad Sci U S A* *110*, E4849–E4857.

Kirkham, M., Müller-Reichert, T., Oegema, K., Grill, S., and Hyman, A.A. (2003). SAS-4 is a *C. elegans* centriolar protein that controls centrosome size. *Cell* *112*, 575–587.

Kitagawa, D., Vakonakis, I., Olieric, N., Hilbert, M., Keller, D., Olieric, V., Bortfeld, M., Erat, M.C., Flückiger, I., Gönczy, P., et al. (2011). Structural Basis of the 9-Fold Symmetry of Centrioles. *Cell* *144*, 364–375.

Klebba, J.E., Buster, D.W., McLamarrah, T.A., Rusan, N.M., and Rogers, G.C. (2015). Autoinhibition and relief mechanism for Polo-like kinase 4. *Proceedings of the National Academy of Sciences* *112*, E657–E666.

Klebba, J.E., Buster, D.W., Nguyen, A.L., Swatkoski, S., Gucek, M., Rusan, N.M., and Rogers, G.C. (2013). Polo-like kinase 4 autodeconstructs by generating its Slimb-binding phosphodegron. *Curr. Biol.* *23*, 2255–2261.

Kleylein-Sohn, J., Westendorf, J., Le Clech, M., Habedanck, R., Stierhof, Y.-D., and Nigg, E.A. (2007). Plk4-induced centriole biogenesis in human cells. *Developmental*

Cell *13*, 190–202.

Klos Dehring, D.A., Vladar, E.K., Werner, M.E., Mitchell, J.W., Hwang, P., and Mitchell, B.J. (2013). Deuterosome-mediated centriole biogenesis. *Developmental Cell* *27*, 103–112.

Kohlmaier, G., Lončarek, J., Meng, X., McEwen, B.F., Mogensen, M.M., Spektor, A., Dynlacht, B.D., Khodjakov, A., and Gönczy, P. (2009). Overly Long Centrioles and Defective Cell Division upon Excess of the SAS-4-Related Protein CPAP. *Current Biology* *19*, 1012–1018.

Kotak, S., and Gönczy, P. (2013). Mechanisms of spindle positioning: cortical force generators in the limelight. *Current Opinion in Cell Biology* *25*, 741–748.

Kratz, A.-S., Bärenz, F., Richter, K.T., and Hoffmann, I. (2015). Plk4-dependent phosphorylation of STIL is required for centriole duplication. *Biology Open* *4*, 370–377.

Kumar, A., Girimaji, S.C., Duvvari, M.R., and Blanton, S.H. (2009). Mutations in STIL, Encoding a Pericentriolar and Centrosomal Protein, Cause Primary Microcephaly. *The American Journal of Human Genetics* *84*, 286–290.

Kuriyama, R., and Boris, G.G. (1981). Centriole cycle in Chinese hamster ovary cells as determined by whole-mount electron microscopy. *J Cell Biol* *91*, 814–821.

Kuriyama, R., Dasgupta, S., and Boris, G.G. (1986). Independence of centriole formation and initiation of DNA synthesis in Chinese hamster ovary cells. *Cell Motil. Cytoskeleton* *6*, 355–362.

Kwon, M., Godinho, S.A., Chandhok, N.S., Ganem, N.J., Azioune, A., Théry, M., and Pellman, D. (2008). Mechanisms to suppress multipolar divisions in cancer cells with extra centrosomes. *Genes & Development* *22*, 2189–2203.

La Terra, S. (2005). The de novo centriole assembly pathway in HeLa cells: cell cycle progression and centriole assembly/maturation. *The Journal of Cell Biology* *168*, 713–722.

Lane, H.A., and Nigg, E.A. (1996). Antibody microinjection reveals an essential role for human polo-like kinase 1 (Plk1) in the functional maturation of mitotic centrosomes. *J Cell Biol* *135*, 1701–1713.

Lawo, S., Hasegan, M., Gupta, G.D., and Pelletier, L. (2012). Subdiffraction imaging of centrosomes reveals higher-order organizational features of pericentriolar material. *Nature Cell Biology* *14*, 1–13.

Leidel, S., and Gönczy, P. (2003). SAS-4 Is Essential for Centrosome Duplication in *C. elegans* and Is Recruited to Daughter Centrioles Once per Cell Cycle. *Developmental Cell* *4*, 431–439.

Leidel, S., and Gönczy, P. (2005). Centrosome duplication and nematodes: recent insights from an old relationship. *Developmental Cell* *9*, 317–325.

- Leidel, S., Delattre, M., Cerutti, L., Baumer, K., and Gönczy, P. (2005). SAS-6 defines a protein family required for centrosome duplication in *C. elegans* and in human cells. *Nature* *7*, 115–125.
- Leung, G.C., Hudson, J.W., Kozarova, A., Davidson, A., Dennis, J.W., and Sicheri, F. (2002). The Sak polo-box comprises a structural domain sufficient for mitotic subcellular localization. *Nat Struct Biol* *9*, 719–724.
- Levine, M.S., and Holland, A.J. (2014). Polo-like Kinase 4 Shapes Up. *Structure* *22*, 1071–1073.
- Lončarek, J., Hergert, P., and Khodjakov, A. (2010). Centriole Reduplication during Prolonged Interphase Requires Procentriole Maturation Governed by Plk1. *Current Biology* *20*, 1277–1282.
- Lončarek, J., Hergert, P., Magidson, V., and Khodjakov, A. (2008). Control of daughter centriole formation by the pericentriolar material. *Nature Cell Biology* *10*, 322–328.
- Lowery, D.M., Lim, D., and Yaffe, M.B. (2005). Structure and function of Polo-like kinases. *Oncogene* *24*, 248–259.
- Lukinavičius, G., Lavogina, D., Orpinell, M., Umezawa, K., Reymond, L., Garin, N., Gönczy, P., and Johnsson, K. (2013). Selective chemical crosslinking reveals a Cep57-Cep63-Cep152 centrosomal complex. *Curr. Biol.* *23*, 265–270.
- Lupas, A., Van Dyke, M., and Stock, J. (1991). Predicting coiled coils from protein sequences. *Science* *252*, 1162–1164.
- Lüders, J., and Stearns, T. (2007). Microtubule-organizing centres: a re-evaluation. *Nature Publishing Group* *8*, 161–167.
- Malecki, M.J., Sanchez-Irizarry, C., Mitchell, J.L., Histen, G., Xu, M.L., Aster, J.C., and Blacklow, S.C. (2006). Leukemia-associated mutations within the NOTCH1 heterodimerization domain fall into at least two distinct mechanistic classes. *Molecular and Cellular Biology* *26*, 4642–4651.
- Manandhar, G., Schatten, H., and Sutovsky, P. (2005). Centrosome reduction during gametogenesis and its significance. *Biol. Reprod.* *72*, 2–13.
- Mardin, B.R., and Schiebel, E. (2012). Breaking the ties that bind: new advances in centrosome biology. *The Journal of Cell Biology* *197*, 11–18.
- Mardin, B.R., Agircan, F.G., Lange, C., and Schiebel, E. (2011). Plk1 Controls the Nek2A-PP1 $\gamma$ ; Antagonism in Centrosome Disjunction. *Current Biology* *21*, 1145–1151.
- Martin, C.-A., Ahmad, I., Klingseisen, A., Hussain, M.S., Bicknell, L.S., Leitch, A., Nürnberg, G., Toliat, M.R., Murray, J.E., Hunt, D., et al. (2014). Mutations in PLK4, encoding a master regulator of centriole biogenesis, cause microcephaly, growth failure and retinopathy. *Nature Genetics* *46*, 1283–1292.

- Mason, J.M., and Arndt, K.M. (2004). Coiled Coil Domains: Stability, Specificity, and Biological Implications. *5*, 170–176.
- Matsumoto, Y., Hayashi, K., and Nishida, E. (1999). Cyclin-dependent kinase 2 (Cdk2) is required for centrosome duplication in mammalian cells. *Current Biology* *9*, 429–432.
- Matsuo, K., Ohsumi, K., Iwabuchi, M., Kawamata, T., Ono, Y., and Takahashi, M. (2012). Kendrin is a novel substrate for separase involved in the licensing of centriole duplication. *Curr. Biol.* *22*, 915–921.
- Mayor, T., Stierhof, Y.D., Tanaka, K., Fry, A.M., and Nigg, E.A. (2000). The Centrosomal Protein C-Nap1 Is Required for Cell Cycle-Regulated Centrosome Cohesion. *The Journal of Cell Biology* *151*, 837–846.
- Mazé, A., Glatter, T., and Bumann, D. (2014). The central metabolism regulator EIIAGlc switches *Salmonella* from growth arrest to acute virulence through activation of virulence factor secretion. *Cell Reports* *7*, 1426–1433.
- Mennella, V., Keszthelyi, B., McDonald, K.L., Chhun, B., Kan, F., Rogers, G.C., Huang, B., and Agard, D.A. (2012). Subdiffraction-resolution fluorescence microscopy reveals a domain of the centrosome critical for pericentriolar material organization. *Nature Cell Biology* *14*, 1159–1168.
- Meraldi, P.P., Lukas, J.J., Fry, A.M.A., Bartek, J.J., and Nigg, E.A.E. (1999). Centrosome duplication in mammalian somatic cells requires E2F and Cdk2-cyclin A. *Nature Cell Biology* *1*, 88–93.
- Meunier, S., and Vernos, I. (2012). Microtubule assembly during mitosis - from distinct origins to distinct functions? *Journal of Cell Science* *125*, 2805–2814.
- Moritz, M., Braunfeld, M.B., Sedat, J.W., Alberts, B., and Agard, D.A. (1995). Microtubule nucleation by gamma-tubulin-containing rings in the centrosome. *Nature* *378*, 638–640.
- Moyer, T.C., Clutario, K.M., Lambrus, B.G., Daggubati, V., and Holland, A.J. (2015). Binding of STIL to Plk4 activates kinase activity to promote centriole assembly. *The Journal of Cell Biology* *209*, 863–878.
- Nakazawa, Y., Hiraki, M., Kamiya, R., and Hirono, M. (2007). SAS-6 is a cartwheel protein that establishes the 9-fold symmetry of the centriole. *Curr. Biol.* *17*, 2169–2174.
- Nigg, E.A. (2006). Origins and consequences of centrosome aberrations in human cancers. *International Journal of Cancer* *119*, 2717–2723.
- Nigg, E.A. (2007). Centrosome duplication: of rules and licenses. *Trends Cell Biol.* *17*, 215–221.
- Nigg, E.A., and Raff, J.W. (2009). Centrioles, centrosomes, and cilia in health and disease. *Cell* *139*, 663–678.
- Nigg, E.A., and Stearns, T. (2011). The centrosome cycle: Centriole biogenesis,

- duplication and inherent asymmetries. *Nature Cell Biology* *13*, 1154–1160.
- Nigg, E.A.E. (2002). Centrosome aberrations: cause or consequence of cancer progression? *Nat Rev Cancer* *2*, 815–825.
- O'Connell, C.B., and Khodjakov, A.L. (2007). Cooperative mechanisms of mitotic spindle formation. *Journal of Cell Science* *120*, 1717–1722.
- O'Connell, K.F., Caron, C., Kopish, K.R., Hurd, D.D., Kempfues, K.J., Li, Y.J., and White, J.G. (2001). The *C-elegans zyg-1* gene encodes a regulator of centrosome duplication with distinct maternal and paternal roles in the embryo. *Cell* *105*, 547–558.
- O'Connell, K.F., Leys, C.M., and White, J.G. (1998). A genetic screen for temperature-sensitive cell-division mutants of *Caenorhabditis elegans*. *Genetics* *149*, 1303–1321.
- Ohta, M., Ashikawa, T., Nozaki, Y., Kozuka-Hata, H., Goto, H., Inagaki, M., Oyama, M., and Kitagawa, D. (2014). Direct interaction of Plk4 with STIL ensures formation of a single procentriole per parental centriole. *Nature Communications* *5*, 5267.
- Park, S.-Y., Park, J.-E., Kim, T.-S., Kim, J.H., Kwak, M.-J., Ku, B., Tian, L., Murugan, R.N., Ahn, M., Komiyama, S., et al. (2014). Molecular basis for unidirectional scaffold switching of human Plk4 in centriole biogenesis. *Nat Struct Mol Biol* *21*, 696–703.
- Peel, N., Stevens, N.R., Basto, R., and Raff, J.W. (2007). Overexpressing Centriole-Replication Proteins In Vivo Induces Centriole Overduplication and De Novo Formation. *Current Biology* *17*, 834–843.
- Pelletier, L.L., Ozlü, N.N., Hannak, E.E., Cowan, C.C., Habermann, B.B., Ruer, M.M., Müller-Reichert, T.T., and Hyman, A.A.A. (2004). The *Caenorhabditis elegans* Centrosomal Protein SPD-2 Is Required for both Pericentriolar Material Recruitment and Centriole Duplication. *Current Biology* *14*, 11–11.
- Pelletier, L., O'Toole, E., Schwager, A., Hyman, A.A., and Müller-Reichert, T. (2006). Centriole assembly in *Caenorhabditis elegans*. *Nature* *444*, 619–623.
- Pfaff, K.L., Straub, C.T., Chiang, K., Bear, D.M., Zhou, Y., and Zon, L.I. (2007). The Zebra fish *cassiopeia* Mutant Reveals that SIL Is Required for Mitotic Spindle Organization. *Molecular and Cellular Biology* *27*, 5887–5897.
- Piperno, G., LeDizet, M., and Chang, X.J. (1987). Microtubules containing acetylated alpha-tubulin in mammalian cells in culture. *J Cell Biol* *104*, 289–302.
- Puklowski, A., Homsy, Y., Keller, D., May, M., Chauhan, S., Kossatz, U., Grünwald, V., Kubicka, S., Pich, A., Manns, M.P., et al. (2011). The SCF--FBXW5 E3-ubiquitin ligase is regulated by PLK4 and targets HsSAS-6 to control centrosome duplication. *Nature Cell Biology* *13*, 1004–1009.
- Quintyne, N.J. (2005). Spindle Multipolarity Is Prevented by Centrosomal Clustering. *Science* *307*, 127–129.
- Rodrigues-Martins, A., Riparbelli, M., Callaini, G., Glover, D.M., and Bettencourt-

- Dias, M. (2007). Revisiting the Role of the Mother Centriole in Centriole Biogenesis. *Science* *316*, 1046–1050.
- Rogers, G.C., Rusan, N.M., Roberts, D.M., Peifer, M., and Rogers, S.L. (2009). The SCF Slimb ubiquitin ligase regulates Plk4/Sak levels to block centriole reduplication. *The Journal of Cell Biology* *184*, 225–239.
- Santamaria, A., Wang, B., Elowe, S., Malik, R., Zhang, F., Bauer, M., Schmidt, A., Sillje, H.H.W., Korner, R., and Nigg, E.A. (2010). The Plk1-dependent Phosphoproteome of the Early Mitotic Spindle. *Molecular & Cellular Proteomics* *10*, M110.004457–M110.004457.
- Saunders, W. (2005). Centrosomal amplification and spindle multipolarity in cancer cells. *Seminars in Cancer Biology* *15*, 25–32.
- Schmidt, T.I., Kleylein-Sohn, J., Westendorf, J., Le Clech, M., Lavoie, S.B., Stierhof, Y.-D., and Nigg, E.A. (2009). Control of Centriole Length by CPAP and CP110. *Current Biology* *19*, 1005–1011.
- Schöckel, L., Möckel, M., Mayer, B., Boos, D., and Stemmann, O. (2011). Cleavage of cohesin rings coordinates the separation of centrioles and chromatids. *Nature* *13*, 966–972.
- Shaheen, R., Tala, A.I., Almoisheer, A., and Alkuraya, F.S. (2014). Mutation in PLK4, encoding a master regulator of centriole formation, defines a novel locus for primordial dwarfism. *J. Med. Genet.* *51*, 814–816.
- Shimanovskaya, E., Viscardi, V., Lesigang, J., Lettman, M.M., Qiao, R., Svergun, D.I., Round, A., Oegema, K., and Dong, G. (2014). Structure of the *C. elegans* ZYG-1 cryptic polo box suggests a conserved mechanism for centriolar docking of Plk4 kinases. *Structure* *22*, 1090–1104.
- Sievers, F., Wilm, A., Dineen, D., Gibson, T.J., Karplus, K., Li, W., Lopez, R., McWilliam, H., Remmert, M., Soding, J., et al. (2011). Fast, scalable generation of high-quality protein multiple sequence alignments using Clustal Omega. *Mol Syst Biol* *7*, 539–539.
- Silkworth, W.T., Nardi, I.K., Scholl, L.M., and Cimini, D. (2009). Multipolar spindle pole coalescence is a major source of kinetochore mis-attachment and chromosome mis-segregation in cancer cells. *PLoS ONE* *4*, e6564.
- Siller, K.H., and Doe, C.Q. (2009). Spindle orientation during asymmetric cell division. *Nature Cell Biology* *11*, 365–374.
- Sir, J.-H., Barr, A.R., Nicholas, A.K., Carvalho, O.P., Khurshid, M., Sossick, A., Reichelt, S., D'Santos, C., Woods, C.G., and Gergely, F. (2011). A primary microcephaly protein complex forms a ring around parental centrioles. *Nature Genetics* *43*, 1147–1153.
- Sir, J.-H., Pütz, M., Daly, O., Morrison, C.G., Dunning, M., Kilmartin, J.V., and Gergely, F. (2013). Loss of centrioles causes chromosomal instability in vertebrate

- somatic cells. *The Journal of Cell Biology* 203, 747–756.
- Slevin, L.K., Nye, J., Pinkerton, D.C., Buster, D.W., Rogers, G.C., and Slep, K.C. (2012). The Structure of the Plk4 Cryptic Polo Box Reveals Two Tandem Polo Boxes Required for Centriole Duplication. *Structure/Folding and Design* 20, 1905–1917.
- Sonnen, K.F., Gabryjonczyk, A.M., Anselm, E., Stierhof, Y.D., and Nigg, E.A. (2013). Human Cep192 and Cep152 cooperate in Plk4 recruitment and centriole duplication. *Journal of Cell Science* 126, 3223–3233.
- Sonnen, K.F., Schermelleh, L., Leonhardt, H., and Nigg, E.A. (2012). 3D-structured illumination microscopy provides novel insight into architecture of human centrosomes. *Biology Open* 1, 965–976.
- SOROKIN, S.P. (1968). Reconstructions of centriole formation and ciliogenesis in mammalian lungs. *Journal of Cell Science* 3, 207–230.
- Stevens, N.R., Dobbelaere, J., Brunk, K., Franz, A., and Raff, J.W. (2010a). *Drosophila* Ana2 is a conserved centriole duplication factor. *The Journal of Cell Biology* 188, 313–323.
- Stevens, N.R., Raposo, A.A.S.F., Basto, R., St Johnston, D., and Raff, J.W. (2007). From Stem Cell to Embryo without Centrioles. *Current Biology* 17, 1498–1503.
- Stevens, N.R., Roque, H., and Raff, J.W. (2010b). DSas-6 and Ana2 coassemble into tubules to promote centriole duplication and engagement. *Developmental Cell* 19, 913–919.
- Strnad, P., Leidel, S., Vinogradova, T., Euteneuer, U., Khodjakov, A., and Gönczy, P. (2007). Regulated HsSAS-6 Levels Ensure Formation of a Single Procentriole per Centriole during the Centrosome Duplication Cycle. *Developmental Cell* 13, 203–213.
- Swallow, C.J., Ko, M.A., Siddiqui, N.U., Hudson, J.W., and Dennis, J.W. (2005). Sak/Plk4 and mitotic fidelity. *Oncogene* 24, 306–312.
- SZOLLOSI, D., Calarco, P., and DONAHUE, R.P. (1972). Absence of centrioles in the first and second meiotic spindles of mouse oocytes. *Journal of Cell Science* 11, 521–541.
- Tang, C.-J.C., Fu, R.-H., Wu, K.-S., Hsu, W.-B., and Tang, T.K. (2009). CPAP is a cell-cycle regulated protein that controls centriole length. *Nature Cell Biology* 11, 825–831.
- Tang, C.-J.C., Lin, S.-Y., Hsu, W.-B., Lin, Y.-N., Wu, C.-T., Lin, Y.-C., Chang, C.-W., Wu, K.-S., and Tang, T.K. (2011). The human microcephaly protein STIL interacts with CPAP and is required for procentriole formation. *The EMBO Journal* 30, 4790–4804.
- Tanos, B.E., Yang, H.J., Soni, R., Wang, W.J., Macaluso, F.P., Asara, J.M., and Tsou, M.F.B. (2013). Centriole distal appendages promote membrane docking, leading to cilia initiation. *Genes & Development* 27, 163–168.
- Thein, K.H., Kleylein-Sohn, J., Nigg, E.A., and Gruneberg, U. (2007). Astrin is

required for the maintenance of sister chromatid cohesion and centrosome integrity. *The Journal of Cell Biology* 178, 345–354.

Tsou, M.-F.B., and Stearns, T. (2006a). Controlling centrosome number: licenses and blocks. *Current Opinion in Cell Biology* 18, 74–78.

Tsou, M.-F.B., and Stearns, T. (2006b). Mechanism limiting centrosome duplication to once per cell cycle. *Nature* 442, 947–951.

Tsou, M.-F.B., Wang, W.-J., George, K.A., Uryu, K., Stearns, T., and Jallepalli, P.V. (2009). Polo Kinase and Separase Regulate the Mitotic Licensing of Centriole Duplication in Human Cells. *Developmental Cell* 17, 344–354.

Uetake, Y., Loncarek, J., Nordberg, J.J., English, C.N., La Terra, S., Khodjakov, A., and Sluder, G. (2007). Cell cycle progression and de novo centriole assembly after centrosomal removal in untransformed human cells. *The Journal of Cell Biology* 176, 173–182.

Van Beneden, É. (1876). Recherches sur les Dicyémides, survivants actuels d'un embranchement des Mésozoaires. *Bulletins De l'Académie Royale Des Sciences, Des Lettres Et Des Beaux-Arts De Belgique* 41.

van Breugel, M., Hirono, M., Andreeva, A., Yanagisawa, H.A., Yamaguchi, S., Nakazawa, Y., Morgner, N., Petrovich, M., Ebong, I.O., Robinson, C.V., et al. (2011). Structures of SAS-6 Suggest Its Organization in Centrioles. *Science* 331, 1196–1199.

van Breugel, M., Wilcken, R., McLaughlin, S.H., Rutherford, T.J., and Johnson, C.M. (2014). Structure of the SAS-6 cartwheel hub from *Leishmania major*. *eLife* 3, e01812.

Vulprecht, J.J., David, A.A., Tibelius, A.A., Castiel, A.A., Konotop, G.G., Liu, F.F., Bestvater, F.F., Raab, M.S.M., Zentgraf, H.H., Izraeli, S.S., et al. (2012). STIL is required for centriole duplication in human cells. *Journal of Cell Science* 125, 1353–1362.

Wadsworth, P., and Khodjakov, A. (2004). E pluribus unum: towards a universal mechanism for spindle assembly. *Trends Cell Biol.* 14, 413–419.

Wang, X., Tsai, J.-W., Imai, J.H., Lian, W.-N., Vallee, R.B., and Shi, S.-H. (2009). Asymmetric centrosome inheritance maintains neural progenitors in the neocortex. *Nature* 461, 947–955.

Winey, M., and O'Toole, E. (2014). Centriole structure. *Philos. Trans. R. Soc. Lond., B, Biol. Sci.* 369.

Wolff, A., de Néchaud, B., Chillet, D., Mazarguil, H., Desbruyeres, E., Audebert, S., Eddé, B., Gros, F., and Denoulet, P. (1992). Distribution of glutamylated alpha and beta-tubulin in mouse tissues using a specific monoclonal antibody, GT335. *Eur J Cell Biol.* 59, 425–432.

Wong, C., and Stearns, T. (2003). Centrosome number is controlled by a centrosome-intrinsic block to reduplication. *Nature Cell Biology* 5, 539–544.

- Xu, J., Shen, C., Wang, T., and Quan, J. (2013). Structural basis for the inhibition of Polo-like kinase 1. *Nat Struct Mol Biol* *20*, 1047–1053.
- Yamashita, Y.M., and Fuller, M.T. (2008). Asymmetric centrosome behavior and the mechanisms of stem cell division. *The Journal of Cell Biology* *180*, 261–266.
- Yang, Z., Lončarek, J., Khodjakov, A., and Rieder, C.L. (2008). Extra centrosomes and/or chromosomes prolong mitosis in human cells. *Nature Cell Biology* *10*, 748–751.
- Yoshio Nakagawa, Y.Y.T.O.S.T.S.T. (2001). Outer Dense Fiber 2 Is a Widespread Centrosome Scaffold Component Preferentially Associated with Mother Centrioles: Its Identification from Isolated Centrosomes. *Molecular Biology of the Cell* *12*, 1687.
- Zhang, H., and Dawe, R.K. (2011). Mechanisms of plant spindle formation. *Chromosome Res* *19*, 335–344.
- Zhao, H., Zhu, L., Zhu, Y., Cao, J., Li, S., Huang, Q., Xu, T., Huang, X., Yan, X., and Zhu, X. (2013). The Cep63 paralogue Deup1 enables massive de novo centriole biogenesis for vertebrate multiciliogenesis. *Nature Cell Biology* *15*, 1434–1444.
- Zhu, F., Lawo, S., Bird, A., Pinchev, D., Ralph, A., Richter, C., Müller-Reichert, T., Kittler, R., Hyman, A.A., and Pelletier, L. (2008). The Mammalian SPD-2 Ortholog Cep192 Regulates Centrosome Biogenesis. *Current Biology* *18*, 136–141.
- Zitouni, S., Nabais, C., Jana, S.C., Guerrero, A., and Bettencourt-Dias, M. (2014). Polo-like kinases: structural variations lead to multiple functions. *Nature Publishing Group* *15*, 433–452.
- Zyss, D., and Gergely, F. (2008). Centrosome function in cancer: guilty or innocent? *Trends Cell Biol.* *19*, 334–346.

## 9 PUBLICATIONS

Large parts of this study have been published in:

Sonnen, K.F., **Gabryjonczyk, A.-M.**, Anselm, E., Stierhof, Y.-D., and Nigg, E.A. (2013). Human Cep192 and Cep152 cooperate in Plk4 recruitment and centriole duplication. *Journal of Cell Science* *126*, 3223–3233.

Arquint, C.\*, **Gabryjonczyk, A.-M.\***, Imseng, S.\*, Böhm, R.\*, Sauer, E., Hiller, S., Nigg, E.A., and Maier, T. (2015). STIL binding to Polo-box 3 of PLK4 regulates centriole duplication. *eLife* *4*. (\* authors contributed equally)

Additionally, the following review article has been published during this study:

Arquint, C.\*, **Gabryjonczyk, A.-M.\***, and Nigg, E.A. (2014). Centrosomes as signalling centres. *Philos. Trans. R. Soc. Lond., B, Biol. Sci.* *369*. (\* authors contributed equally)

## 10 ACKNOWLEDGEMENTS

First of all, I would like to thank Erich Nigg for giving me the opportunity to do my PhD in his lab and for supervising my thesis. I also thank Peter Scheiffle for joining the thesis committee as a co-referee.

Furthermore, I am grateful to all present and past members of the Nigg group for their companionship and support in the lab (Christian, Ina, Lukas, Dominik, Conrad, Patrick, Fabien, Anna B., Ana A., Cristina, Manuel, Eduard, Jasmine, Anna S., Gary, Luca). Especially, I would like to thank Ina and Christian for their help with experiments and the nice teamwork during the shared projects.

In addition, I am grateful to Stefan, Evelyn, Timm, Raphael, and Sebastian (from the Maier and Hiller laboratories at the Biozentrum) for the enjoyable collaboration and their invaluable contribution to this study. Thank you for carrying out the biophysical and crystallographic experiments, determining the structure, and conducting the NMR analysis.

I further thank the people from the Biozentrum's Core Facilities. Specifically, my thanks go to Oliver, Alexia, and Niko (Imaging Core Facility), Alex, Timo, Erik, and Jovan (Proteomics Core Facility), and Tim (Biophysics Core Facility) for their technical advice and expert support.

I am also grateful to Elena for her help and technical assistance, and to Fabien for lab management. Additionally, I thank Nadine for her support with administrative issues and Vaclav for excellent floor management.

Last but not least, I thank my family and friends – thank you for being around!